TABLE 5-9c
VERTICAL/HORIZONTAL RATIO MODELS USED BY EACH EXPERT

RATIO MODEL	ANDERSON	BOORE	CAMPBELL	MCGARR	SILVA	SOMERVILLE	WALCK
Campbell (1997) empirical	No	No	No	No	No	No	Yes
Silva (YM point source)	No	No	Yes	Yes	Yes	No	Yes
Abrahamson and Silva (1997) empirical	No	No	No	No	No	No	No
Spudich *et al.* (1997) empirical	No	No	No	No	No	No	No
Sabetta and Pugliese (1996) empirical	No	No	No	No	No	No	No
Zeng and Anderson finite fault	No	No	No	No	No	No	No
Somerville finite fault	No	No	No	No	No	No	No

TABLE 5-9d
PEAK VELOCITY/SA(F) RATIO MODELS USED BY EACH EXPERT

RATIO MODEL	ANDERSON	BOORE	CAMPBELL	MCGARR	SILVA	SOMERVILLE	WALCK
pgv/pga Campbell (1997) empirical	No	No	No	No	No	No	No
pgv/pga Silva (YM point source)	No	No	No	No	Yes	No	No
pgv/pga Joyner and Boore (1988) empirical	No	No	No	No	No	No	No
pgv/pga Sabetta and Pugliese (1996) empirical	No	No	No	No	No	No	No
pgv/pga Zeng and Anderson finite fault	No	No	No	No	No	No	No
pgv/pga Somerville finite fault	No	No	No	No	No	No	No
pgv/pga Silva finite fault	No	No	No	No	No	No	No
pgv/Sa (f=1Hz) Campbell (1997) empirical	No	No	No	No	No	No	No
pgv/Sa (f=1Hz) Silva (YM point source)	No	Yes	No	No	No	No	No
pgv/Sa (f=1Hz) Joyner and Boore (1988) empirical	No	No	No	No	No	No	No
pgv/Sa (f=1Hz) Sabetta and Pugliese (1996) empirical	No	No	No	No	No	No	No
pgv/Sa (f=1Hz) Zeng and Anderson finite fault	No	No	No	No	No	No	No
pgv/Sa (f=1Hz) Somerville finite fault	No	No	No	No	No	No	No
pgv/Sa (f=1Hz) Silva finite fault	No	No	No	No	No	No	No

TABLE 5-9e
HORIZONTAL COMPONENT-TO-COMPONENT VARIABILITY MODELS USED BY EACH EXPERT

VARIABILITY MODEL	ANDERSON	BOORE	CAMPBELL	MCGARR	SILVA	SOMERVILLE	WALCK
Boore *et al.* (1997) empirical	Yes	Yes	Yes	Yes	Yes	Yes	Yes
Spudich *et al.* (1996) empirical	No	No	No	No	No	No	No

TABLE 5-9f
20 HZ SPECTRAL ACCELERATION INTERPOLATION MODELS USED BY EACH EXPERT

INTERPOLATION MODEL	ANDERSON	BOORE	CAMPBELL	MCGARR	SILVA	SOMERVILLE	WALCK
Average coefficients for pga and 10 Hz	Yes	No	No	Yes	No	No	No
log-log interpolation between 33 Hz (pga) and 10 Hz	No	No	Yes	No	No	No	Yes
Boore scaling (Appendix F)	No	Yes	No	No	Yes	No	Yes

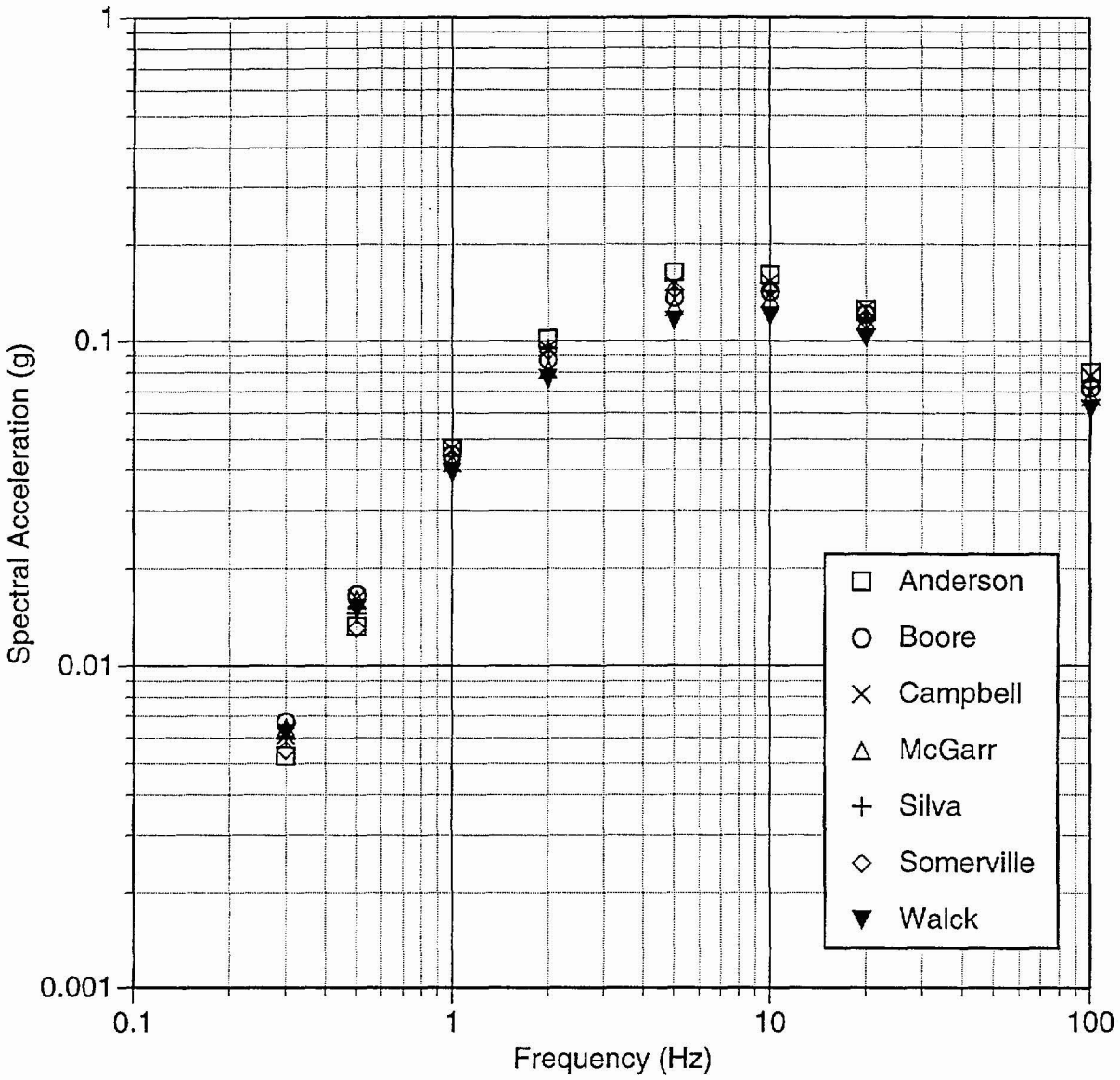

Figure 5-1 Median horizontal ground motion estimates for a M_W 5.8 earthquake at 17 km (rupture distance), normal faulting, hanging wall (Case 6)

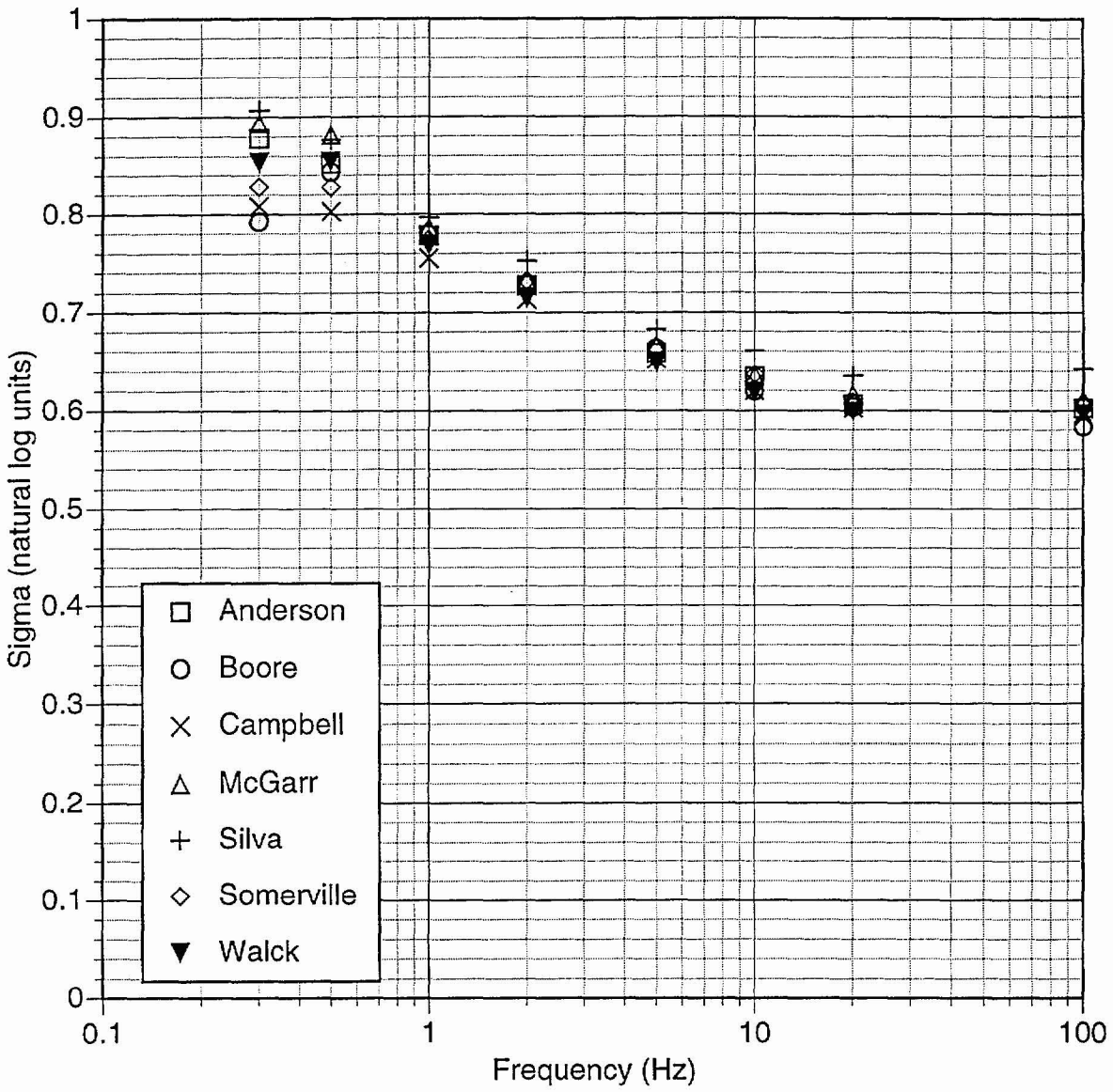

Figure 5-2 Aleatory variability in horizontal ground motion estimates for a M_W 5.8 earthquake at 17 km (rupture distance), normal faulting, hanging wall (Case 6)

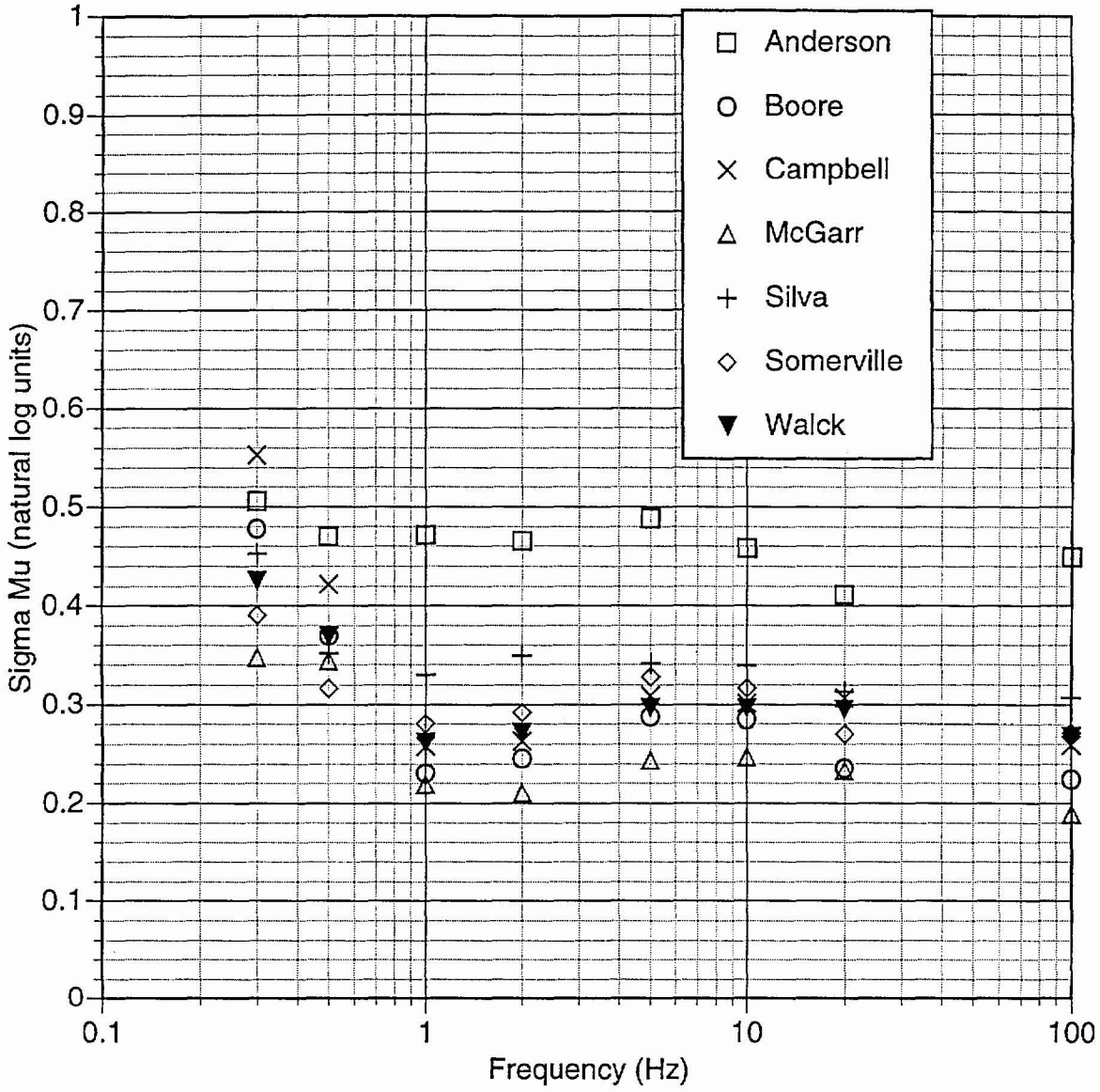

Figure 5-3 Epistemic uncertainty on the median horizontal ground motion estimates for a M_W 5.8 earthquake at 17 km (rupture distance), normal faulting, hanging wall (Case 6)

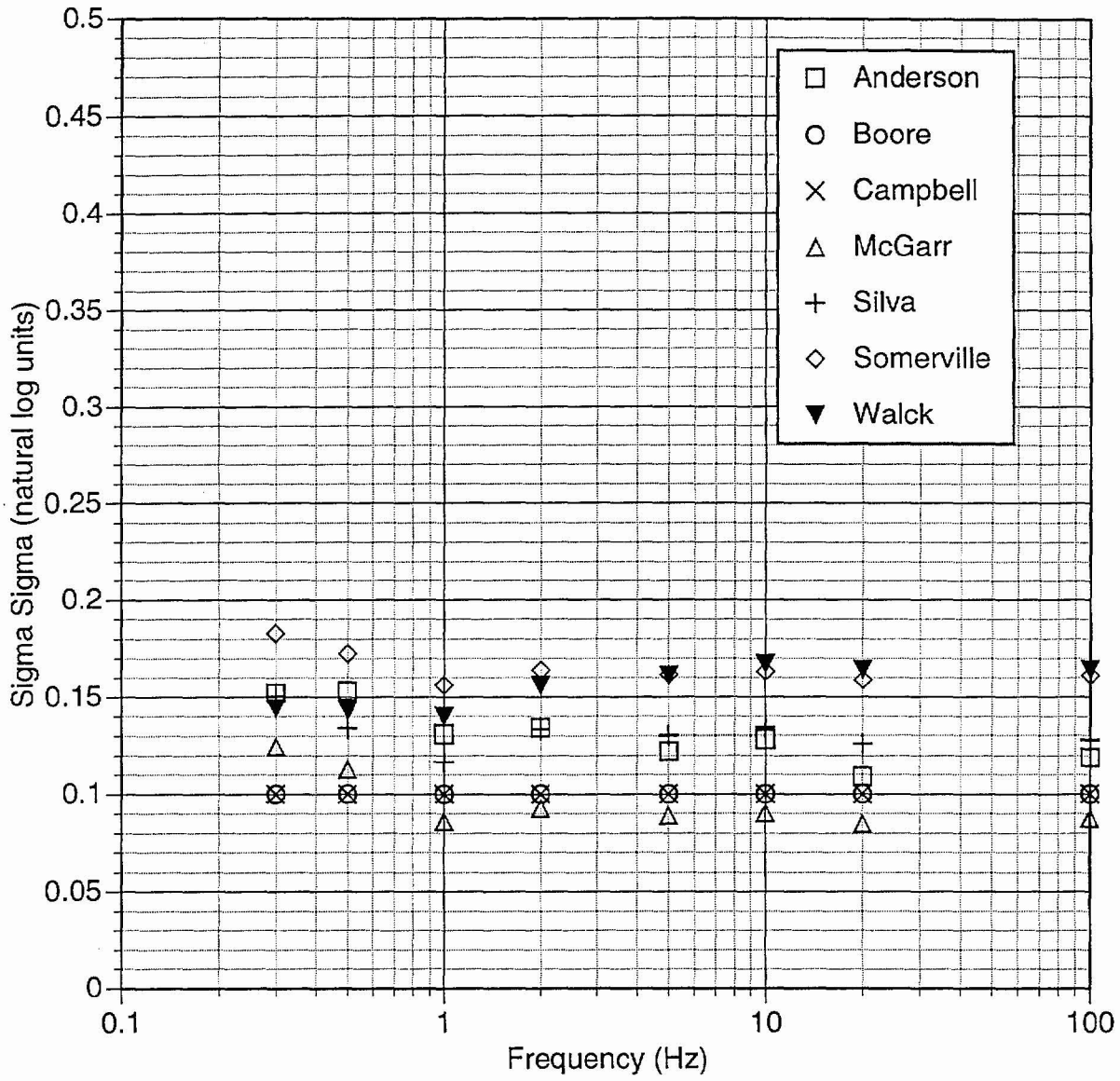

Figure 5-4 Epistemic uncertainty on the aleatory variability of horizontal ground motion estimates for a M_W 5.8 earthquake at 17 km (rupture distance), normal faulting, hanging wall (Case 6)

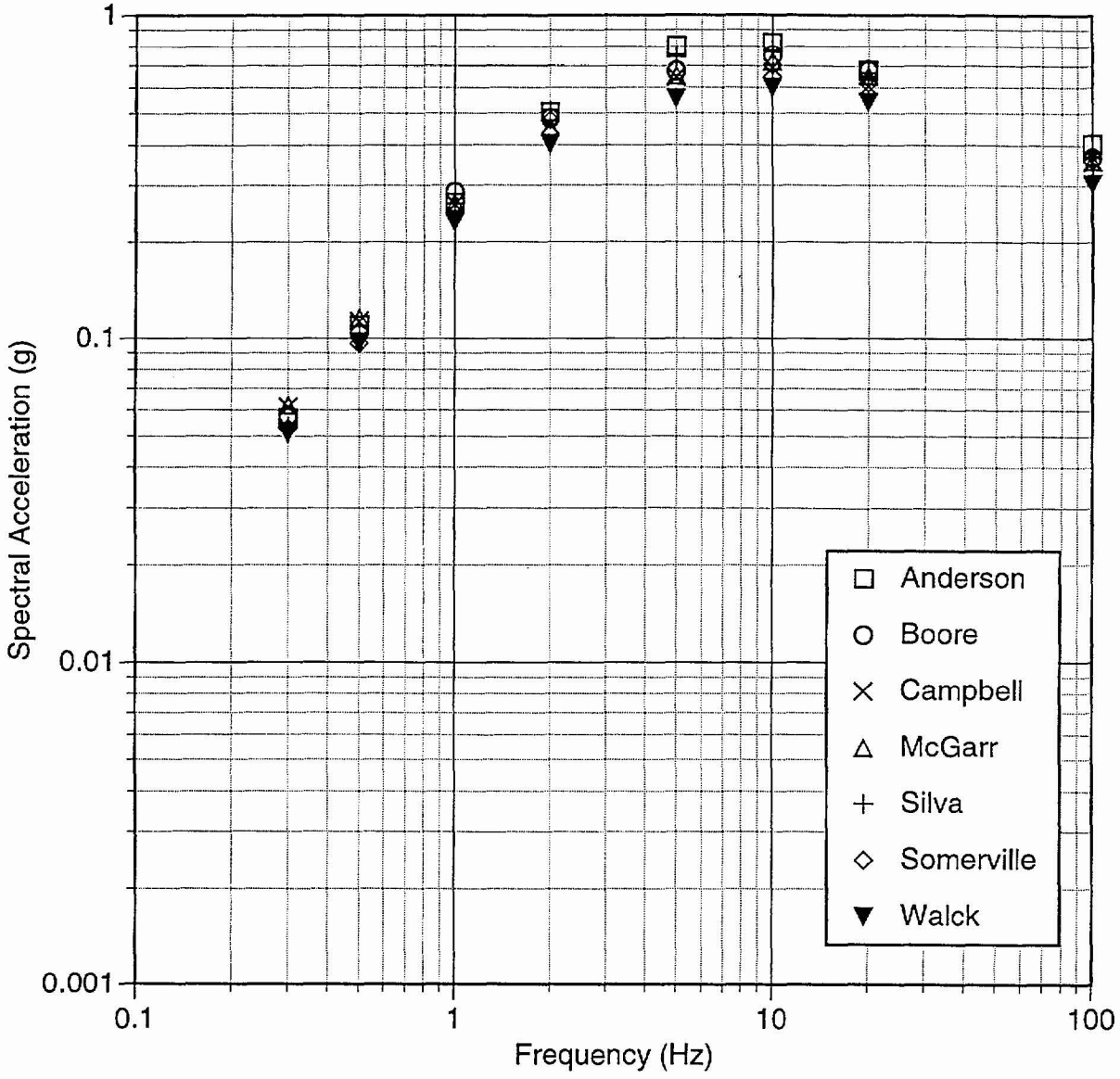

Figure 5-5 Median horizontal ground motion estimates for a M_W 6.5 earthquake at 4 km (rupture distance), normal faulting, hanging wall (Case 10)

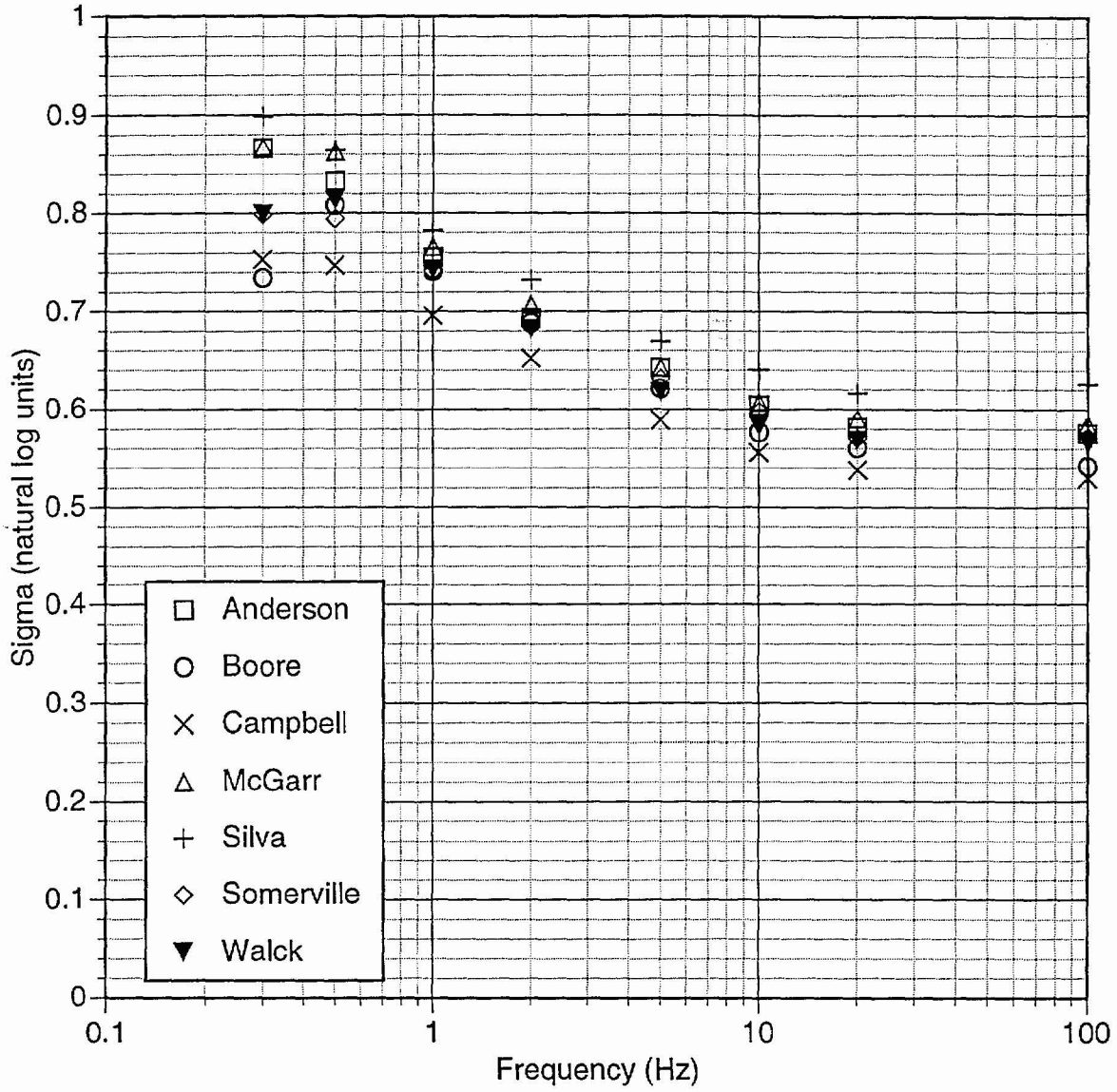

Figure 5-6 Aleatory variability in horizontal ground motion estimates for a M_W 6.5 earthquake at 4 km (rupture distance), normal faulting, hanging wall (Case 10)

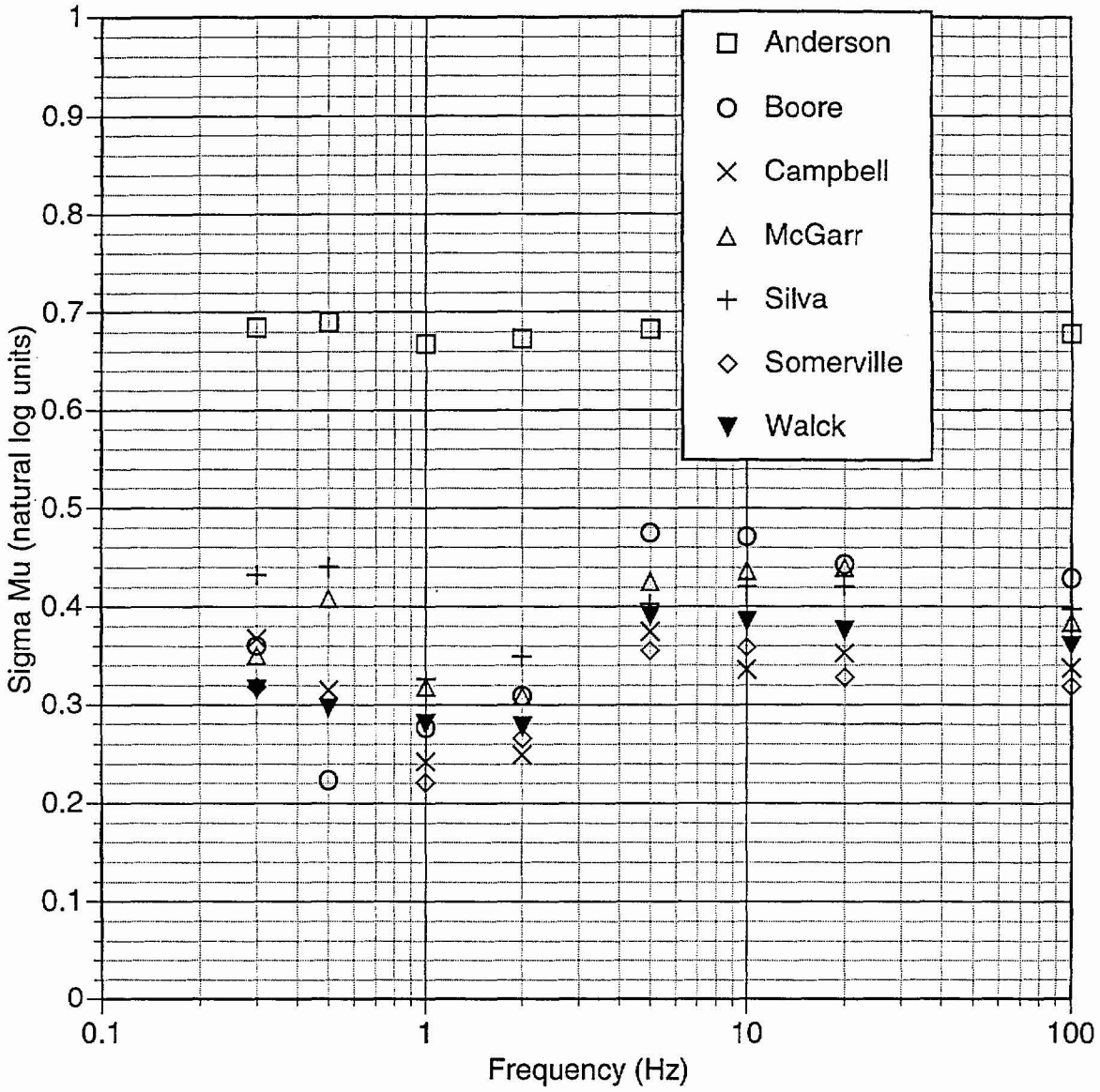

Figure 5-7 Epistemic uncertainty on the median horizontal ground motion estimates for a Mw 6.5 earthquake at 4 km (rupture distance), normal faulting, hanging wall (Case 10)

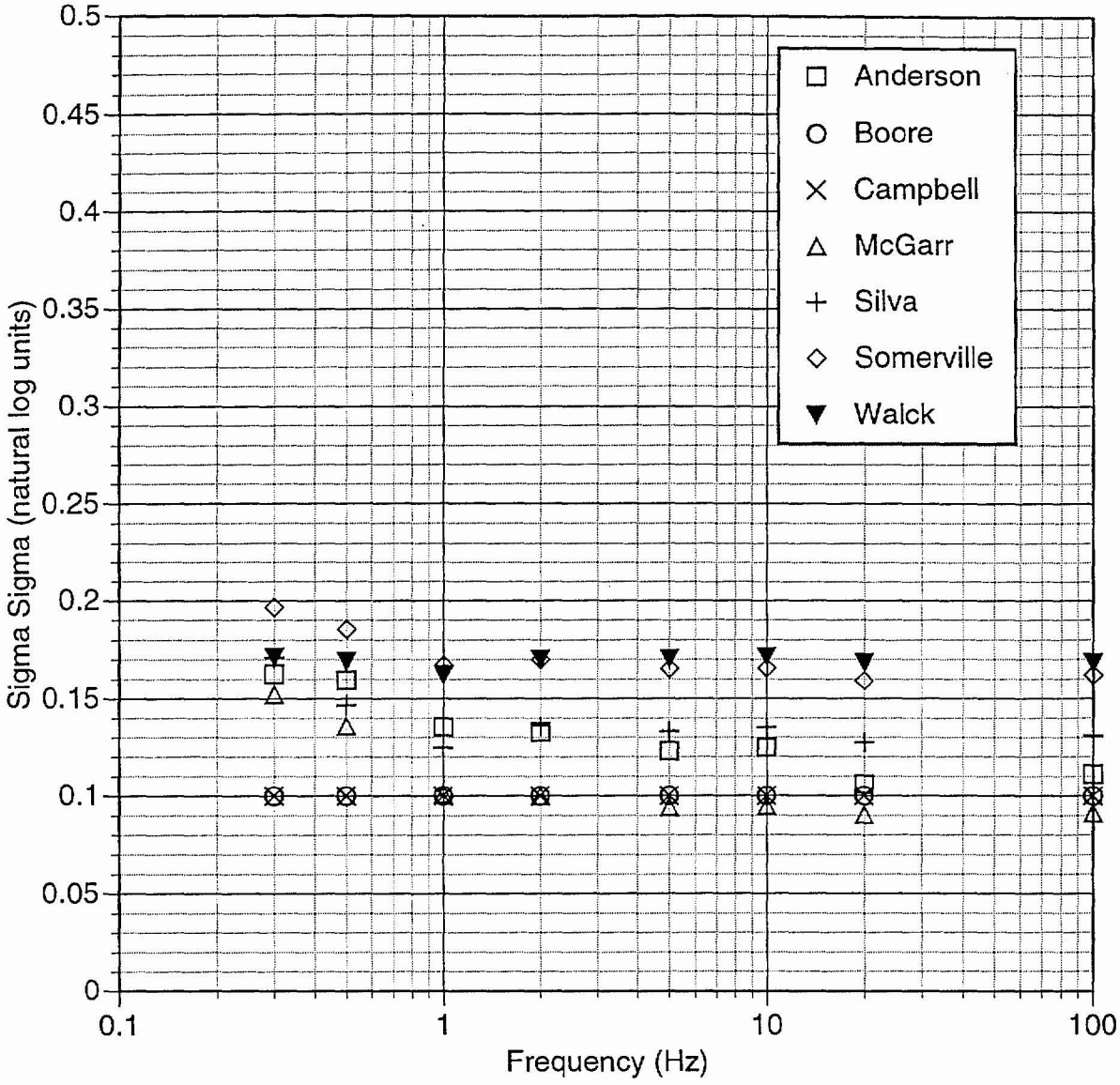

Figure 5-8 Epistemic uncertainty on the aleatory variability of horizontal ground motion estimates for a Mw 6.5 earthquake at 4 km (rupture distance), normal faulting, hanging wall (Case 10)

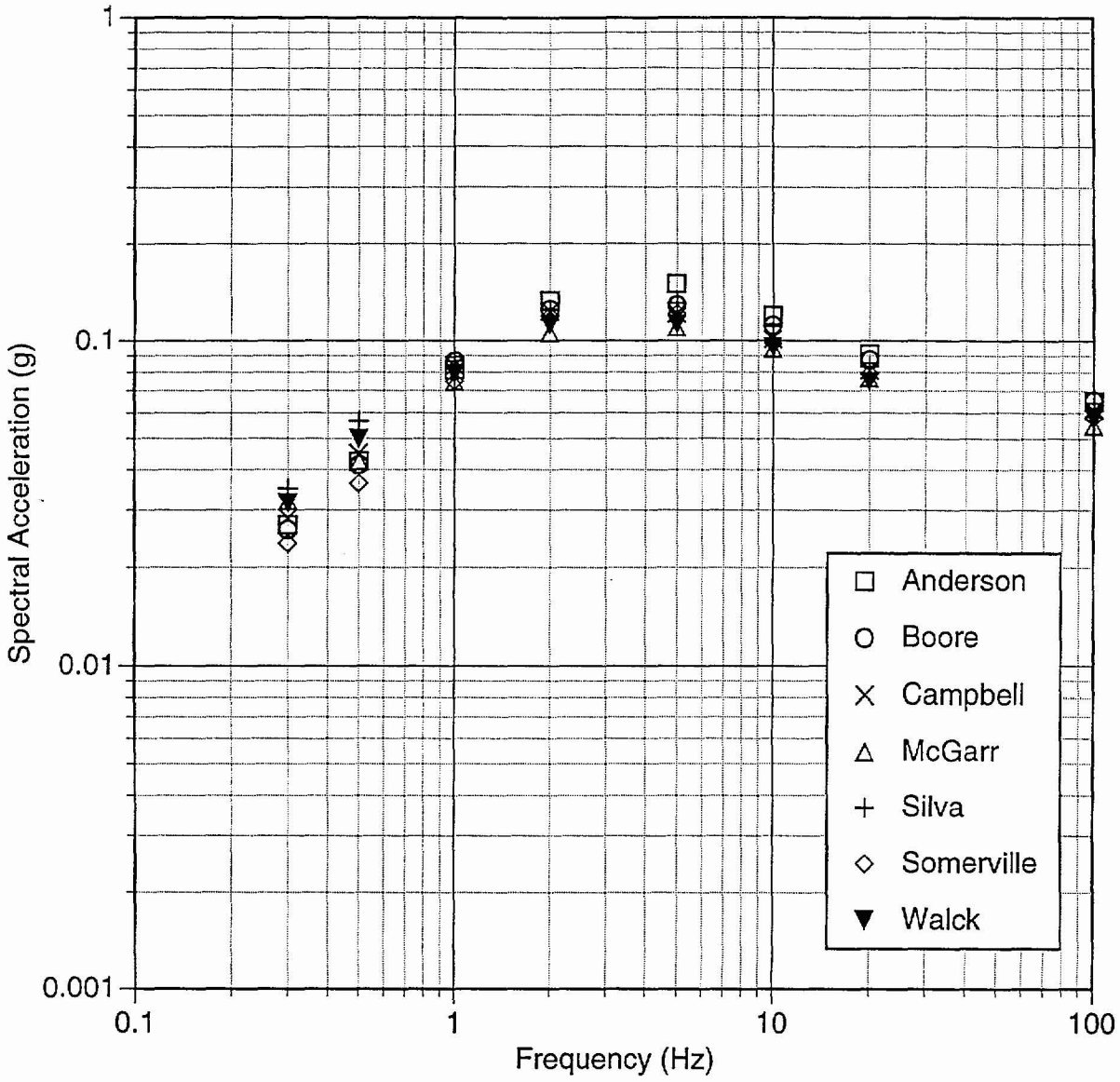

Figure 5-9 Median horizontal ground motion estimates for a M_W 7.5 earthquake at 50 km (rupture distance) strike-slip faulting (Case 15)

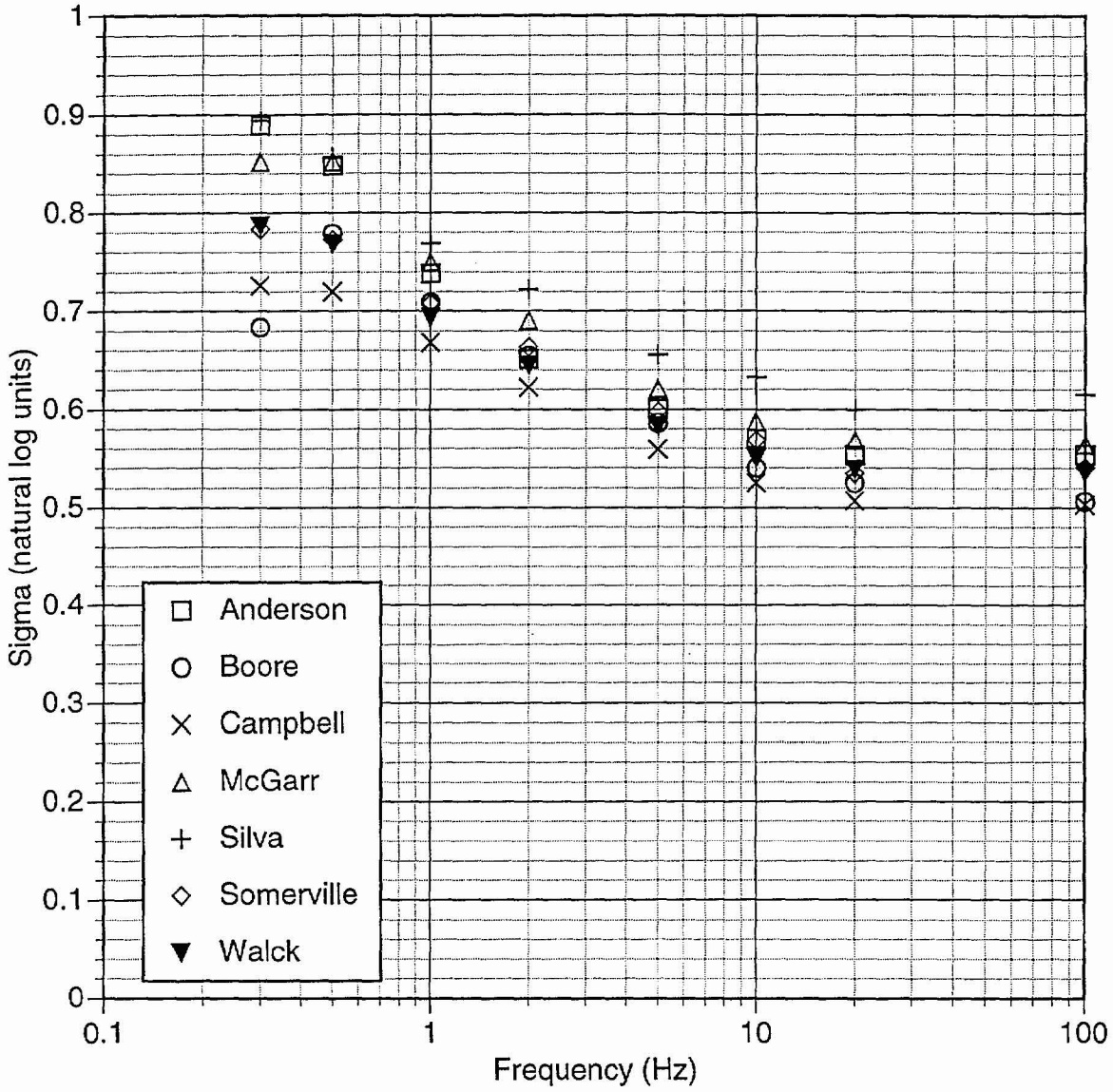

Figure 5-10 Aleatory variability in horizontal ground motion estimates for a Mw 7.5 earthquake at 50 km (rupture distance), strike-slip faulting (Case 15)

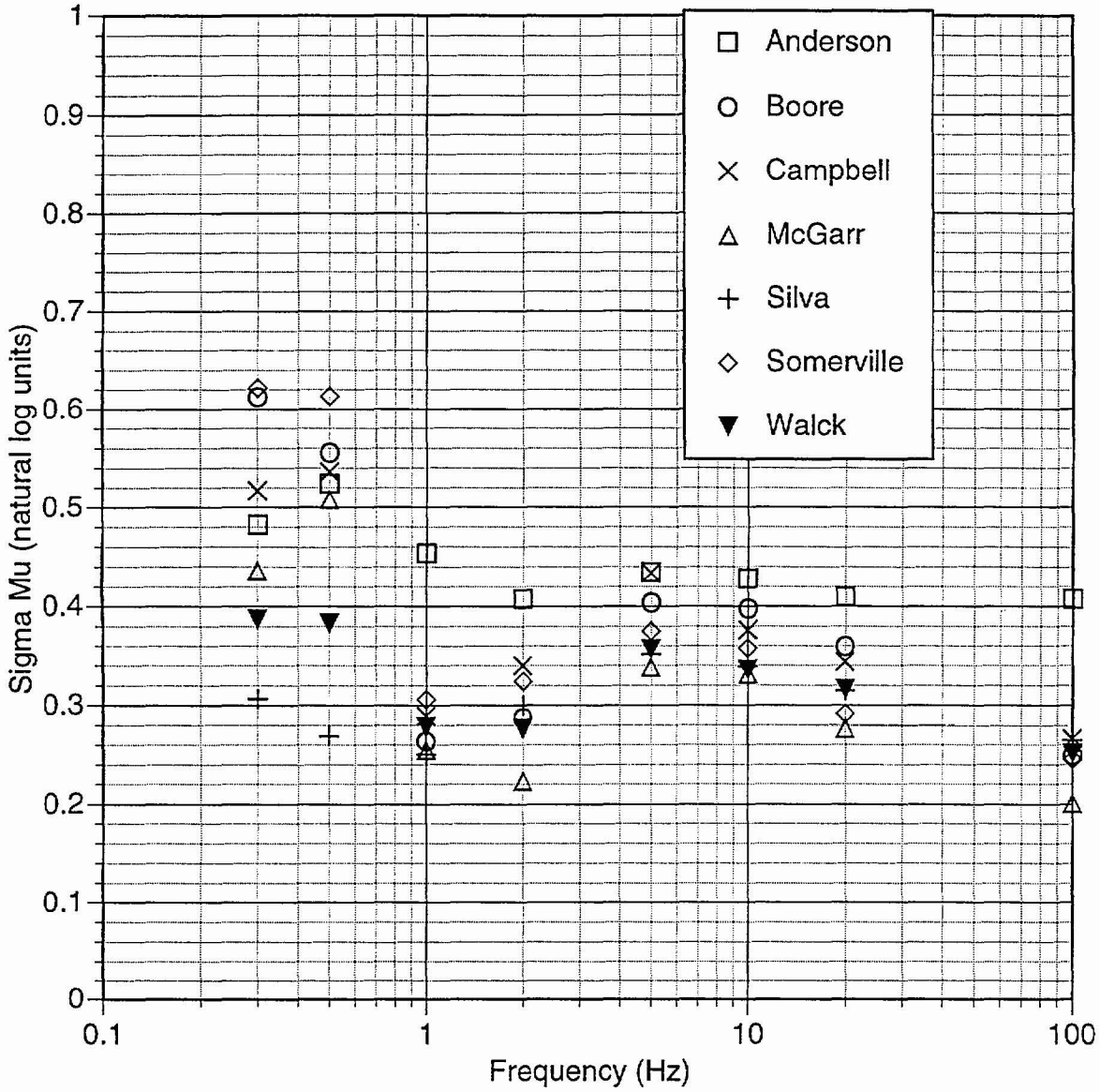

Figure 5-11 Epistemic uncertainty on the median horizontal ground motion estimates for a M_W 7.5 earthquake at 50 km (rupture distance), strike-slip faulting (Case 15)

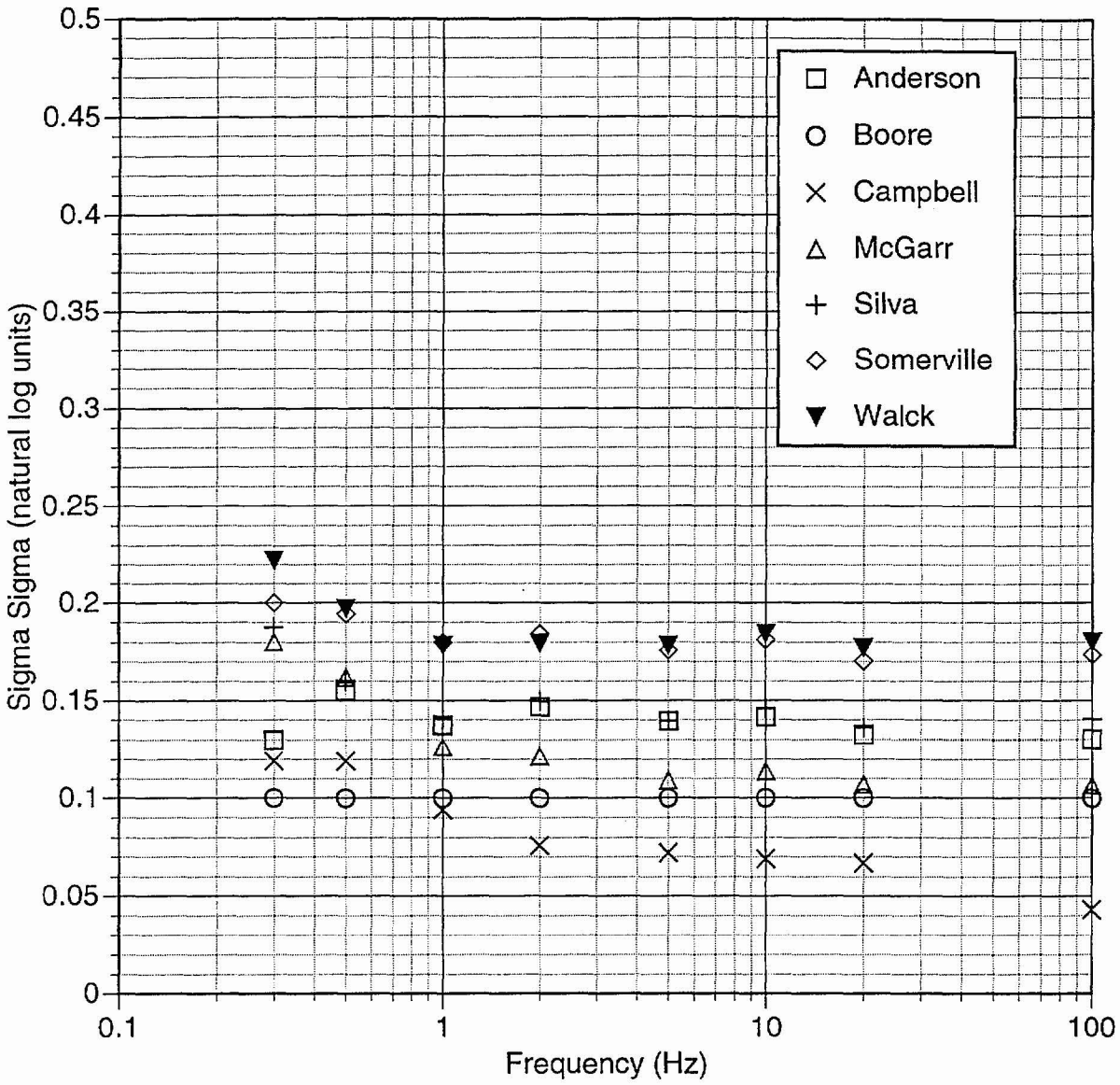

Figure 5-12 Epistemic uncertainty on the aleatory variability of horizontal ground motion estimates for a Mw 7.5 earthquake at 50 km (rupture distance), strike-slip faulting (Case 15)

6.0
GROUND MOTION ATTENUATION RELATIONS

To facilitate the use of the ground motion models in the hazard calculation, the experts' point estimates were parameterized by attenuation relations. The regression analysis to develop the attenuation relations was performed by the GM Facilitation Team. Each expert selected the distance measure used in the regression analyses for his/her point estimates. They chose whether the footwall and hanging wall point estimates were regressed together, resulting in a single normal faulting attenuation equation, or separately, yielding separate models for sites on the hanging wall and footwall. In addition, the experts could constrain the degree of magnitude saturation at close distances.

The experts reviewed the resulting regression models and either approved the models or made revisions to their point estimates or to the functional form used in the regression. This process was repeated until each expert was satisfied with the resulting models and is documented in Data Package Vols. 3 through 12. The final regression results are presented in this chapter.

6.1 REGRESSION MODEL FORM

Based on an examination of the experts' point estimates and with feedback from the experts, general functional forms were selected. Different functional forms were used for the median estimates, the aleatory variability, and the epistemic uncertainties.

The independent variables used in all regressions correspond to:

- M_w Moment magnitude
- R Distance (experts' selected distance measure in km)
- F Mechanism flag (0=strike-slip, 1 = normal)
- W_H Hanging wall flag (1=hanging wall, 0 = not hanging wall)
- W_F Footwall flag (1=footwall, 0=not footwall)

The predicted values for μ are in natural logarithm of g for spectral acceleration and natural logarithm of cm/sec for peak velocity. The σ_{al}, σ_{μ}, and σ_{σ} are all in natural log units. All of

the experts except for Campbell selected "rupture distance," defined as the closest distance from the site to the fault rupture as the distance metric. Campbell selected "seismogenic distance," the closest distance from the site to the assumed seismogenic part of the rupture (herein used as the part of the rupture that is at a depth of least 3 km)

The adopted general forms for the regression model are given below. As noted above, in some instances the experts added constraints to these general forms. These constraints are summarized in Table 6-1.

Median (μ):

For $M < m_1$,

$$\mu = a_1 + a_2(M - m_1) + a_6(8.5 - M)^2 + \left[a_3 + a_5(M - m_1)\right] \cdot \ln\sqrt{R^2 + a_8^2} + a_7 F + a_9 W_H f_1(M,R) + a_{10} W_F f_1(M,R) \quad (6\text{-}1a)$$

For $M \geq m_1$,

$$\mu = a_1 + a_4(M - m_1) + a_6(8.5 - M)^2 + \left[a_3 + a_5(M - m_1)\right] \cdot \ln\sqrt{R^2 + a_8^2} + a_7 F + a_9 W_H f_1(M,R) + a_{10} W_F f_1(M,R) \quad (6\text{-}1b)$$

in which

$$f_1(M,R) = \begin{cases} 0 & \text{for } R \leq x_1 \\ \dfrac{R - x_1}{x_2 - x_1} & x_1 < R < x_2 \\ 1 & x_2 \leq R \leq x_3 \\ \dfrac{x_4 - R}{x_4 - x_3} & x_3 < R < x_4 \\ 0 & \text{for } R \geq x_4 \end{cases} \cdot \begin{cases} 0 & \text{for } M < a_{11} \\ \dfrac{M - a_{11}}{a_{12} - a_{11}} & \text{for } a_{11} \leq M \leq a_{12} \\ 1 & \text{for } M > a_{12} \end{cases} \quad (6\text{-}2)$$

Aleatory Variability (σ_{al}):

For $M < b_4$,

$$\sigma_{al} = b_1 + b_2(M - b_4) \quad (6\text{-}3a)$$

For $M \geq b_4$,

$$\sigma_{al} = b_1 \tag{6-3b}$$

Epistemic Uncertainty in the Median (σ_μ):

$$\sigma_\mu = c_1 + c_2(M - c_6) + c_3 \ln(R+1) + c_4[\ln(R+1)]^2 + c_5 F \tag{6-4}$$

Epistemic Uncertainty in the Aleatory Variability (σ_σ):

For $M < d_4$, $$\sigma_\sigma = d_1 + d_2(M - d_4) \tag{6-5a}$$

For $M \geq d_4$, $$\sigma_\sigma = d_1 \tag{6-5b}$$

6.2 REGRESSION RESULTS

The following values are used for all models and for all periods:

$x_1 = 3$

$x_2 = 8$

$x_3 = 20$

$x_4 = 30$

$m_1 = 6.25$

Coefficients a_i, b_i, c_i, and d_i are listed in Appendix I. The process of fitting the experts' point estimates with a smooth equation leads to additional aleatory variability due to the misfit between the equation and the point estimates. To account for this additional variability, the total aleatory variability is given by the combination of the experts' estimate of the aleatory variability (parameterized by the regression equation as σ_{al}) and the standard deviation of the fit to the median ground motion (listed as Sigma Fit in the Appendix I tables). The total aleatory variability is given by

$$\sigma_{total} = \sqrt{\sigma_{fit}^2 + \sigma_{al}^2} \tag{6-6}$$

Comparisons of the regression model fits and the experts' point estimates are contained in Data Package Vols. 11A through 11G. Examples of the resulting attenuation relations for the

seven experts are compared for peak ground acceleration and for 1 Hz spectral acceleration for two faulting cases: a M_w 6.5 normal earthquake on the hanging wall and a M_w 7.5 strike-slip earthquake. The models for the horizontal component median ground motions are compared on Figures 6-1 through 6-4. These figures show that the range in the median ground motions from these models is generally less than a factor of 1.5. The models for the horizontal component aleatory variability are compared on Figures 6-5 and 6-6 for peak acceleration and spectral acceleration at a period of 1.0 sec. The range in the aleatory variability in the models is generally less than 0.1 natural log unit. The epistemic variability in the median horizontal ground motion is compared on Figures 6-7 to 6-10. The range of the models is generally less than 0.1 natural log units except for Anderson's model, which has much larger values due to his larger estimates of the epistemic uncertainty for the proponent model median estimates. Finally, the epistemic uncertainty in the aleatory variability is shown on Figures` 6-11 to 6-12. The range of these models is generally less than 0.1 natural log unit.

A corresponding set of plots of the models for the vertical component are shown on Figures 613 through 6-24. The vertical median ground motion models tend to be more variable between experts than the horizontal models. This larger variability is due to having fewer vertical proponent models available and much less validation for the numerical simulations. The experts individual estimates of the epistemic uncertainty also tend to be larger for the vertical component than for the horizontal component.

6.3 HYPOCENTRAL-BASED MODELS

The seismic source characterization also includes areal source zones, which are treated as point sources in the hazard calculation. Since the GM expert point estimates and the attenuation relations were developed for closest distance, a conversion factor is needed to make the model applicable to hypocentral distance, which is the relevant distance for areal sources.

The use of hypocentral distance rather than closest distance affects both the median ground motion and the aleatory variability since for a given hypocentral distance, there is a range of possible closest distances. Rather than developing independent attenuation models based on

hypocentral distance, the GM Facilitation Team evaluated the relation between hypocentral distance and rupture distance based on an assumed distribution of hypocenters on the fault plane. Note that this distribution is not the same as the distribution of hypocenters with depth in an earthquake catalog, but rather the distribution of the hypocenters on the rupture plane for a specific rupture dimension. With this relation between hypocentral distance and rupture distance, the uncertainty of the ground motion due to uncertainty in the closest-distance can be directly propagated using standard methods for propagation of errors (see Appendix J).

The adjustments using hypocentral distance are presented as a mapping of the mean rupture distance (as a function of the hypocentral distance and magnitude) and additional aleatory variability. The additional epistemic uncertainty in the median ground motion and aleatory variability due to the uncertainty in the distribution of hypocenters on the rupture plane are also estimated, but they are negligible. The development of these correction factors is given in Appendix J. Here, just the final models are presented.

For a given hypocentral distance H (in km) and magnitude M, the mean rupture distance R (in km) is given by

$$R = \begin{cases} H\left(1 + e_1 + e_2(M-5)\right) + H^2\left(e_3 + e_4(M-5)\right) & \text{for } H \le 30 \text{ km} \\ H + 30\left(e_1 + e_2(M-5)\right) + 900\left(e_3 + e_4(M-5)\right) & \text{for } H > 30 \text{ km} \end{cases} \tag{6-7}$$

in which the estimated coefficients are listed in Table 6-2.

The aleatory variability of the rupture distance as a function of the hypocentral distance and M is given by:

$$\sigma_R(H,M) = \sqrt{\left[\left(e_5 + e_6(M-5)\right)\tanh\left\{H\left(e_7 + e_8(M-5)\right)\right\}\right]^2 + 1.2^2} \tag{6-8}$$

with the coefficients listed in Table 6-2.

The additional aleatory variability in ground motion due to the use of hypocentral distance is given by

$$\sigma_{Hypo} = \left|\frac{\partial Y}{\partial R}\right| \sigma_R(H,M) \tag{6-9}$$

in which Y is the natural log of the ground motion parameter of interest. Ignoring hanging wall and footwall effects, then

$$\frac{\partial Y}{\partial R} = \left(a_3 + a_5(M - 6.25)\right)\frac{R(H,M)}{R^2(H,M) + a_8^2} \tag{6-10}$$

in which a_3, a_5, and a_8 are coefficients in the regression equations for each expert (Appendix I tables). This additional aleatory variability is combined with the total aleatory variability for the experts' models (Equation 6-6) to give the total aleatory variability of ground motion for the hypocentral model:

$$\sigma_{total}^{hypo} = \sqrt{\sigma_{hypo}^2 + \sigma_{total}^2} \tag{6-11}$$

The additional epistemic uncertainties in ground motion for a hypocentral distance model are computed in Appendix J. They are small enough to be neglected.

6.4 SPECIAL CASES

The experts developed scaling rules to apply their ground motion models to the two special cases discussed in Chapter 5.0: rupture of multiple (parallel) faults, and a shallow detachment fault.

6.4.1 Multiple Rupture Case

In the hazard calculation, the multiple rupture case is simplified and approximated by summing the moment of all of the ruptures and using the closest distance of any of the ruptures to the site. The resulting ground motion estimates must be adjusted, however, because using the total moment at the closest distance is not conservative compared to the case of multiple faults rupturing near the site. Multiple ruptures with small magnitude events can produce constructive interference that will result in larger ground motion than would be predicted for a single larger-magnitude event. Therefore, the GM Facilitation Team developed scale factors for the calculated ground motions, based on rules given by each of the experts.

Most of the experts used the concept of random vibration theory to predict the effect of multiple ruptures on ground motion. The main issue is whether the ground motions from the

multiple ruptures are correlated or are independent. In general, the experts considered the ground motions to be independent.

The scale factors for multiple ruptures are the ratios of ground motion as predicted by the experts' rules to the ground motion predicted from the experts' attenuation relations, using the full moment at the closest distance. Each expert's rules for developing the multiple rupture scale factors are given in the experts' documentation in Appendix F.

The scale factors are presented for cases of 2, 3, 4, and 5 faults rupturing simultaneously. The faults are assumed to be separated by 2 to 3 km (between any two faults). The ground motion was evaluated for several locations within 5 km of any of the faults. The average adjustment factors for the median, the aleatory uncertainty, and epistemic uncertainties are listed in Tables 6-3 to 6-9. The experts provided their adjustment factors for the uncertainties in either of two ways: as a scale factor or as an addition (in a square root of the sum of the squares method) to the total.

6.4.2 Detachment Fault Case

The second special case is a low-angle detachment fault with a dip of about 30 degrees. At Workshop #2, this case was presented as a combination of a low-angle detachment and multiple parallel faults that splayed off from the detachment fault. Six of the seven experts addressed the low-angle detachment separately from the multiple parallel faults; Somerville addressed the combined case. The adjustment factors for this case are listed in Tables 6-10 and 6-11. These factors should be applied to the computed ground motions based on the experts' attenuation relations.

TABLE 6-1
CONSTRAINTS ON THE REGRESSION

EXPERT	MEDIAN: INCREASE SATURATION AT SHORT DISTANCES?	MEDIAN: INCLUDE FOOTWALL AND HANGING WALL DIFFERENCES?	σ_μ: MAGNITUDE DEPENDENCE?	σ_μ: DISTANCE DEPENDENCE?
Anderson	Yes	Yes	No	Yes
Boore	No	Yes	Yes	Yes
Campbell	Yes	No	No	Yes
McGarr	Yes	No	No	Yes
Silva	Yes	Yes	No	No
Somerville	No	Yes	Yes	Yes
Walck	Yes	Yes	No	Yes

TABLE 6-2
REGRESSION MODEL COEFFICIENTS FOR THE HYPOCENTRAL-BASED MODELS

COEFFICIENT	ESTIMATE
e_1	-0.207
e_2	-0.323
e_3	0.0058
e_4	0.0059
e_5	1.894
e_6	3.854
e_7	0.0116
e_8	0.0094
e_9	-0.177
e_{10}	0.0055
e_{11}	0.0111

TABLE 6-3
J. G. ANDERSON: MULTIPLE RUPTURE SCENARIO
FACTORS APPLIED TO MEDIAN ESTIMATES

COMPONENT	FREQUENCY (HZ)	MEDIAN 2 FAULTS	MEDIAN 3 FAULTS	MEDIAN 4 FAULTS	MEDIAN 5 FAULTS	FACTOR SIGMA	FACTOR SIGMA-MU	ADDITIONAL SIGMA (SRSS)	ADDITIONAL SIGMA-MU (SRSS)
Horizontal	PGA	1.20	1.31	1.40	1.47	1.0	1.0	-	-
	20.	1.21	1.33	1.42	1.50	1.0	1.0	-	-
	10.	1.20	1.31	1.41	1.48	1.0	1.0	-	-
	5.	1.19	1.30	1.39	1.45	1.0	1.0	-	-
	2.	1.16	1.24	1.31	1.36	1.0	1.0	-	-
	1.	1.13	1.21	1.27	1.32	1.0	1.0	-	-
	0.5	1.09	1.13	1.17	1.21	1.0	1.0	-	-
	0.3	1.05	1.05	1.07	1.08	1.0	1.0	-	-
	PGV	1.13	1.20	1.25	1.29	1.0	1.0	-	-
Vertical	PGA	1.11	1.17	1.21	1.24	1.0	1.0	-	-
	20.	1.11	1.17	1.21	1.24	1.0	1.0	-	-
	10.	1.17	1.27	1.35	1.41	1.0	1.0	-	-
	5.	1.18	1.30	1.39	1.45	1.0	1.0	-	-
	2.	1.14	1.22	1.29	1.35	1.0	1.0	-	-
	1.	1.12	1.18	1.24	1.29	1.0	1.0	-	-
	0.5	1.04	1.04	1.06	1.07	1.0	1.0	-	-
	0.3	1.00	0.98	0.98	0.98	1.0	1.0	-	-
	PGV	1.11	1.16	1.20	1.24	1.0	1.0	-	-

TABLE 6-4
D. M. BOORE: MULTIPLE RUPTURE SCENARIO
FACTORS APPLIED TO MEDIAN ESTIMATES

COMPONENT	FREQUENCY (HZ)	MEDIAN 2 FAULTS	MEDIAN 3 FAULTS	MEDIAN 4 FAULTS	MEDIAN 5 FAULTS	FACTOR SIGMA	FACTOR SIGMA-MU	ADDITIONAL SIGMA (SRSS)	ADDITIONAL SIGMA-MU (SRSS)
Horizontal	PGA	1.25	1.38	1.48	1.55	1.0	1.0	-	-
	20.	1.26	1.38	1.48	1.55	1.0	1.0	-	-
	10.	1.25	1.37	1.47	1.53	1.0	1.0	-	-
	5.	1.24	1.37	1.46	1.53	1.0	1.0	-	-
	2.	1.21	1.31	1.39	1.45	1.0	1.0	-	-
	1.	1.18	1.26	1.33	1.37	1.0	1.0	-	-
	0.5	1.17	1.25	1.31	1.36	1.0	1.0	-	-
	0.3	1.10	1.13	1.16	1.18	1.0	1.0	-	-
	PGV	1.15	1.22	1.26	1.30	1.0	1.0	-	-
Vertical	PGA	1.22	1.33	1.41	1.46	1.0	1.0	-	-
	20.	1.22	1.32	1.4	1.45	1.0	1.0	-	-
	10.	1.22	1.32	1.39	1.44	1.0	1.0	-	-
	5.	1.21	1.31	1.39	1.44	1.0	1.0	-	-
	2.	1.19	1.28	1.35	1.39	1.0	1.0	-	-
	1.	1.17	1.24	1.3	1.34	1.0	1.0	-	-
	0.5	1.13	1.18	1.22	1.25	1.0	1.0	-	-
	0.3	1.09	1.11	1.14	1.16	1.0	1.0	-	-
	PGV	1.15	1.20	1.24	1.27	1.0	1.0	-	-

TABLE 6-5
K. W CAMPBELL: MULTIPLE RUPTURE SCENARIO
FACTORS APPLIED TO MEDIAN ESTIMATES

COMPONENT	FREQUENCY (HZ)	MEDIAN 2 FAULTS	MEDIAN 3 FAULTS	MEDIAN 4 FAULTS	MEDIAN 5 FAULTS	FACTOR SIGMA	FACTOR SIGMA-MU	ADDITIONAL SIGMA (SRSS)	ADDITIONAL SIGMA-MU (SRSS)
Horizontal	PGA	1.0	1.0	1.0	1.0	1.2	1.0	-	-
	20.	1.0	1.0	1.0	1.0	1.2	1.0	-	-
	10.	1.0	1.0	1.0	1.0	1.2	1.0	-	-
	5.	1.0	1.0	1.0	1.0	1.2	1.0	-	-
	2.	1.0	1.0	1.0	1.0	1.2	1.0	-	-
	1.	1.0	1.0	1.0	1.0	1.2	1.0	-	-
	0.5	1.0	1.0	1.0	1.0	1.2	1.0	-	-
	0.3	1.0	1.0	1.0	1.0	1.2	1.0	-	-
	PGV	1.0	1.0	1.0	1.0	1.2	1.0	-	-
Vertical	PGA	1.0	1.0	1.0	1.0	1.2	1.0	-	-
	20.	1.0	1.0	1.0	1.0	1.2	1.0	-	-
	10.	1.0	1.0	1.0	1.0	1.2	1.0	-	-
	5.	1.0	1.0	1.0	1.0	1.2	1.0	-	-
	2.	1.0	1.0	1.0	1.0	1.2	1.0	-	-
	1.	1.0	1.0	1.0	1.0	1.2	1.0	-	-
	0.5	1.0	1.0	1.0	1.0	1.2	1.0	-	-
	0.3	1.0	1.0	1.0	1.0	1.2	1.0	-	-
	PGV	1.0	1.0	1.0	1.0	1.2	1.0	-	-

TABLE 6-6
A. MCGARR MULTIPLE RUPTURE SCENARIO
FACTORS APPLIED TO MEDIAN ESTIMATES

COMPONENT	FREQUENCY (HZ)	MEDIAN 2 FAULTS	MEDIAN 3 FAULTS	MEDIAN 4 FAULTS	MEDIAN 5 FAULTS	FACTOR SIGMA	FACTOR SIGMA-MU	ADDITIONAL SIGMA (SRSS)	ADDITIONAL SIGMA-MU (SRSS)
Horizontal	PGA	1.0	1.0	1.0	1.0	1.2	1.0	-	-
	20.	1.0	1.0	1.0	1.0	1.2	1.0	-	-
	10.	1.0	1.0	1.0	1.0	1.2	1.0	-	-
	5.	1.0	1.0	1.0	1.0	1.2	1.0	-	-
	2.	1.0	1.0	1.0	1.0	1.2	1.0	-	-
	1.	1.0	1.0	1.0	1.0	1.2	1.0	-	-
	0.5	1.0	1.0	1.0	1.0	1.2	1.0	-	-
	0.3	1.0	1.0	1.0	1.0	1.2	1.0	-	-
	PGV	1.0	1.0	1.0	1.0	1.2	1.0	-	-
Vertical	PGA	1.0	1.0	1.0	1.0	1.2	1.0	-	-
	20.	1.0	1.0	1.0	1.0	1.2	1.0	-	-
	10.	1.0	1.0	1.0	1.0	1.2	1.0	-	-
	5.	1.0	1.0	1.0	1.0	1.2	1.0	-	-
	2.	1.0	1.0	1.0	1.0	1.2	1.0	-	-
	1.	1.0	1.0	1.0	1.0	1.2	1.0	-	-
	0.5	1.0	1.0	1.0	1.0	1.2	1.0	-	-
	0.3	1.0	1.0	1.0	1.0	1.2	1.0	-	-
	PGV	1.0	1.0	1.0	1.0	1.2	1.0	-	-

TABLE 6-7
W. J. SILVA: MULTIPLE RUPTURE SCENARIO
FACTORS APPLIED TO MEDIAN ESTIMATES

COMPONENT	FREQUENCY (HZ)	MEDIAN 2 FAULTS	MEDIAN 3 FAULTS	MEDIAN 4 FAULTS	MEDIAN 5 FAULTS	FACTOR SIGMA	FACTOR SIGMA-MU	ADDITIONAL SIGMA (SRSS)	ADDITIONAL SIGMA-MU (SRSS)
Horizontal	PGA	1.29	1.44	1.56	1.66	1.0	1.0	-	-
	20.	1.30	1.46	1.58	1.68	1.0	1.0	-	-
	10.	1.29	1.45	1.57	1.66	1.0	1.0	-	-
	5.	1.29	1.44	1.56	1.65	1.0	1.0	-	-
	2.	1.25	1.39	1.49	1.57	1.0	1.0	-	-
	1.	1.22	1.34	1.43	1.50	1.0	1.0	-	-
	0.5	1.46	1.56	1.64	1.70	1.0	1.0	-	-
	0.3	1.40	1.45	1.50	1.54	1.0	1.0	-	-
	PGV	1.21	1.32	1.40	1.46	1.0	1.0	-	-
Vertical	PGA	1.29	1.45	1.57	1.66	1.0	1.0	-	-
	20.	1.30	1.46	1.58	1.67	1.0	1.0	-	-
	10.	1.29	1.43	1.55	1.63	1.0	1.0	-	-
	5.	1.28	1.43	1.54	1.63	1.0	1.0	-	-
	2.	1.25	1.38	1.48	1.55	1.0	1.0	-	-
	1.	1.22	1.34	1.42	1.49	1.0	1.0	-	-
	0.5	1.45	1.55	1.62	1.69	1.0	1.0	-	-
	0.3	1.39	1.45	1.49	1.51	1.0	1.0	-	-
	PGV	1.22	1.33	1.42	1.48	1.0	1.0	-	-

TABLE 6-8
P. G. SOMERVILLE: MULTIPLE RUPTURE SCENARIO
FACTORS APPLIED TO MEDIAN ESTIMATES

COMPONENT	FREQUENCY (HZ)	MEDIAN 2 FAULTS	MEDIAN 3 FAULTS	MEDIAN 4 FAULTS	MEDIAN 5 FAULTS	FACTOR SIGMA	FACTOR SIGMA-MU	ADDITIONAL SIGMA (SRSS)	ADDITIONAL SIGMA-MU (SRSS)
Horizontal	PGA	1.63	1.63	1.63	1.63	-	-	0.3	0.2
	20.	1.63	1.63	1.63	1.63	-	-	0.3	0.2
	10.	1.63	1.63	1.63	1.63	-	-	0.3	0.2
	5.	1.63	1.63	1.63	1.63	-	-	0.3	0.2
	2.	1.58	1.58	1.58	1.58	-	-	0.3	0.2
	1.	1.5	1.5	1.5	1.5	-	-	0.3	0.2
	0.5	1.5	1.5	1.5	1.5	-	-	0.3	0.2
	0.3	1.5	1.5	1.5	1.5	-	-	0.3	0.2
	PGV	1.5	1.5	1.5	1.5	-	-	0.3	0.2
Vertical	PGA	1.63	1.63	1.63	1.63	-	-	0.3	0.2
	20.	1.63	1.63	1.63	1.63	-	-	0.3	0.2
	10.	1.63	1.63	1.63	1.63	-	-	0.3	0.2
	5.	1.63	1.63	1.63	1.63	-	-	0.3	0.2
	2.	1.58	1.58	1.58	1.58	-	-	0.3	0.2
	1.	1.5	1.5	1.5	1.5	-	-	0.3	0.2
	0.5	1.5	1.5	1.5	1.5	-	-	0.3	0.2
	0.3	1.5	1.5	1.5	1.5	-	-	0.3	0.2
	PGV	1.5	1.5	1.5	1.5	-	-	0.3	0.2

TABLE 6-9
M. C. WALCK: MULTIPLE RUPTURE SCENARIO
FACTORS APPLIED TO MEDIAN ESTIMATES

COMPONENT	FREQUENCY (HZ)	MEDIAN 2 FAULTS	MEDIAN 3 FAULTS	MEDIAN 4 FAULTS	MEDIAN 5 FAULTS	FACTOR SIGMA	FACTOR SIGMA-MU	ADDITIONAL SIGMA (SRSS)	ADDITIONAL SIGMA-MU (SRSS)
Horizontal	PGA	1.28	1.42	1.53	1.61	-	-	0.0	0.1
	20.	1.30	1.45	1.58	1.67	-	-	0.0	0.1
	10.	1.29	1.43	1.55	1.63	-	-	0.0	0.1
	5.	1.27	1.42	1.53	1.61	-	-	0.0	0.1
	2.	1.23	1.35	1.45	1.52	-	-	0.0	0.1
	1.	1.20	1.30	1.38	1.43	-	-	0.0	0.1
	0.5	1.17	1.25	1.31	1.36	-	-	0.0	0.2
	0.3	1.13	1.17	1.22	1.25	-	-	0.0	0.2
	PGV	1.21	1.32	1.40	1.46	-	-	0.0	0.1
Vertical	PGA	1.25	1.37	1.46	1.53	-	-	0.0	0.1
	20.	1.26	1.39	1.48	1.55	-	-	0.0	0.1
	10.	1.26	1.39	1.49	1.56	-	-	0.0	0.1
	5.	1.25	1.38	1.47	1.54	-	-	0.0	0.1
	2.	1.20	1.30	1.38	1.43	-	-	0.0	0.1
	1.	1.18	1.26	1.33	1.37	-	-	0.0	0.1
	0.5	1.14	1.19	1.23	1.26	-	-	0.0	0.2
	0.3	1.09	1.11	1.13	1.14	-	-	0.0	0.2
	PGV	1.20	1.28	1.35	1.40	-	-	0.0	0.1

TABLE 6-10
LOW-ANGLE DETACHMENT FAULT SCENARIO
SCALE FACTORS

EXPERT	MEDIAN SCALE FACTOR	SIGMA-MU SCALE FACTOR	SIGMA SCALE FACTOR	ADDITIONAL SIGMA-MU (SRSS[1])	ADDITIONAL SIGMA (SRSS[1])
Anderson	1.0	1.0	1.0	-	-
Boore	1.0	1.0	1.0	-	-
Campbell (D = depth to bottom of rupture)	1.0 for D < 8 1.0+0.2*(D-8)/7 + 1 for 8<D<15 1.2 for D > 15	1.2	1.2	-	-
McGarr	1.0	1.3	1.0	-	-
Silva	1.0	1.0	1.0	-	-
Somerville[2]	See Table 4-17	-	-	0.3	0.2
Walck	1.0	-	-	0.25	0.0

[1] Square root of the sum of the squares method.

[2] Somerville addressed the case of a low-angle detachment fault combined with multiple parallel faults splaying off of the detachment (as requested). All of the other experts addressed the detachment fault by itself.

TABLE 6-11
ADJUSTMENT FACTORS FOR SIMULTANEOUS RUPTURES ON PARALLEL FAULTS AND A DEEP DETACHMENT SURFACE (SOMERVILLE)

FREQUENCY (HZ)	MEDIAN SCALE FACTOR	ADDITIONAL SIGMA (SRSS[1])	ADDITIONAL SIGMA-MU (SRSS[1])
PGA	1.0	0.3	0.2
20	1.0	0.3	0.2
10	1.0	0.3	0.2
5	1.0	0.3	0.2
2	1.2	0.3	0.2
1	2.2	0.3	0.2
0.5	2.2	0.3	0.2
0.3	1.7	0.3	0.2
PGV	2.2	0.3	0.2

[1] Square root of the sum of the squares method.

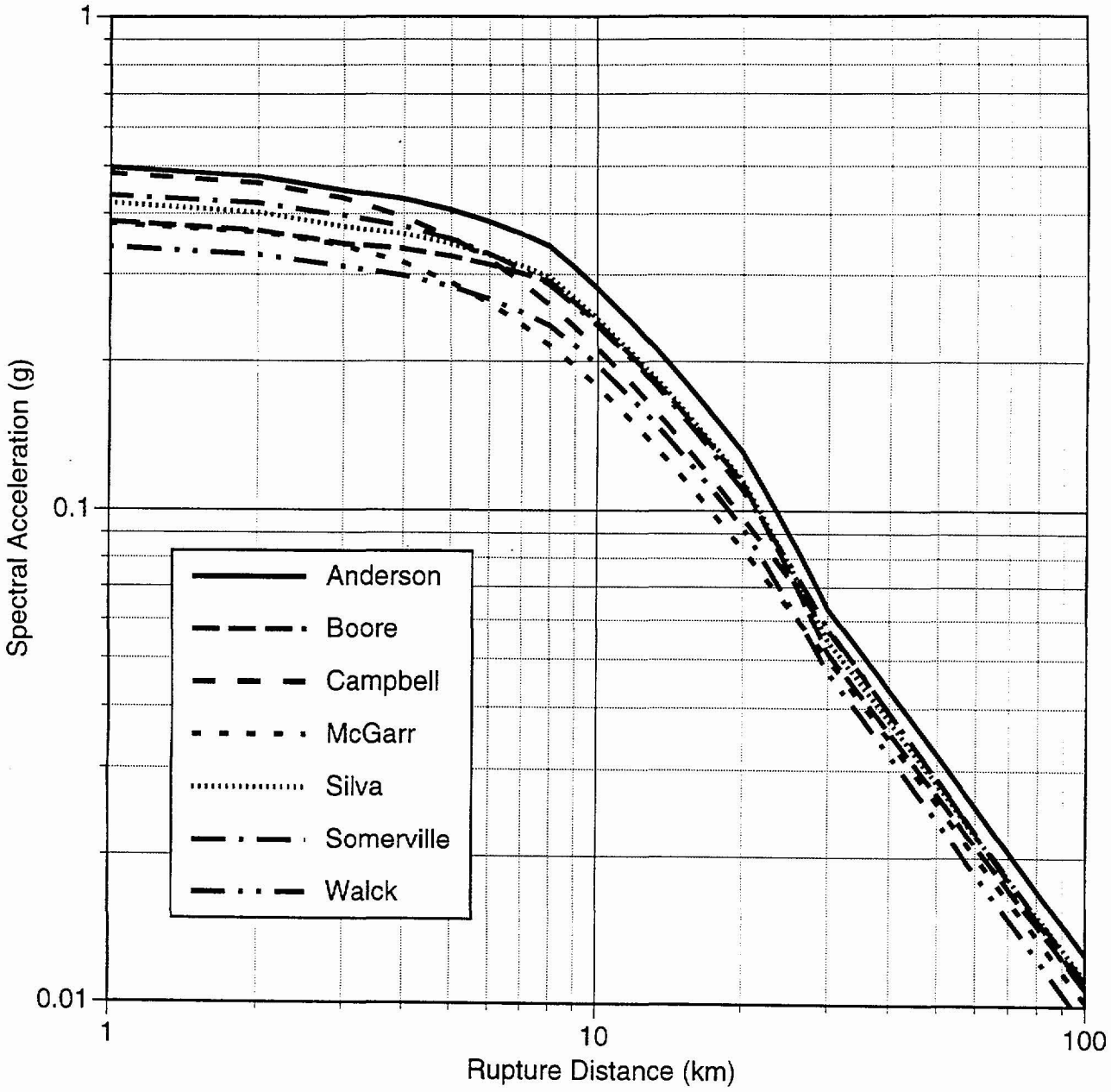

Figure 6-1 Comparison of median attenuation of horizontal PGA for M_w 6.5, normal faulting, hanging wall

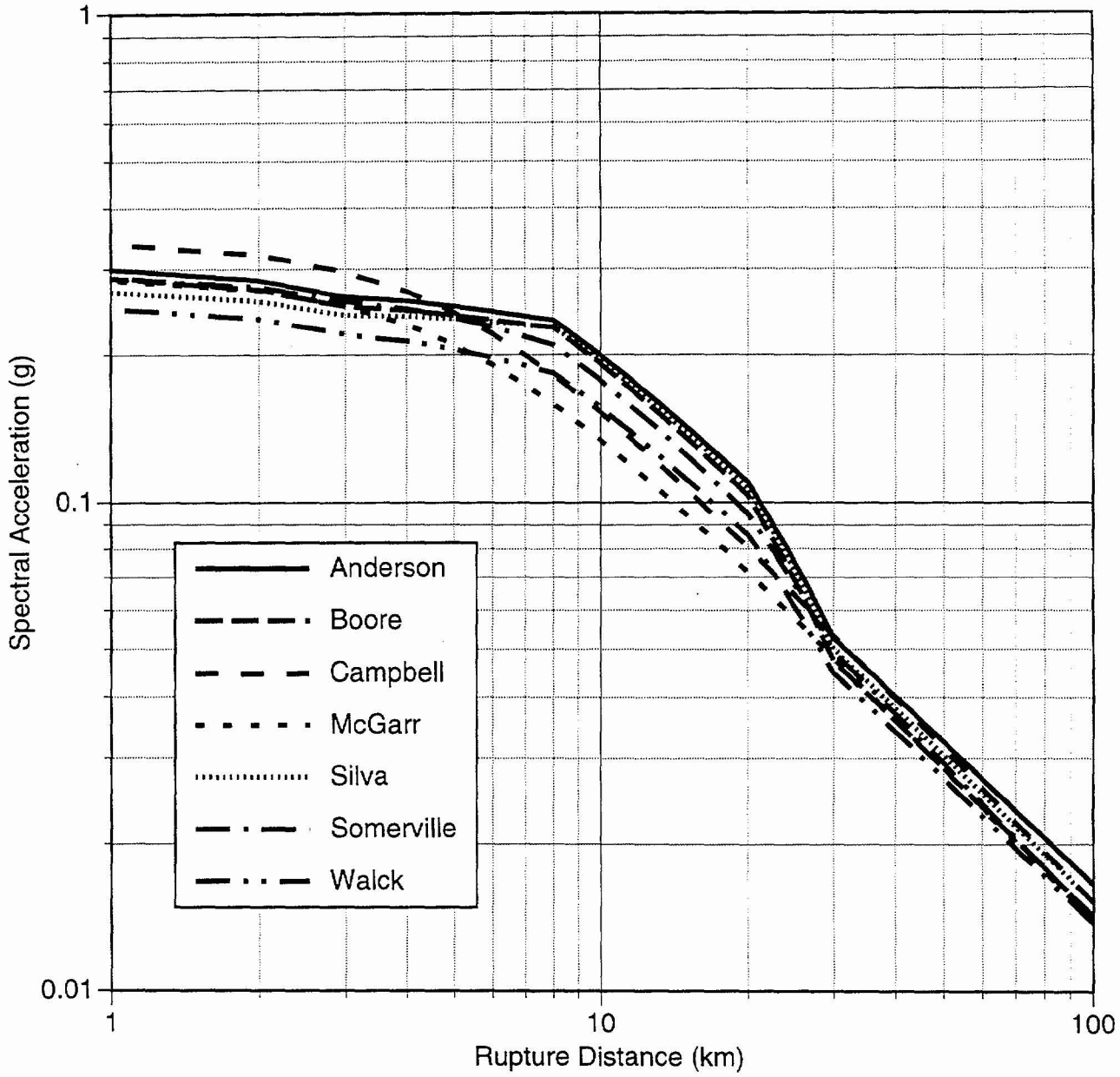

Figure 6-2 Comparison of median attenuation of horizontal spectral acceleration (T = 1.0 sec, 5% damping) for M_W 6.5, normal faulting, hanging wall

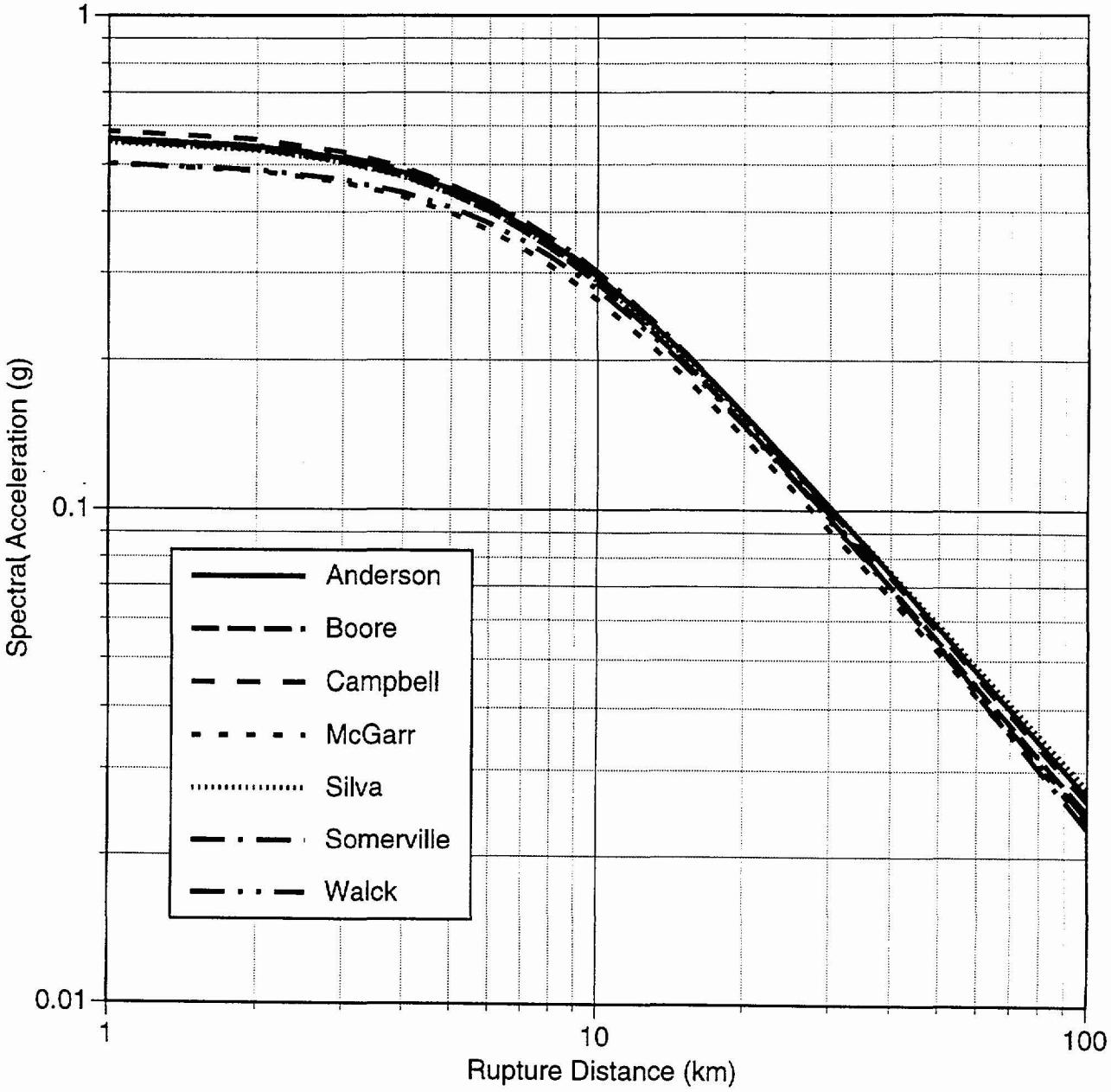

Figure 6-3 Comparison of median attenuation of horizontal PGA for Mw 7.5, strike-slip faulting

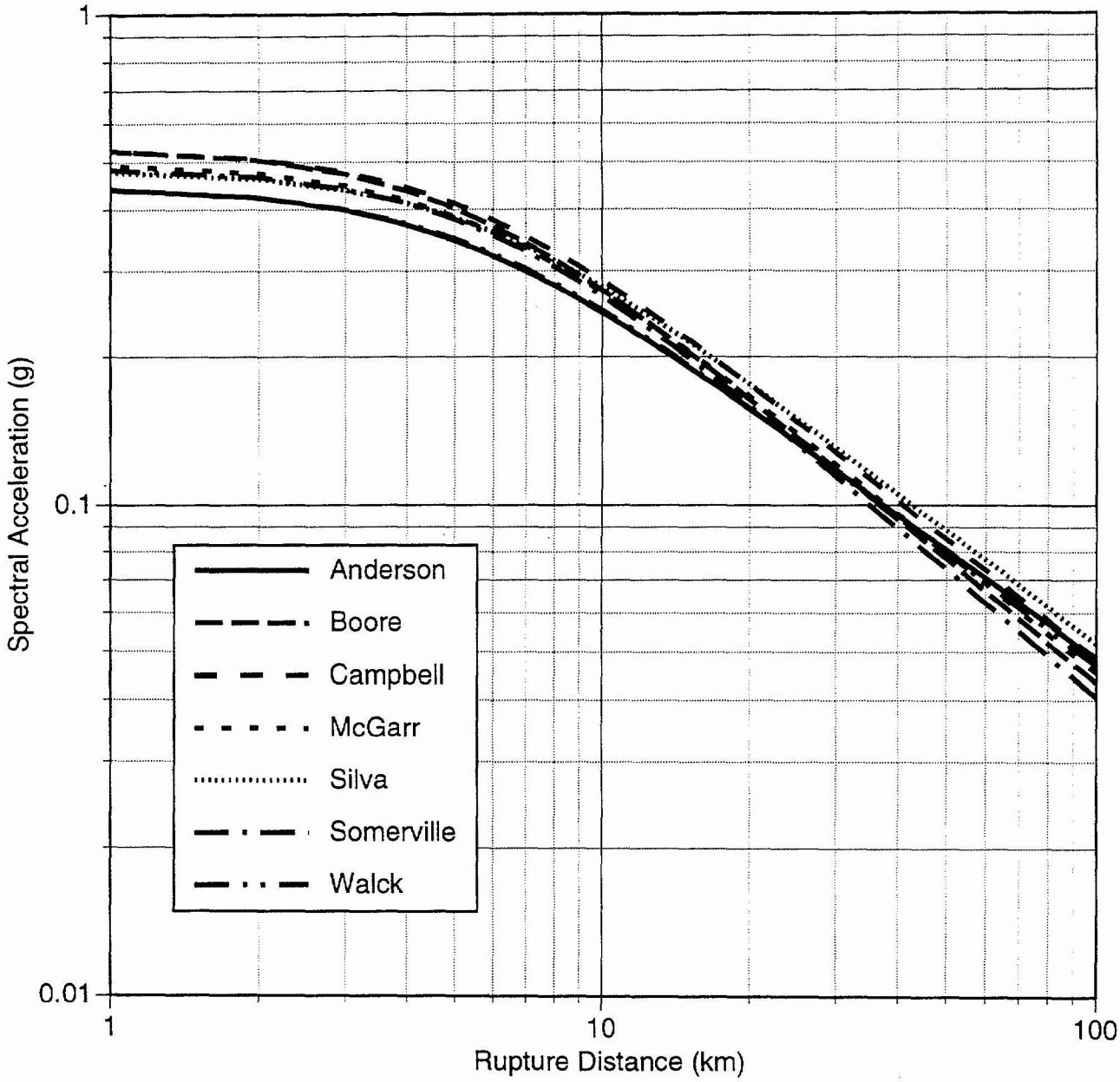

Figure 6-4 Comparison of median attenuation of horizontal spectral acceleration (T = 1.0 sec, 5% damping) for M_W 7.5, strike-slip faulting

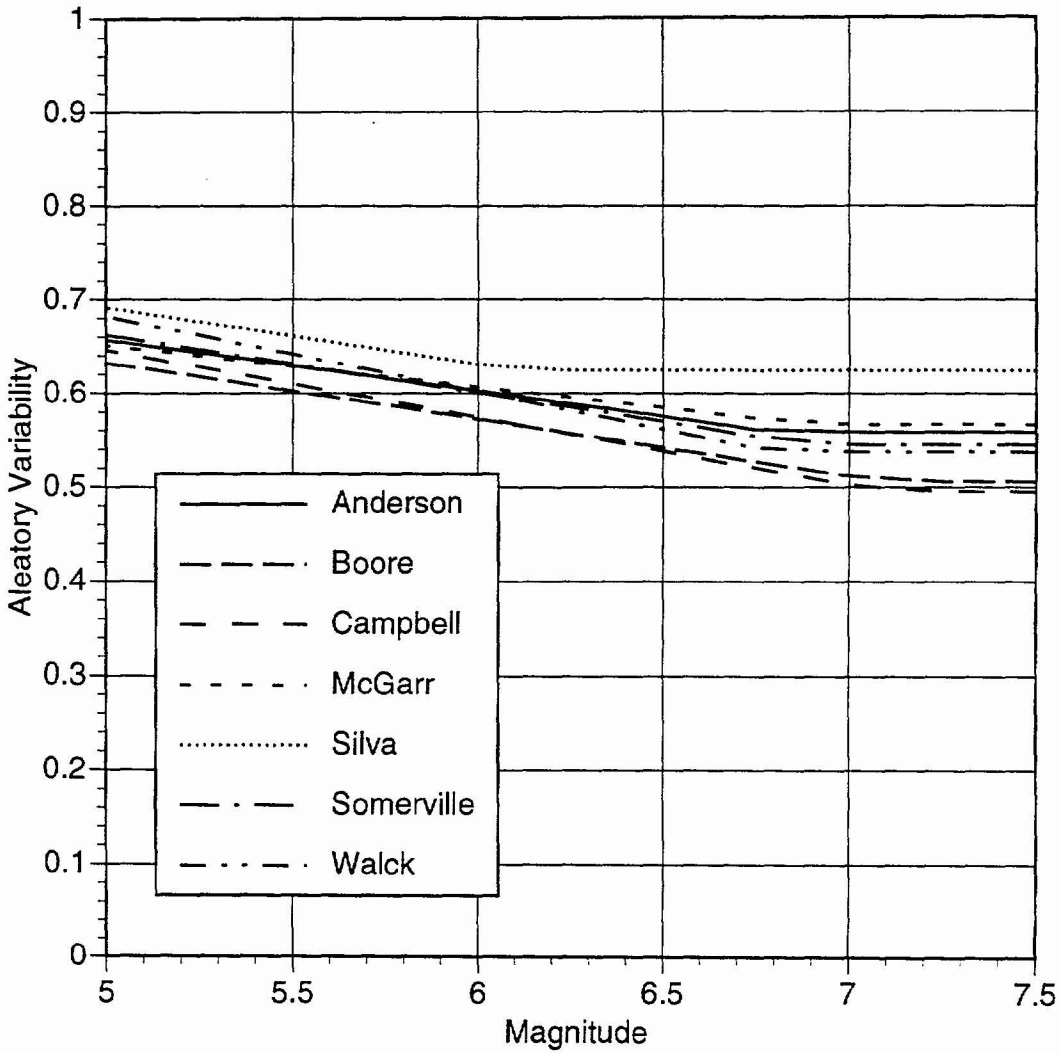

Figure 6-5 Comparison of aleatory variability of horizontal PGA

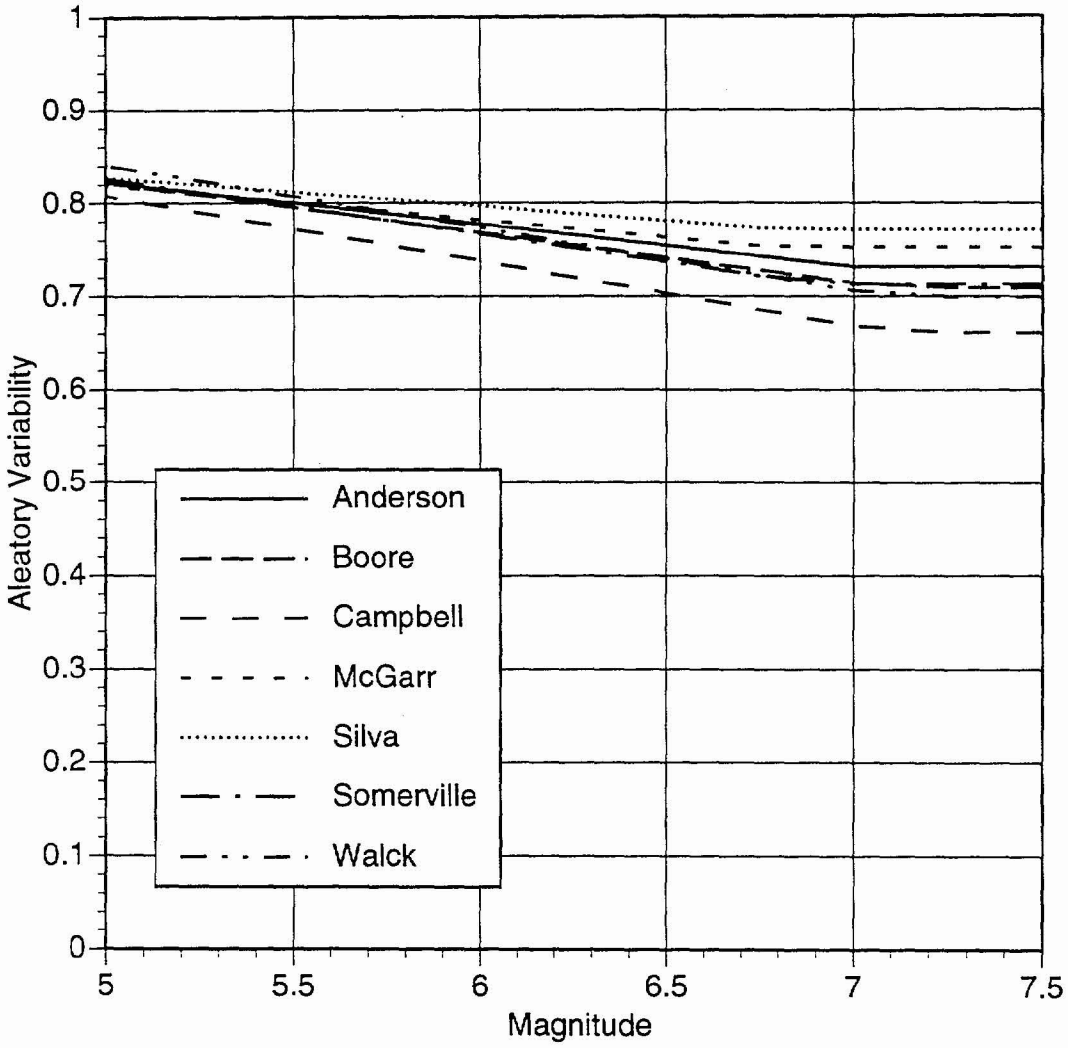

Figure 6-6 Comparison of aleatory variability of 1.0 sec horizontal spectral acceleration (at 5% damping)

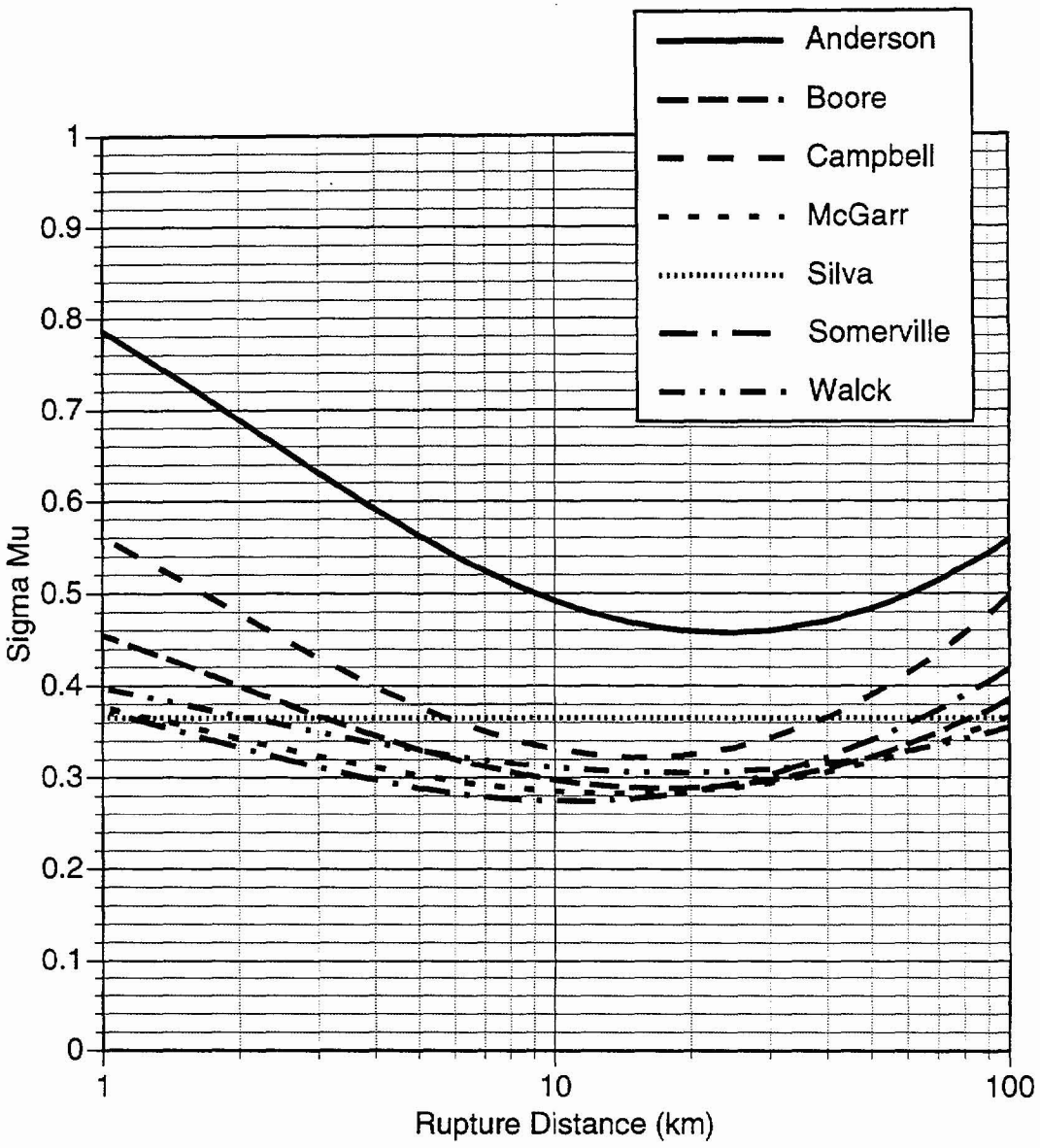

Figure 6-7 Comparison of epistemic uncertainty in the median horizontal PGA for M_W 6.5, normal faulting

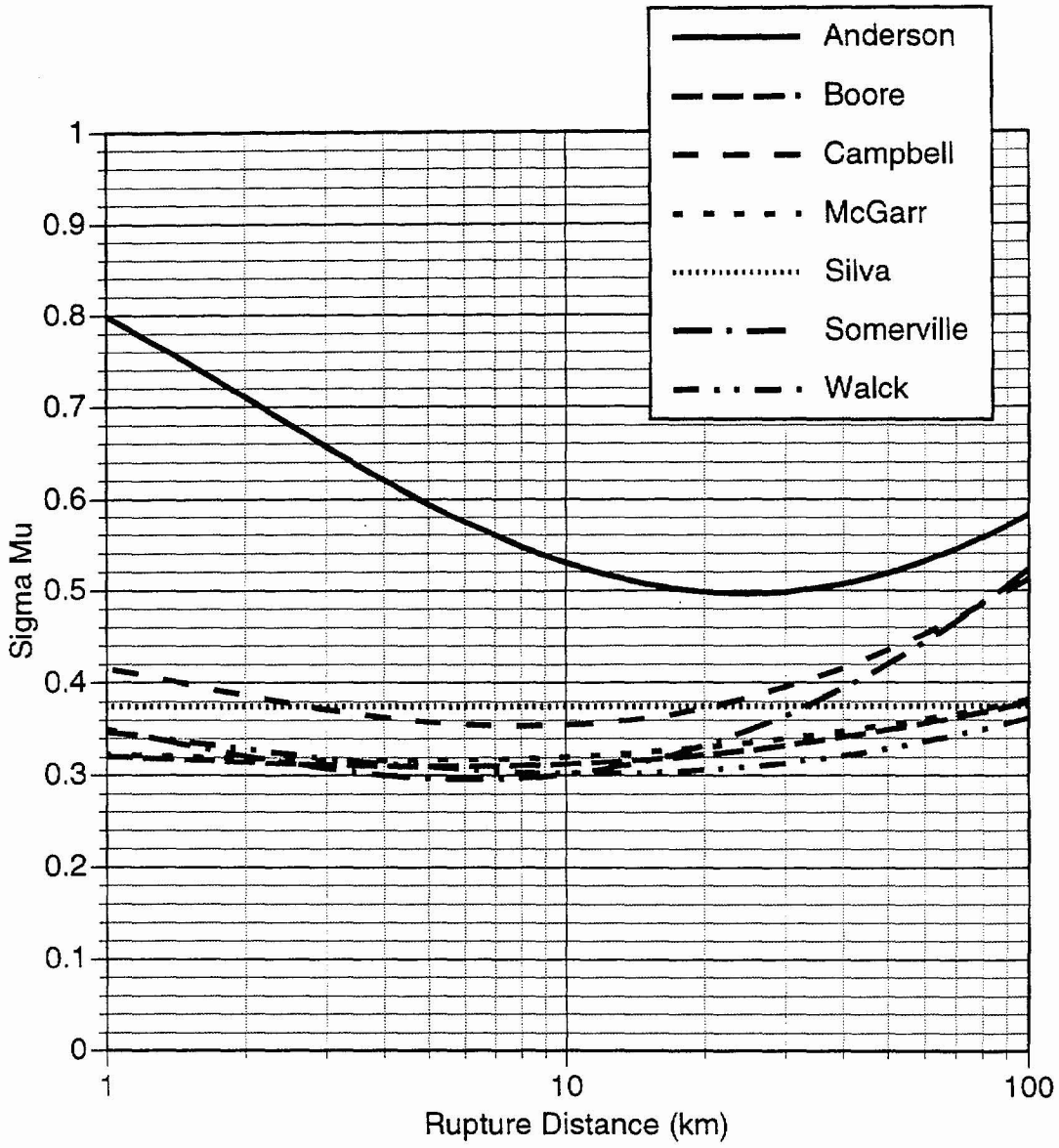

Figure 6-8 Comparison of epistemic uncertainty in the median 1.0 sec horizontal spectral acceleration (at 5% damping) for M_W 6.5, normal faulting

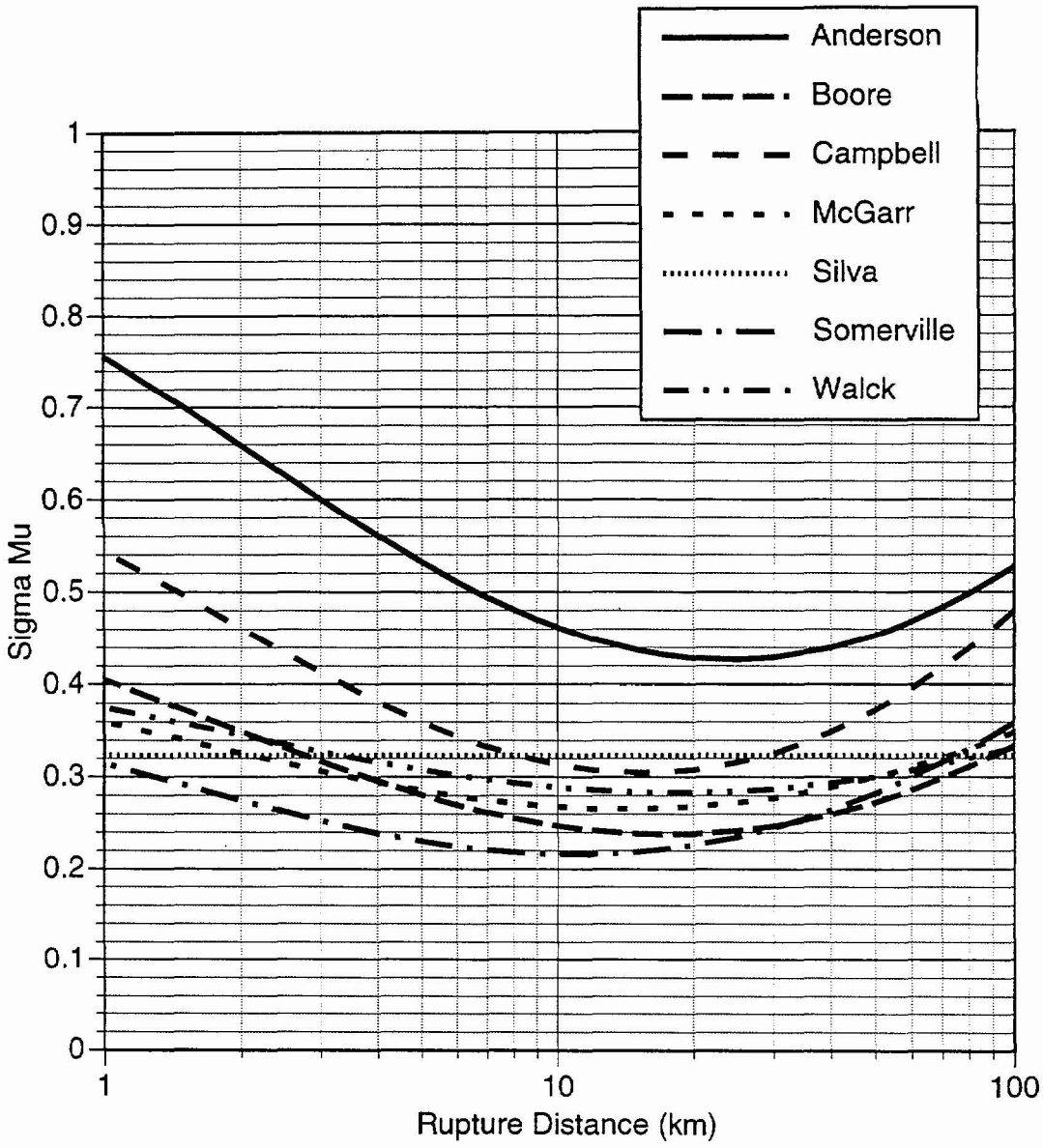

Figure 6-9 Comparison of epistemic uncertainty in the median horizontal PGA for M_W 7.5, normal faulting

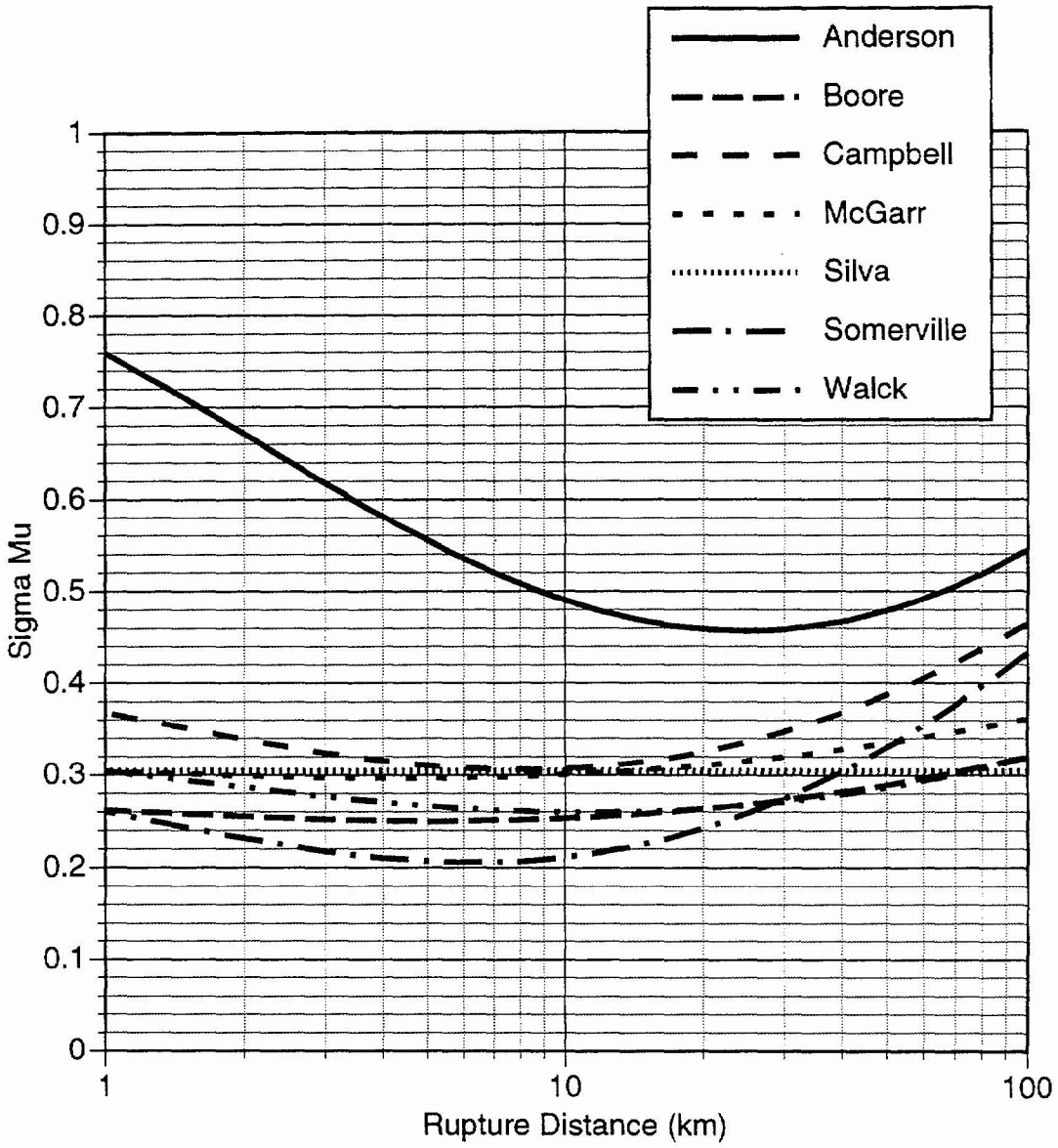

Figure 6-10 Comparison of epistemic uncertainty in the median 1.0 sec horizontal spectral acceleration (at 5% damping) for Mw 7.5, normal faulting

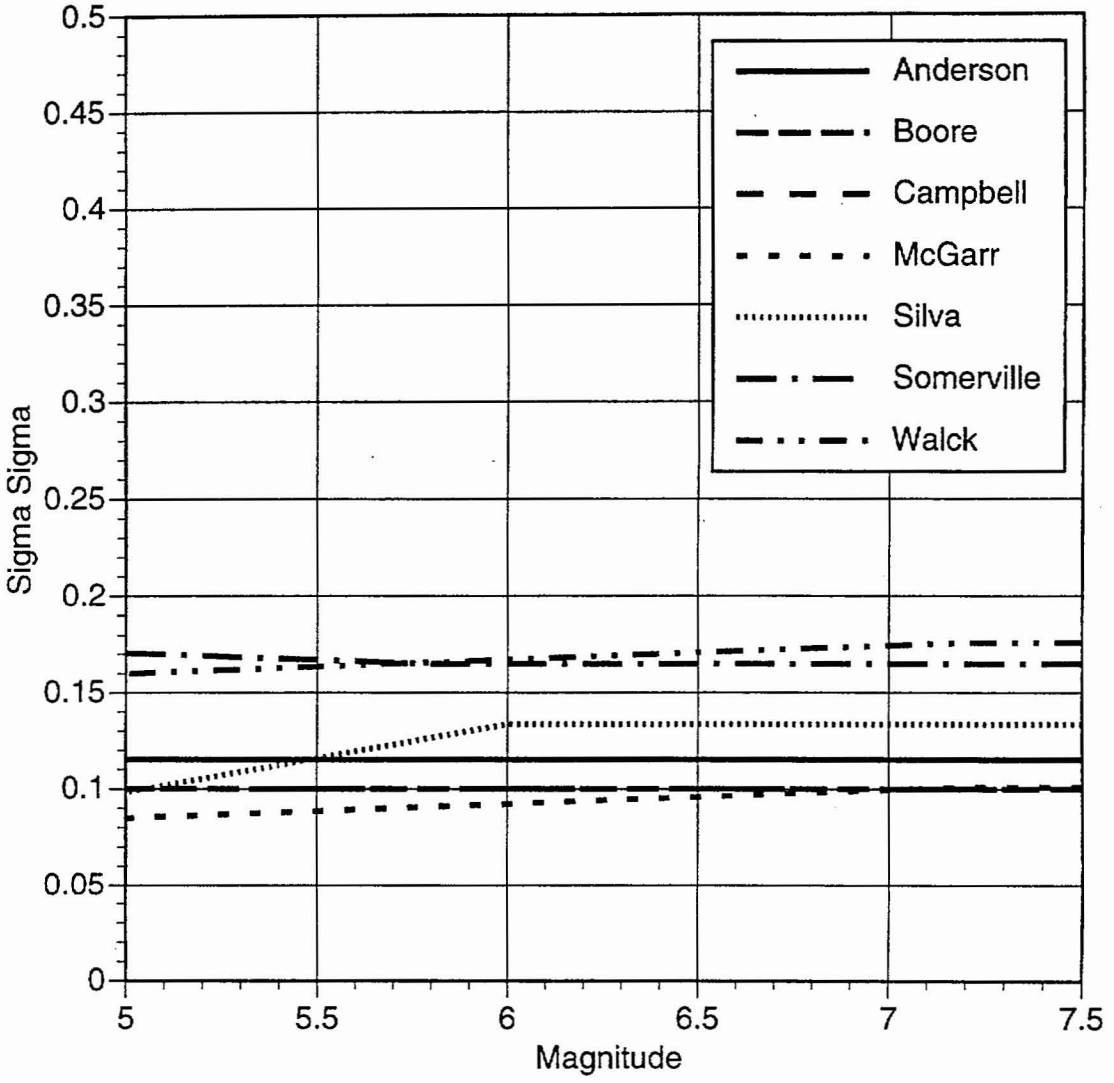

Figure 6-11 Comparison of epistemic uncertainty in the aleatory variability of horizontal PGA.

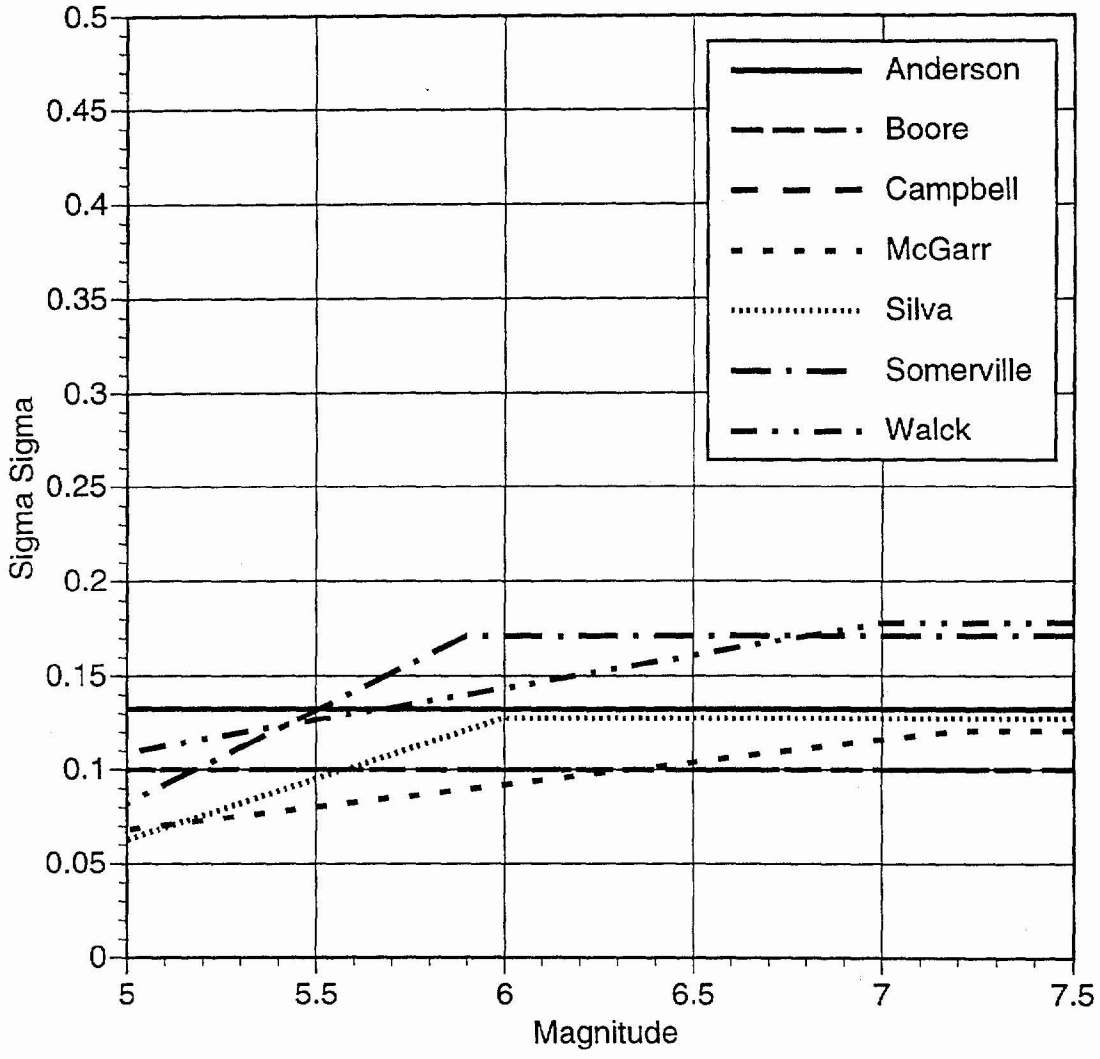

Figure 6-12 Comparison of epistemic uncertainty in the aleatory variability of 1 second horizontal spectral acceleration (5% damping).

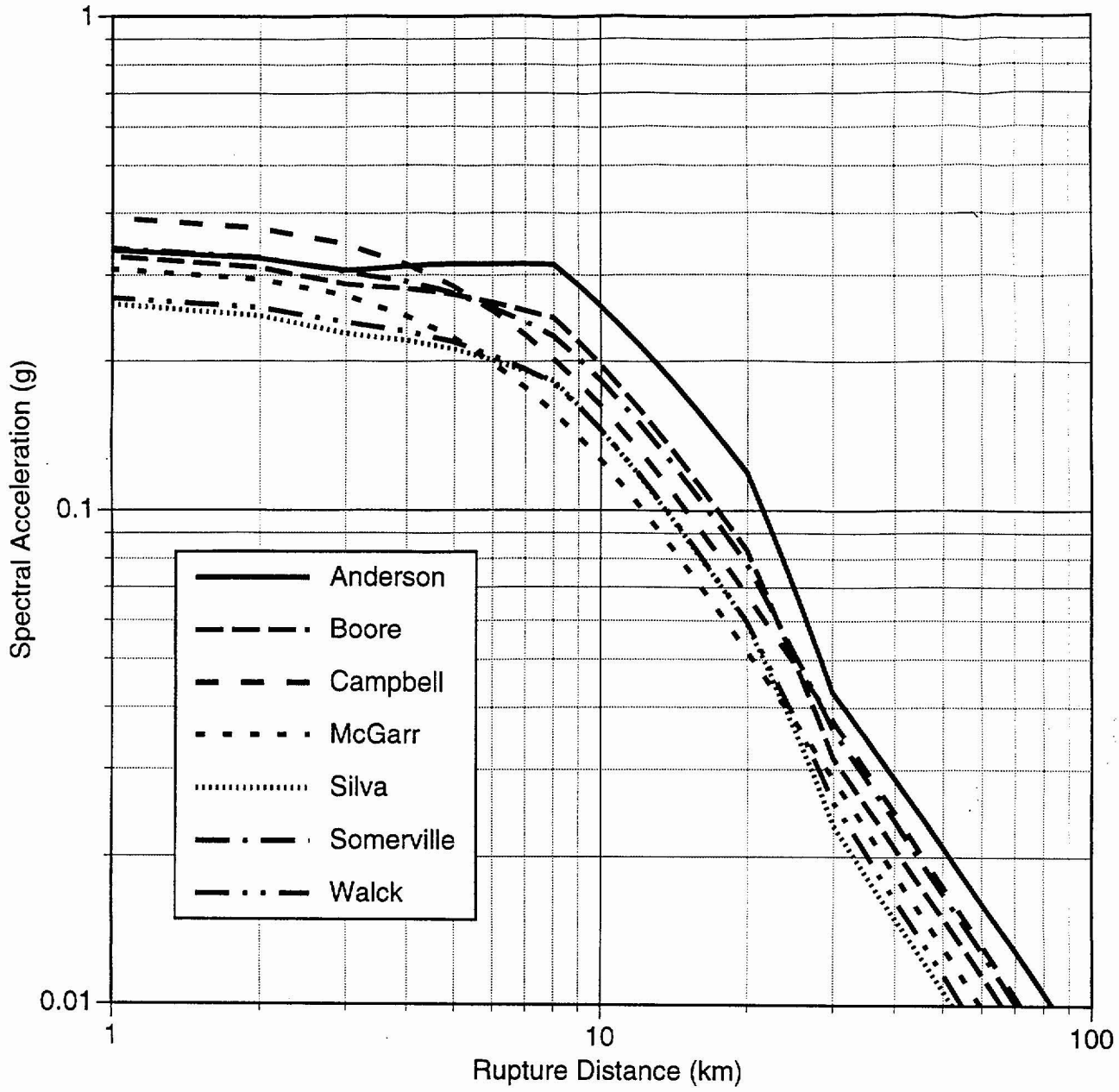

Figure 6-13 Comparison of median attenuation of vertical PGA for M_W 6.5, normal faulting, hanging wall

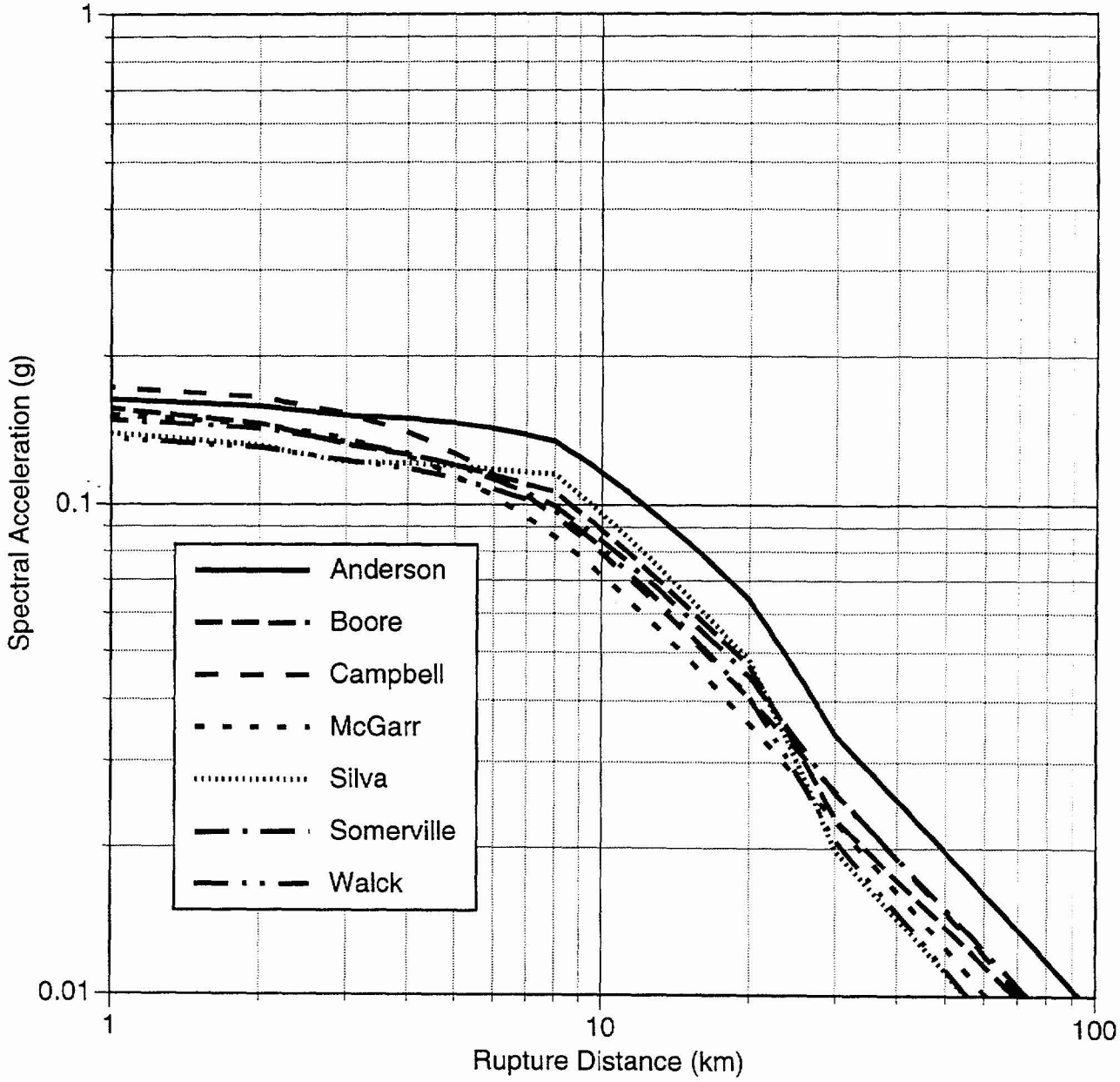

Figure 6-14 Comparison of median attenuation of vertical spectral acceleration (T= 1.0 sec, 5% damping) for M_W 6.5, normal faulting, hanging wall

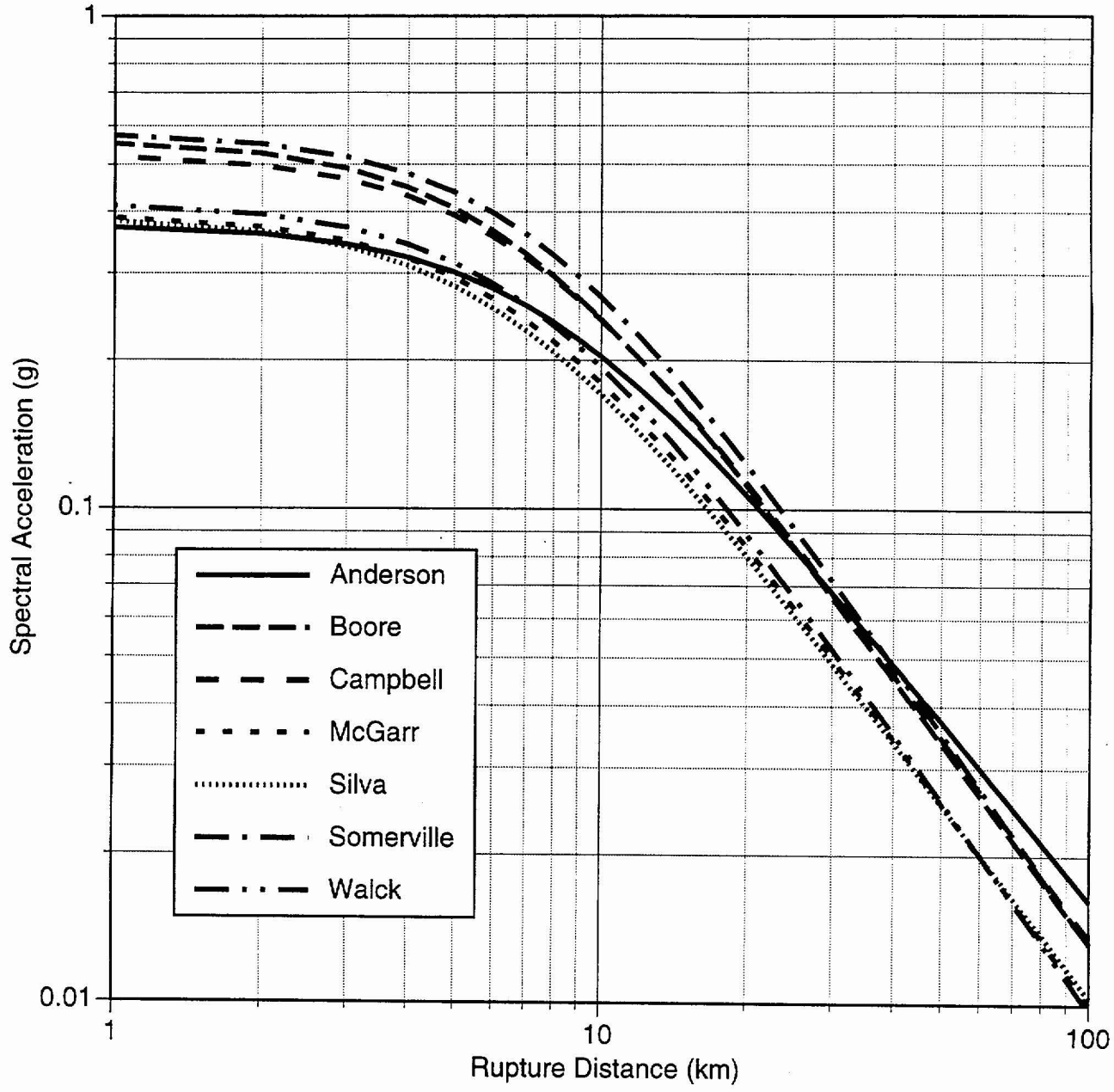

Figure 6-15 Comparison of median attenuation of vertical PGA for M_W 7.5, strike-slip faulting

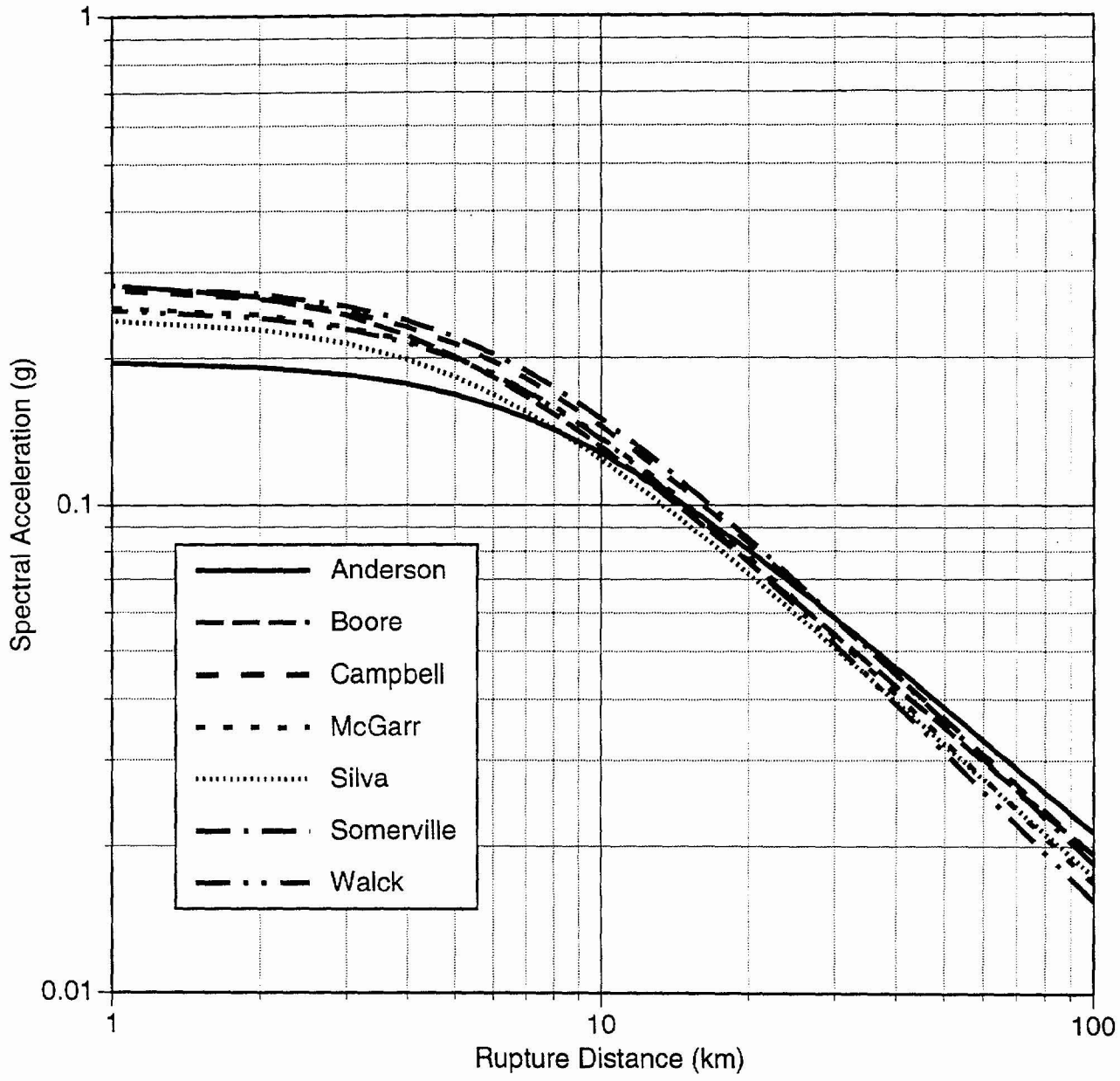

Figure 6-16 Comparison of median attenuation of vertical spectral acceleration (T= 1.0 sec, 5% damping) for M_W 7.5, strike-slip faulting

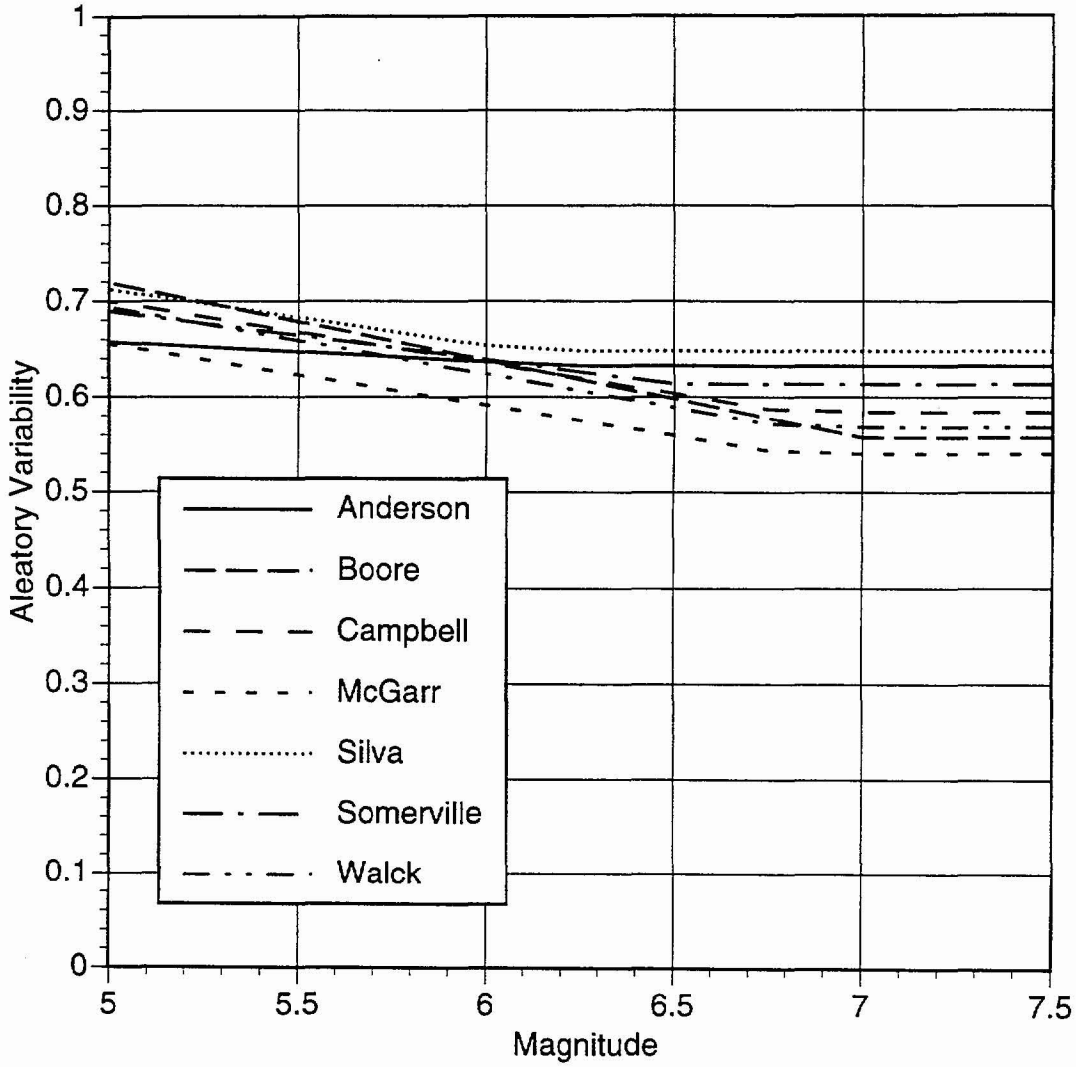

Figure 6-17 Comparison of aleatory variability of vertical PGA

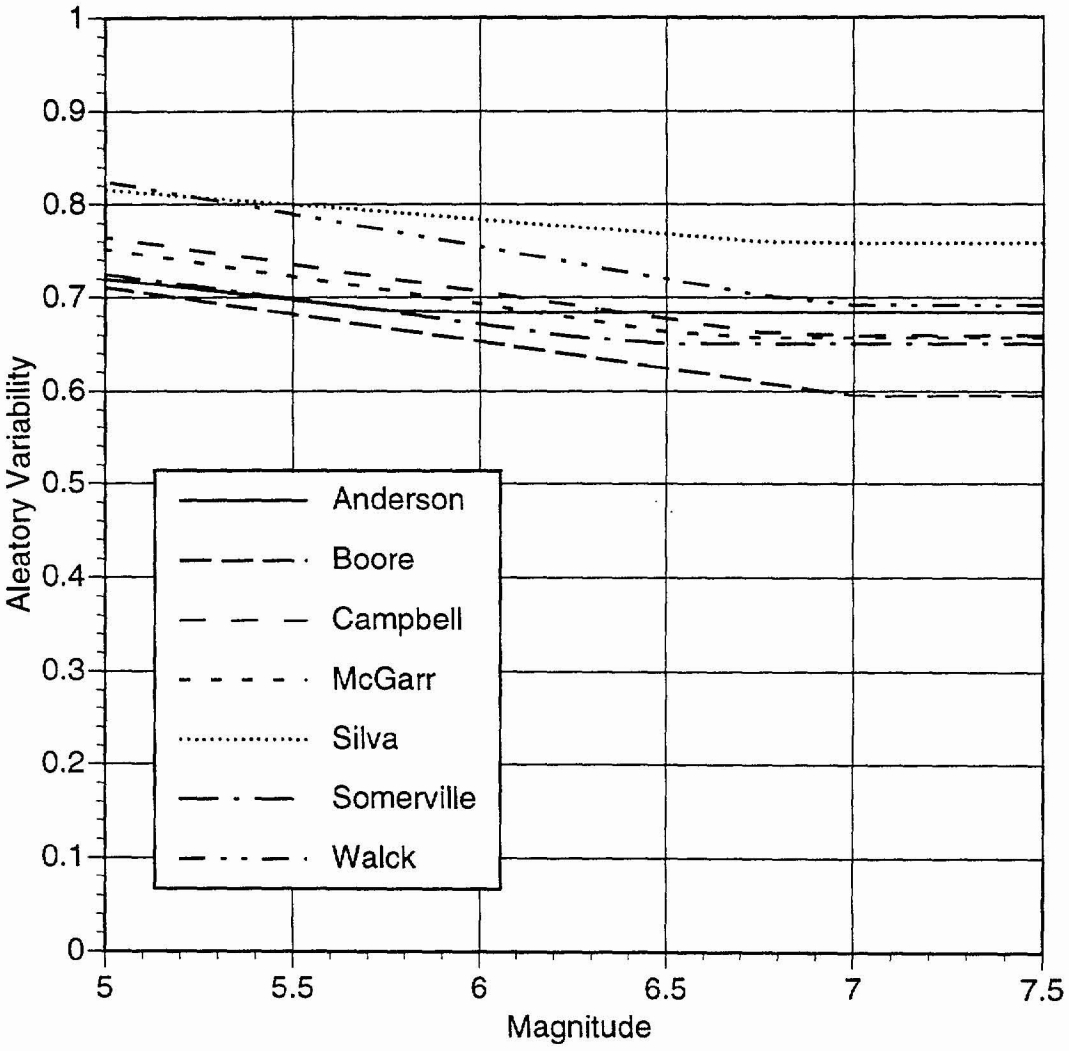

Figure 6-18 Comparison of aleatory variability of 1.0 sec vertical spectral acceleration (at 5% damping)

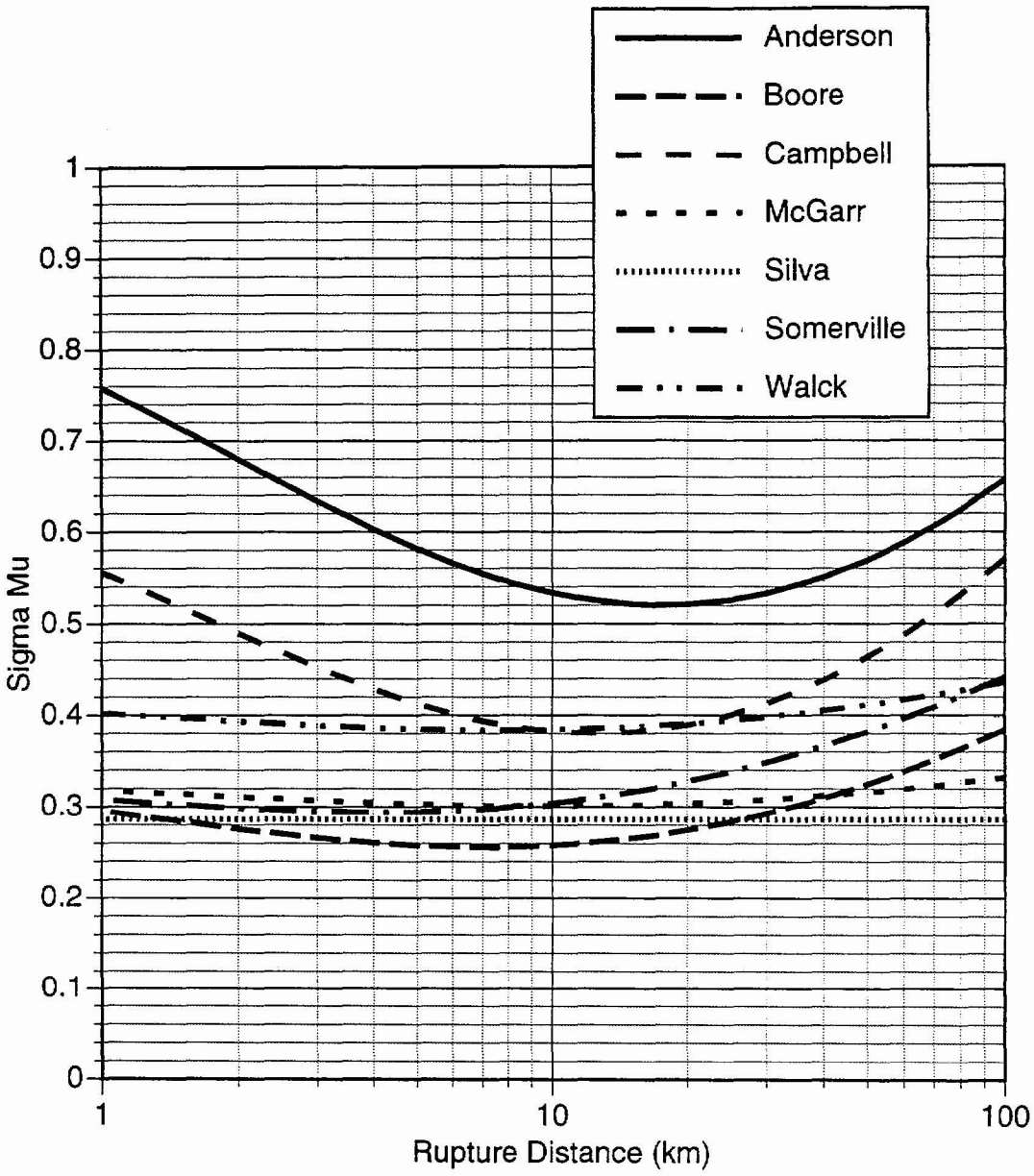

Figure 6-19 Comparison of epistemic uncertainty in the median vertical PGA for M_W 6.5, normal faulting

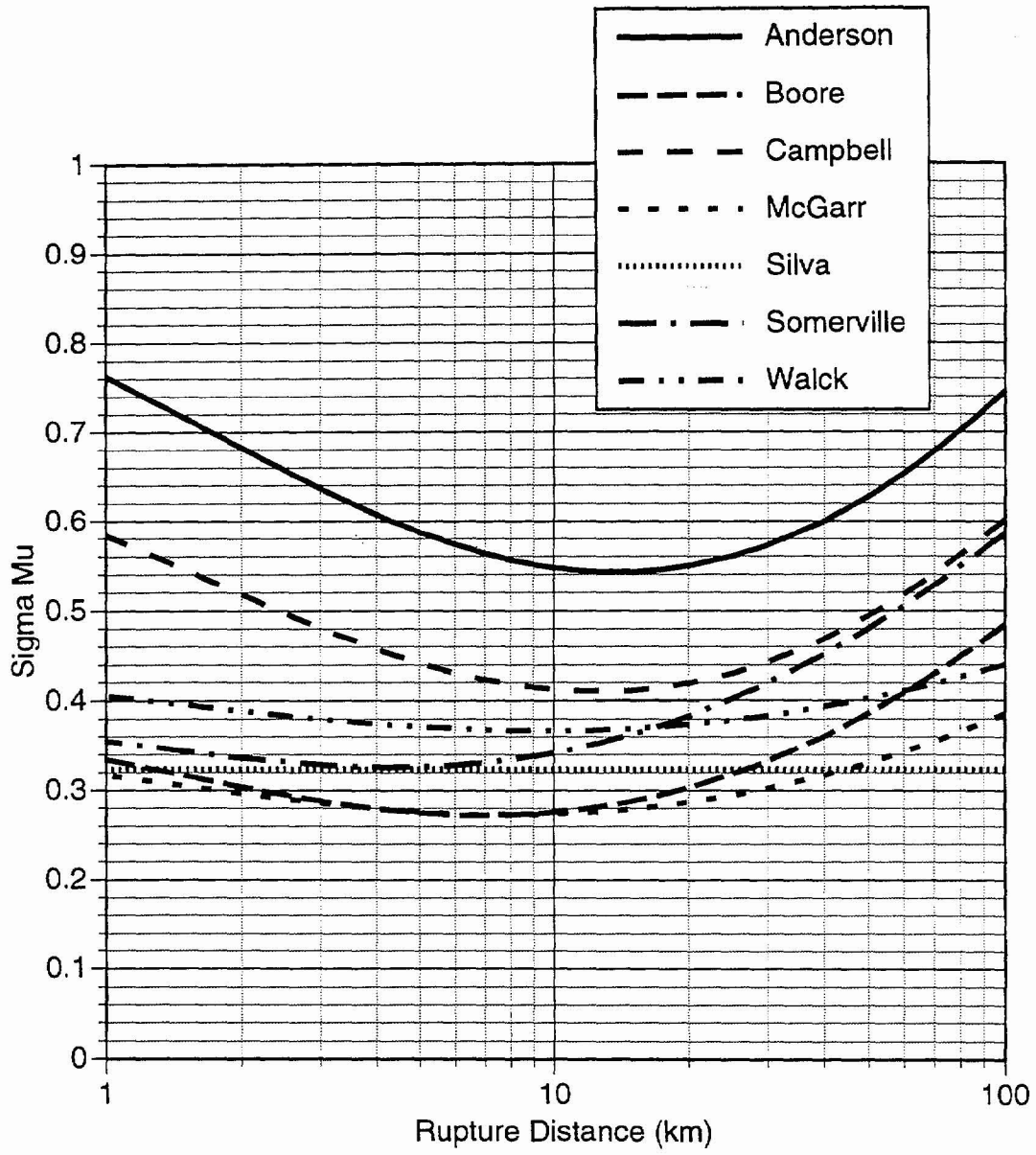

Figure 6-20 Comparison of epistemic uncertainty in the median 1.0 sec vertical spectral acceleration (at 5% damping) for M_w 6.5, normal faulting

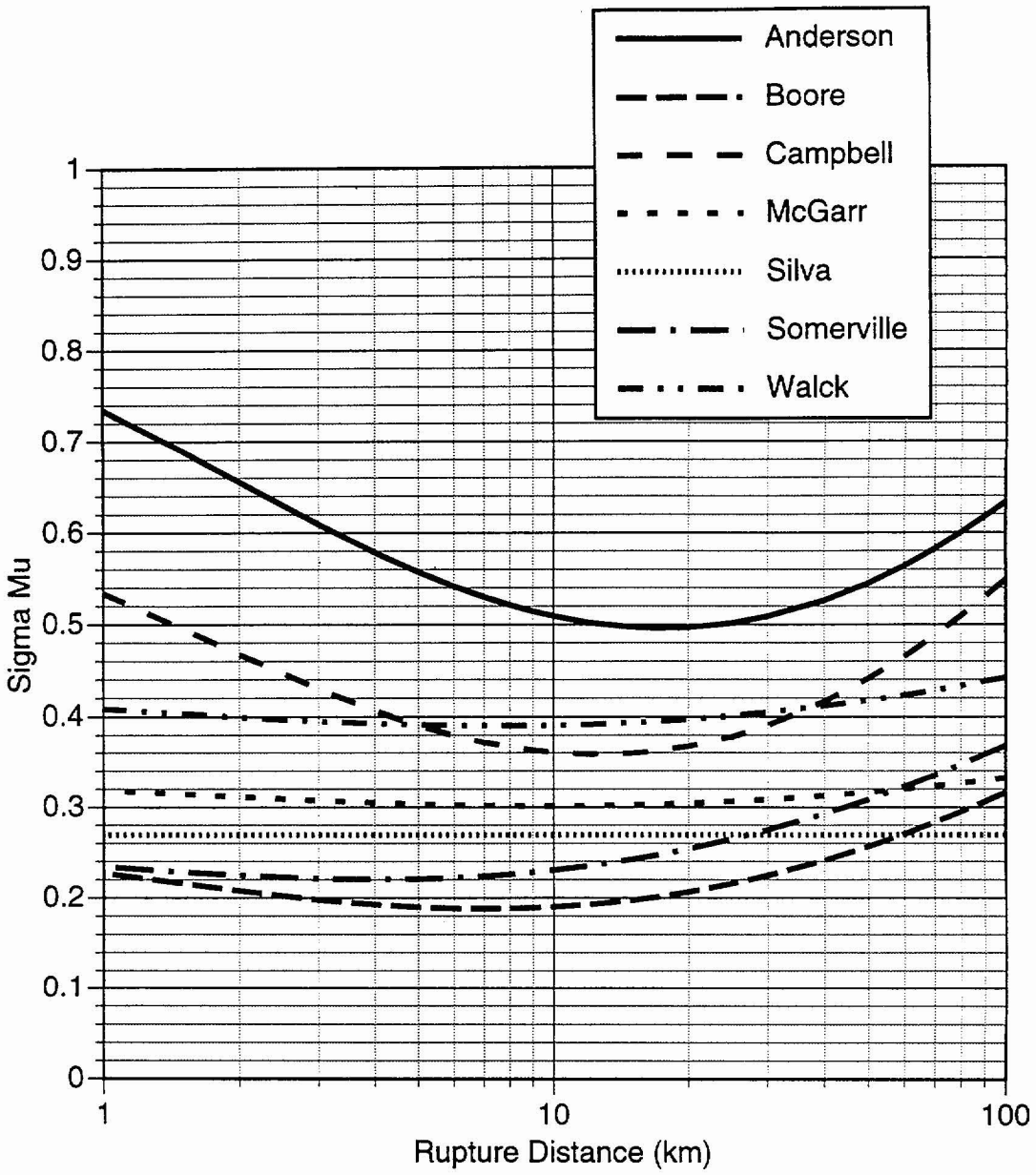

Figure 6-21 Comparison of epistemic uncertainty in the median vertical PGA for M_W 7.5, normal faulting

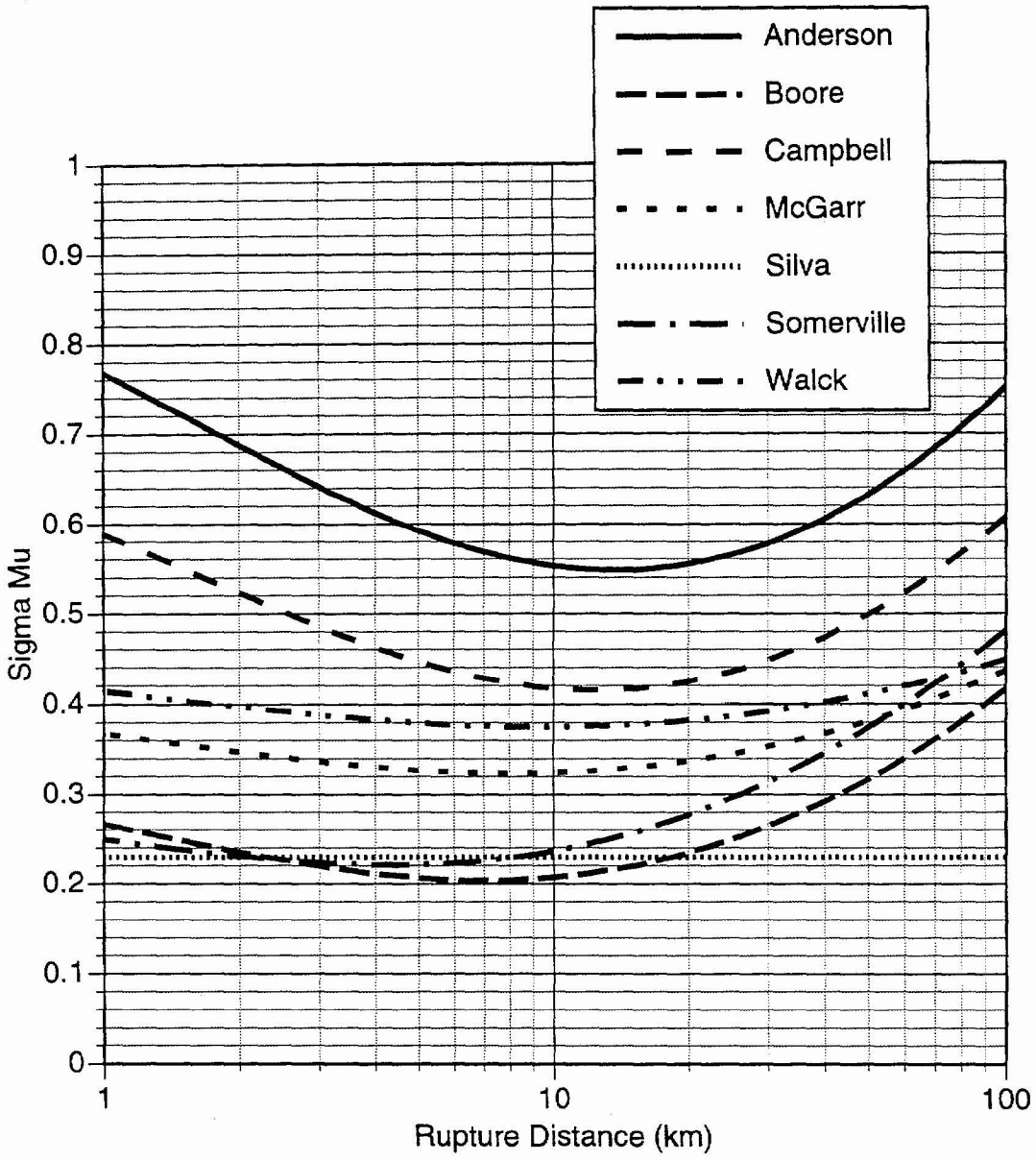

Figure 6-22 Comparison of epistemic uncertainty in the median 1.0 sec vertical spectral acceleration (at 5% damping) for M_W 7.5, normal faulting

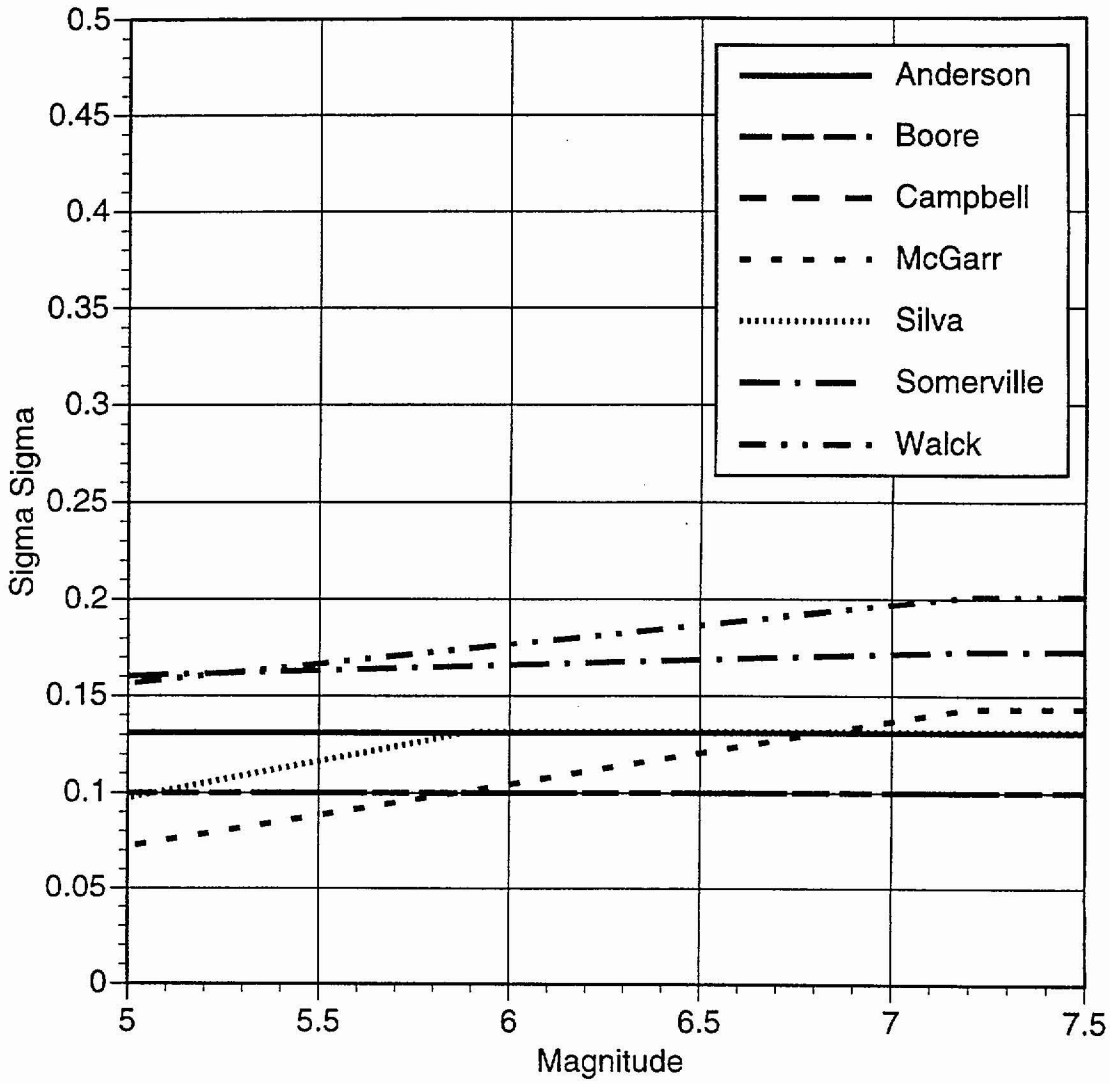

Figure 6-23 Comparison of epistemic uncertainty in the aleatory variability of vertical PGA.

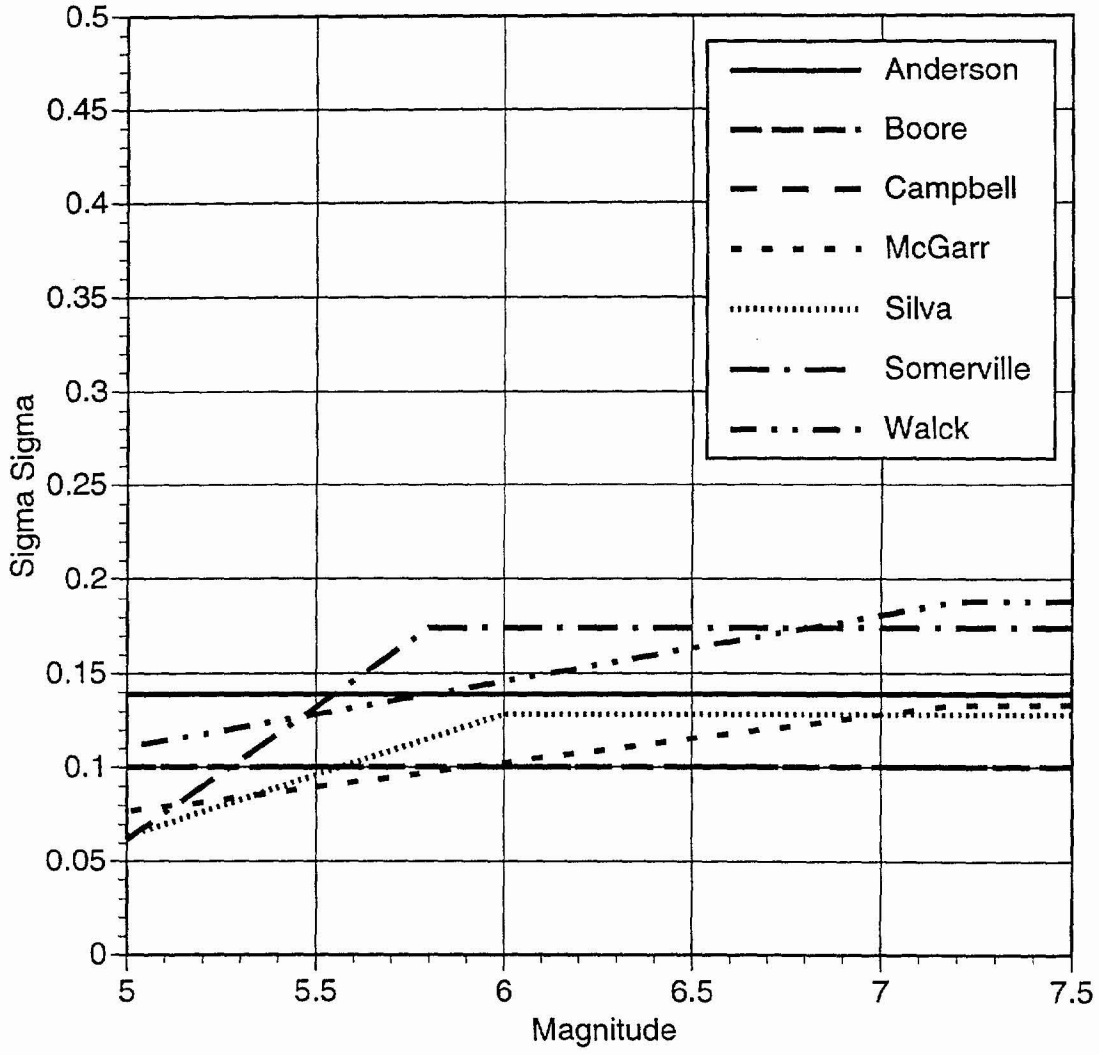

Figure 6-24 Comparison of epistemic uncertainty in the aleatory variability of 1 second vertical spectral acceleration (5% damping).

7.0
PSHA METHODOLOGY AND RESULTS FOR GROUND MOTION HAZARD

This chapter describes the methodology used to perform the PSHA for vibratory ground motion and the resulting calculations for the Yucca Mountain site. Section 7.1 provides an overview of the PSHA approach and introduces some key terms. Section 7.2 provides details about the implementation of the PSHA methodology specifically for the Yucca Mountain site. Section 7.3 presents the seismic hazard results, integrated over all SSFD expert teams and GM experts. Section 7.4 presents sensitivity results divided into three parts: Section 7.4.1, a comparison of hazard results across SSFD expert teams; Section 7.4.2, sensitivity to the alternative models formulated by each SSFD expert team; and Section 7.4.3, sensitivity to GM experts.

The hazard was calculated for reference rock outcrop (Figure 1-1) at the center of the potential repository block between the Solitario Canyon and Ghost Dance faults. The site coordinates are UTM 547.953 km easting, 4077.750 km northing.

7.1 BASIC PSHA MODEL

The methodology to calculate the probabilistic ground motion hazard at a site is well established in the literature (Cornell, 1968, 1971; McGuire, 1976, 1978). Calculation of the hazard requires specification of the following three inputs:

- The geometry of a seismic source (e.g., source i) relative to the site, and a relationship between rupture size and magnitude determine the conditional probability distribution of distance r from the earthquake rupture to the site (given magnitude): $f_{R(i)|M(i)}(r,m)$. The types of sources are faults and areal source zones.

- The mean annual rate of occurrence ν_i and magnitude distribution $f_{M(i)}(m)$ of earthquakes occurring on each source i. This characterization includes the M_{max} that a seismic source can produce. The M_w scale is used in all the final hazard calculations.

- An attenuation relation for the estimation of ground motion amplitude (e.g., peak ground acceleration [PGA] or spectral acceleration) at the site as a function of earthquake magnitude and distance. This characterization includes both an equation for the median amplitude and a standard deviation σ that describes the site-to-site and event-to-event scatter in ground motion amplitude observations for the same magnitude and distance.

These inputs are illustrated on Figure 7-1, Parts a through c. Figure 7-1a shows the geometry of a seismic source and the distance distribution for a given value of magnitude. The distribution of magnitude $f_{M(i)}(m)$ for an areal source is typically specified as the doubly truncated exponential distribution. Seismicity for a source with the exponential magnitude distribution is completely specified by the minimum magnitude m_o and parameters a and b. Parameter a is a measure of seismic activity, b is a measure of relative frequency of large versus small events, and $\log[\nu_i f_{M(i)}(m)]$ is proportional to $-bm$ for $m \leq m_{max}$. Except for truncation effects near M_{max}, this is the well-known Gutenberg-Richter relation. The distribution of magnitude $f_{M(i)}(m)$ for a fault is specified by an exponential distribution, a characteristic distribution (Youngs and Coppersmith, 1985, as illustrated on Figure 2-1b), or a maximum-moment distribution (Wesnousky *et al.*, 1983). The rate information for these three distribution shapes may be specified, respectively, as the rate ν_i, the rate of large earthquakes (magnitude greater than M_{max} - ½), or the slip rate (for faults only).

The ground motion is modeled by an attenuation function, as illustrated on Figure 7-1c. Attenuation functions are usually of the form $ln[A] = f(M,R) + \varepsilon$, where A is ground motion amplitude, M is magnitude, R is distance, and ε is a random variable (with mean zero and standard deviation σ) that represents scatter in $ln[A]$ for the same magnitude and distance. The attenuation function is used to calculate $G_{A|m,r}(a^*) = P[A > a^*|m,r]$: the probability that the ground motion amplitude A is larger than a^*, for a given M and R. The seismic hazard over all sources is calculated as a summation:

$$v(a^*) = \sum_i \nu_i \iint_r G_{A*m,r}(a^*)\, f_{M(i)}(m) f_{R(i)|M(i)}\, dm\, dr \qquad (7\text{-}1)$$

in which $\nu(a^*)$ is the annual rate of earthquakes that produce amplitudes $A > a^*$ at the site, and the summation is performed over all seismic sources i. The integration on magnitude in Equation 7-1 considers only earthquakes with magnitudes greater than a minimum magnitude m_o, typically taken as M_w 5. Smaller earthquakes are assumed to produce no damage to engineered structures, regardless of the ground motion amplitudes they generate. Thus, both ν and $f_{M(i)}(m)$ are only specified for magnitudes greater than m_o, although smaller magnitudes are considered in the determination of the rate and magnitude distribution.

Equation 7-1 is formulated using the assumption that earthquakes (most particularly, successive earthquakes) are independent in size and location. In all seismic hazard applications, primary interest is focused on computing probabilities for the occurrence of high (rare) ground motions (as a result, the probability of two exceedances in 1 year is negligible). Thus, the quantity on the right side of Equation 7-1, which is the annual rate of earthquakes with amplitude $A > a^*$, is a very good approximation to the probability of exceeding amplitude a^* in one year.

The calculation of hazard from all sources is performed for multiple values of a^*. The result is a hazard curve, which gives the annual probability of exceedance as a function of a^*. This calculation is performed for multiple measures of ground motion amplitude (i.e., PGA and spectral acceleration at multiple frequencies).

7.1.1 Treatment of Uncertainty

The most recent PSHA studies distinguish between two types of uncertainty, namely epistemic and aleatory. Aleatory uncertainty (sometimes called randomness) is probabilistic variability that results from natural physical processes. The size, location, and time of the next earthquake on a fault and the details of the ground motion are examples of quantities considered aleatory. In current practice, these quantities cannot be predicted, even with the collection of additional data. Thus, the aleatory component of uncertainty is irreducible. The second category of uncertainty is epistemic (sometimes called simply uncertainty), which results from imperfect knowledge about earthquakes and their effects. An example of epistemic uncertainty is the shape of the magnitude distribution for a given seismic source. In principle, this uncertainty can be reduced with advances in knowledge and the collection of additional data.

These two types of uncertainty are treated differently in advanced PSHA studies. Integration is carried out over aleatory uncertainties to get a single hazard curve (see Equation 7-1), whereas epistemic uncertainties are expressed by incorporating multiple assumptions, hypotheses, models, or parameter values. These multiple interpretations are propagated through the analysis, resulting in a suite of hazard curves and their associated weights. Results are presented as curves showing statistical summaries (e.g., mean, median, fractiles) of the exceedance probability for each ground motion amplitude. The mean and median hazard curves convey the central tendency of the calculated exceedance probabilities. The separation among fractile curves conveys the net effect of epistemic uncertainty about the source characteristics and ground motion prediction on the calculated exceedance probability.

Epistemic uncertainties are associated with each of the three inputs to the seismic-hazard evaluation. The seismogenic potential of faults and other geologic features is uncertain, as a result of (1) uncertainty about the tectonic regime operating in the region and (2) incomplete knowledge of these geological features. The geometry of these geologic features is also uncertain. Uncertainty in the rate of seismicity is generally divided into uncertainty in M_{max}, uncertainty in the type of magnitude distribution, uncertainty in the rate parameter (i.e., activity rate, rate of large events, or slip rate), and uncertainty in b or other shape parameters of the magnitude distribution $f_{M(i)}(m)$. Finally, the attenuation functions are uncertain, which arises from uncertainty about the dynamic characteristics (source, path, and site effects) of earthquake ground motions in the vicinity of Yucca Mountain. This uncertainty is large because few strong motions have been recorded in the region. Uncertainties in seismic source characterization and ground motion attenuation relations were quantified by considering inputs from six SSFD expert teams and seven GM experts, and by each team's and expert's own assessment of uncertainty.

That is, each SSFD expert team formulated multiple alternative interpretations about the seismogenic characteristics of potential seismic sources, and assigned weights to these hypotheses according to their credibility given the current state of knowledge and the degree to which they are supported by data. Each GM expert applied a similar procedure to alternative interpretations about the source, path, and site characteristics affecting ground motions. The development of these seismic source and ground motion interpretations was described previously in Chapters 4.0, 5.0, and 6.0.

7.2 IMPLEMENTATION OF METHODOLOGY IN THIS STUDY

This section describes the PSHA calculation methodology in more detail, with emphasis on methodological developments that were introduced to represent the specific conditions at Yucca Mountain.

7.2.1 Fault Sources

Fault sources were modeled as planar features and their geometry was represented in three dimensions by a fault trace, a dip angle, and minimum and maximum depths. Earthquakes occurring on these faults are treated as having finite, magnitude-dependent length and width, which are calculated using the Wells and Coppersmith (1994) relationship for subsurface rupture length (all fault types).

Due to the presence of closely spaced parallel local faults, all of the SSFD expert teams included scenarios in which ruptures occur simultaneously on two or more of these faults. The teams specified these seismic sources by indicating the associated faults, their occurrence or slip rates, and their magnitude distributions.

The ASM, RYA, SBK, and SDO expert teams specified the multiple-rupture scenarios as having magnitudes comparable to their M_{max} (i.e., these scenarios have maximum-moment magnitude distributions) and always rupturing all the faults involved. Smaller events on these faults are only considered as part of the respective individual sources, which are not mutually exclusive from the multiple-rupture sources.

The AAR and DFS expert teams specified the multiple-rupture sources as having exponential or characteristic magnitude distributions and being capable of single- as well as multiple-rupture events, depending on their magnitude. Each team specified the range of magnitudes associated with ruptures on one fault, two faults, three faults, etc., for each multiple-rupture scenario. These multiple-rupture sources are therefore mutually exclusive from the corresponding single-rupture fault sources.

For events with multiple ruptures, the rupture length and width on each fault are calculated as $L\ n^{-\alpha}$ and $Wn^{-\alpha}$, respectively, where L is the single-rupture length and W is the single-rupture width given by Wells and Coppersmith (1994), and n is the number of simultaneous ruptures. This equation arises from the assumption that the seismic moment of the multiple-rupture event is divided equally among the various faults and that the stress drop is constant across ruptures and is the same for single-rupture and multiple-rupture events.

The SSFD expert teams specified which simultaneous-rupture sources should be treated as multiple ruptures for the purposes of ground motion evaluation (see below), and which should be treated as single rupture plane events.

The GM experts parameterized ground motion amplitude from multiple-rupture events as a function of the total magnitude of the event, the distance to the closest rupture, and the number of faults that rupture simultaneously. According to some of their interpretations, multiple ruptures affect not only the median amplitude, but also the aleatory and/or the epistemic standard deviations (Section 6.4.1).

7.2.2 Areal Source Zones

Areal source zones are defined by a polygon in latitude-longitude space. In most PSHA studies, areal zones are assumed to have uniform activity rate per unit area (EPRI, 1986; USGS, written communication, 1996, constitute notable exceptions). This study allowed for both uniform and variable rates per unit area. Each SSFD expert team specified the approach to use for each areal zone. If they specified variable seismicity, they also specified the degree of smoothing. The teams could also specify that an areal zone could have both uniform and variable seismicity, or multiple degrees of smoothing, by means of alternative branches in the logic tree. The methodology to calculate variable seismicity utilizes the spatial pattern of historical seismicity within the source, as described in Section 4.1.4.1.

Hypocentral depth is considered explicitly in the hazard integration (as part of the calculation of $f_{R(i)|M(i)}(r;m)$ in Equation 7-1). The SSFD expert teams specified the distribution of hypocentral depth, as well as optional values for the minimum and maximum depths. All distributions specified are well represented by normal distributions.

The depth distributions specified by the SSFD expert teams are assumed to apply to small events (with negligible source dimensions) and are modified for the effect of magnitude-dependent rupture dimensions. The approach followed is described in Appendix J and is summarized below.

The down-dip rupture width for a given magnitude is calculated using the corresponding relationship by Wells and Coppersmith (1994) and projected into a vertical width using a typical dip angle of 70 degrees. The vertical location of the hypocenter is taken as uniformly distributed over the lower 75% of the vertical width. Using this distribution, we calculate the probability that a certain hypocentral depth is realizable, for a given magnitude. This is simply the probability that the top of the rupture is below ground, given hypocentral depth and rupture width. Viewed as a function of depth, this probability has the shape of a ramp. The resulting magnitude-dependent depth distribution is obtained by multiplying the small-event magnitude distribution by the magnitude-dependent probability that each depth is realizable, and then normalizing so that the distribution integrates to unity. The resulting distribution forces the hypocenters of larger events to greater depths. Figure 7-2 illustrates this calculation. This distribution is consistent with the depths on Figure 9-11 of S. K. Pezzopane and T. E. Dawson (USGS, written communication, 1996), which shows focal depths as a function of magnitude for events in the Basin and Range Province.

Because the attenuation equations predict amplitude as a function of magnitude and distance to the rupture, a relationship between hypocentral and rupture distance is required. This relationship takes the form of equations for the conditional mean and standard deviation of rupture distance given magnitude and hypocentral distance (Appendix J). The effect of the conditional standard deviation in rupture distance is to make the aleatory uncertainty given hypocentral distance larger than the aleatory uncertainty given rupture distance, as has been observed in the development of empirical attenuation equations (e.g., Campbell, 1981).

7.2.3 Ground Motion Attenuation

Each GM expert characterized epistemic uncertainty in the median amplitude and the ground motion scatter by means of standard deviations σ_μ and σ_σ, respectively. For the purposes of the PSHA calculations, it is necessary to represent these uncertainties as discrete values of the associated "epistemic" variables ε_μ and ε_σ. Following EPRI (1993) and Toro *et al.* (1997),

ε_μ was discretized into four points at locations $\pm\ 0.74\,\sigma_\mu$ (weight 0.454) and $\pm 2.33\,\sigma_\mu$ (weight 0.0454) (Figure 7-3). The variable ε_σ was discretized conditionally on σ_μ, as follows. For $\varepsilon_\mu = \pm\ 0.74\,\sigma_\mu$, ε_σ was discretized into three points at 0 (weight 2/3) and $\pm\ 1.73\ \sigma_\sigma$ (weight 1/6 each). For $\varepsilon_\mu = \pm\, 2.33\,\sigma_\mu$, ε_σ was discretized into two points at $\pm 1\,\sigma_\sigma$ (weight 0.5 each). Each combination of ε_μ and ε_σ is treated as one attenuation equation in the PSHA calculations. The resulting total number of attenuation equations for all seven experts is 70.

7.2.4 Calculations

Hazard calculations for vibratory ground motions for a single SSFD expert team proceeded in two steps, as follows:

1. Calculation of seismic hazard from each individual source: This calculation was performed for each combination of attenuation equation and seismic source parameters resulting in one hazard curve and one weight for each combination.

2. Calculation of total hazard (i.e., the hazard from all seismic sources) and its epistemic uncertainty. For the calculation of quantities other than the mean hazard, this calculation takes into account the probabilistic dependence introduced by hypotheses in the logic tree that affect more than one source. This calculation considers each possible branch of the overall logic tree (which includes attenuation equations as well as seismic source characteristics). The hazard associated with one branch of the logic tree includes only those sources that are active given that branch and only those source parameters that are consistent with that branch. The result of this calculation is a set of mean and fractile hazard curves. (We compute 11 fractiles in order to carry distribution-shape information into the integration step below.)

Calculation of the integrated hazard (across all SSFD expert teams) was performed by combining the expert teams' mean and fractile hazard curves, giving each team equal weight. The result is a set of integrated mean and fractile hazard curves.

In addition to these main results, deaggregation results calculate and display the contributions of various magnitude-distance-ε combinations to the mean hazard. This information is required

for the selection of the magnitude-distance-ε combinations to use in seismic design. Furthermore, sensitivity results provide insights into the effect of various parameters and assumptions on the calculated seismic hazard and its uncertainty.

7.3 INTEGRATED RESULTS

The integrated results provide a representation of seismic hazard and its uncertainty at the site, based on the interpretations and parameters developed by the six SSFD expert teams and seven GM experts. Separate results are obtained for PGA and spectral accelerations at 0.3, 0.5, 1, 2, 5, 10, and 20 Hz. The results for each ground motion measure are in the form of summary hazard curves. Figures 7-4 through 7-6 show the mean and fractile hazard curves for PGA and for 10- and 1-Hz spectral acceleration. Figures 7-7 and 7-8 show the mean and fractile hazard curves for horizontal and vertical PGVs, respectively. The mean and median hazard curves convey the central tendency of the calculated exceedance probabilities. The separation between the 15th and 85th percentile curves conveys the effect of epistemic uncertainty on the calculated exceedance probability. A large portion of this epistemic uncertainty results from epistemic uncertainty in ground motions, as will be shown in Section 7.4.3. Figure 7-9 shows the uniform hazard spectrum (UHS) for 10^{-4} annual exceedance probability, which is calculated from the spectral acceleration hazard curves (PGA is treated as 100-Hz spectral acceleration for these plots).

Figures 7-10 through 7-13 show analogous hazard curves and spectrum for the vertical component of ground motion. Figure 7-14 shows the horizontal and vertical mean UHS for 10^{-4} annual exceedance probability in a tripartite scale. This scale shows the spectrum in terms of spectral acceleration, spectral velocity, and spectral displacement. Table 7-1 lists the mean UHS values and PGV values for 10^{-3} and 10^{-4} annual exceedance probability, and for both horizontal and vertical motions.

Figures 7-15 and 7-16 show the deaggregation of the mean hazard (for 10^{-4} annual exceedance probability) into magnitude-distance-ε bins, where ε is the difference between the logarithm of the ground motion amplitude and the mean logarithm of ground motion (for that M and R) measured in units of the standard deviation σ of log (ground motion). Figure 7-15 indicates that the 5 to 10-Hz ground motions (and other high-frequency motions as well) are dominated by

events of less than M_w 6.5 at distances less than 15 km. In contrast, ground motions at 1 to 2 Hz (and other low-frequency motions as well) contain a sizable contribution from M_w 7 and greater events at distances beyond 50 km. Results in Section 7.4 will show this contribution is primarily from the Death Valley, Furnace Creek, and Fish Lake Valley faults, which have higher M_{max} and much higher activity rates than the local faults.

7.4 SENSITIVITY RESULTS

Sensitivity results provide insights into the effect of various interpretations and parameters on the calculated seismic hazard and its uncertainty. These results provide insight into the PSHA process. They also provide a consistency check for the experts and analysts.

7.4.1 Comparisons Across SSFD Expert Teams

Figures 7-17 through 7-20 compare the mean hazard curves obtained by the six SSFD expert teams, for PGAs and spectral accelerations at 10, 1, and 0.3 Hz. These results show a reasonable degree of consistency among the mean estimates of the expert teams, with less than a factor of three (in annual exceedance probability) between the lowest and the highest teams. This consistency among experts is likely the result of using a large common information base and of having an elicitation and feedback format that minimizes differences in knowledge or understanding among experts.

7.4.2 Sensitivity Results for Each SSFD Expert Team's Interpretations

Several types of sensitivity results are presented in this section for each SSFD expert team. (AAR, Figures 7-21 through 7-52; ASM, Figures 7-53 through 7-80; DFS, Figures 7-81 through 7-104; RYA, Figures 7-105 through 7-132; SBK, Figures 7-133 through 7-158; and SDO, Figures 7-159 through 7-177). Table 7-2 provides a "road map" for these figures, whereas the following text first describes the results generally, then discusses results specifically for each team. The number and type of figures shown vary somewhat between teams, as each team defined different logic trees and different sources.

The most straightforward type of sensitivity results are obtained by deaggregating the calculated mean hazard into contributions by source group, by individual source, or by magnitude-

distance-ε bins. Six figures of this type are first presented for each SSFD expert team (three for 10-Hz and three for 1 Hz), as follows:

1. Mean seismic hazard by source type (i.e., local faults, local areal zones, and regional faults). The local fault type is subdivided into single-rupture and multiple-rupture fault sources. This subdivision is based on whether the single-rupture or multiple-rupture attenuation equations apply to a fault or faults, as specified by the SSFD expert team. (Recall that the expert teams specified that the multiple-rupture attenuation equations are applicable to some, but not all, the multiple-rupture fault sources.)

2. Dominant seismic sources, based on their contribution to seismic hazard at 1.1g (for 10 Hz) and at 0.5g (for 1 Hz). Each source is labeled to indicate its type.

3. Magnitude-distance-ε deaggregation of the mean hazard for each source type.

Note two important considerations when examining the figures showing dominant sources. First, the contributions shown on these figures are mean contributions. Thus, the contribution of a source may be written as

$$P\,[\text{Source is Active}] \times \text{Mean Hazard given that the Source is Active}$$

Therefore, a source that can produce a high hazard (if active), but with a low probability of activity, will not necessarily show as having a high contribution to the mean hazard. The importance of this source may be seen in the sensitivity to the logic tree branch that controls whether the source is active. Second, the definition of a "source" for the purposes of this and other figures has some limitations. Consider the Solitario Canyon fault as an example and assume that the SSFD expert team is certain that the fault is active. The Solitario Canyon fault may appear by itself in some branches of the logic tree and also as part of a multiple-rupture source in other branches. These and other figures show separate contributions from Solitario Canyon fault (alone) and from the multiple-rupture source.

Next, sensitivity results with respect to interpretations or parameters are presented separately for a variety of seismic sources. They show the effect of each interpretation or parameter on the

calculated seismic hazard from that type of source. Results for the local faults and areal source zones are shown for 10 Hz; results for the regional faults are shown for 1 Hz because these faults are important only at low frequencies. Sensitivities to all global interpretations and parameters (i.e., those that affect more than one seismic source) were calculated and examined; all important sensitivities are shown here. Sensitivities to source parameters were calculated and examined for the two or three most important sources in each type. Typically, only the results for the most important source in each type are shown here. Results for other sources have smaller contributions to the total uncertainty and are not shown.

Sensitivity results with respect to global interpretations are calculated by computing the mean hazard for each interpretation and then comparing the results obtained with the various interpretations. The weights assigned to the various interpretations or branches of the logic tree are also an important element of these comparisons and are shown (in parentheses) on all figures.

Sensitivity results with respect to source parameters are calculated in a different manner. For instance, to investigate the sensitivity to the M_{max} of the Solitario Canyon fault, the following steps are implemented:

1. Compute the combined hazard from all local faults, for all combinations of global and fault parameters.

2. Group these hazard curves into bins defined so that the parameters of all hazard curves in one bin differ only in the M_{max} for the Solitario Canyon fault (i.e., all other parameters used to compute these hazard curves are the same).

3. For each bin, calculate the mean and standard deviation of hazard and create mean $\pm \sigma$ hazard curves.

4. Compute the average of the mean + σ curves over all bins. Do the same for the mean - σ curves. The resulting difference between the mean - σ and mean + σ curves indicates the sensitivity of the results to uncertainty in the M_{max} of the Solitario Canyon fault. If the fault does not appear in all branches of the logic tree, an additional curve (labeled NA) is also shown, corresponding to the mean hazard from those branches of the logic tree where the fault does not appear. (Recall that the Solitario Canyon fault by itself may not appear in all branches of the logic tree, even if the SSFD expert team considers this fault to be active with certainty.)

This approach is more convenient because source parameters may have distributions that vary as a function of the values of other variables in the logic tree. For instance, the distribution of M_{max} has a range of number of magnitudes, a range of values, and different weights, depending on fault length. Other source parameters, such as the recurrence of areal source zones, have up to 25 different (rate,b) pairs. These factors make it difficult to display and interpret these results in the same manner as the global sensitivity results. It is important to emphasize that this approach shows the mean $\pm$ σ effect *on hazard* of the uncertain parameter, not simply the results associated with the mean - σ and mean + σ values of the parameter.

The following discusses sensitivity results specifically by team. This discussion focuses on the amplitudes associated with 10^{-4} annual exceedance probability (1.1 g for 10 Hz, 0.5 g for 1 Hz). When necessary, the discussion includes a brief description of some elements of a team's seismic source characterization.

7.4.2.1 AAR Team

Figures 7-21 and 7-22 show the contributions of the various source types to the mean hazard. For 10 Hz, both the individual local faults and the areal sources are the major contributors to the hazard. For 1 Hz, the individual local faults, the areal zones, and the regional faults contribute similarly to the hazard.

Figures 7-23 and 7-24 show the contributions of the most important individual seismic sources from all source types. The most important local faults are two coalesced fault systems, namely the East-side (all local faults east of Yucca Mountain; active with a probability of 75%), and West-side #2 (all local faults west of Yucca Mountain except the Solitario Canyon and Iron

Ridge faults; active with a probability of 60%). Both of these fault systems involve simultaneous ruptures on multiple faults. The AAR team associated these fault systems with the single-rupture attenuation equations because most of the seismic moment release is postulated to occur on a single-rupture plane. The most important areal zone is Zone 2, which includes the Nevada Walker Lane, the host areal source zone for Scenario 1 (see Section 4.3.1.1). The most important regional fault is the Death Valley-Furnace Creek fault system, which is also the most important contributor to hazard at 1 Hz.

The 10-Hz deaggregation results (Figure 7-25) show that most of the hazard comes from events of M_w 5 to 6.5 at short distances (<15 km occurring on local faults and generally within areal zones). The 1-Hz results (Figure 7-26) show a shift to higher magnitudes for the local faults and areal sources, and a large contribution from regional faults in the 45 to 60 km distance range and magnitudes greater than M_w 7 (associated with the Death Valley-Furnace Creek fault system).

Figures 7-27 through 7-41 show sensitivity results of the AAR local faults for 10-Hz horizontal spectral acceleration. The major nodes in the AAR global logic tree for local faults represent the existence of NW-SE dextral structures, the type of dextral structure, and the existence of a detachment. Additional branches consider detachment depth, the possibility of coalescence, coalescence pattern (i.e., which groups of faults rupture simultaneously), and seismogenic crustal thickness. The probability of coalesced behavior depends on preceding branches of the logic tree, with a high marginal probability of coalescence. The existence and pattern of coalescence are the only nodes to show significant sensitivity. Other branches of the local fault global logic tree show negligible sensitivity. Of the source parameters for the East-side fault system, recurrence model and recurrence (given the recurrence model and recurrence approach) show moderate sensitivity; b-value, rupture length, M_{max}, and recurrence approach show low sensitivity. Similar trends are observed in the sensitivity to the parameters of the West-side fault system (only results for recurrence model are shown here).

Figures 7-42 through 7-46 show sensitivity results for the AAR areal zones and 10-Hz horizontal spectral acceleration. The major nodes in the AAR global logic tree for areal zones represent three scenarios with differing areal zone configurations, and a fourth scenario containing only one areal zone. The first three scenarios use uniform seismicity; the fourth

scenario uses variable seismicity, with four alternative degrees of smoothing. In all scenarios, a portion of the host areal source zone (20-km radius around the site), is assigned a lower M_{max} by the AAR team due to more detailed knowledge of local fault sources. Sensitivity to scenario and to spatial variability is important. Sensitivity to minimum magnitude used in the recurrence calculations, M_{max}, and recurrence is low.

Figures 7-47 through 7-52 show sensitivity results for the AAR regional faults and 1-Hz spectral acceleration. The only regional faults that make any significant contribution to the hazard are Death Valley and Furnace Creek faults, which may be linked (i.e., rupture together, probability 80%) or independent (i.e., rupture separately, probability 20%). Sensitivity to the recurrence of the Death Valley-Furnace Creek fault system is moderate; sensitivity is low for other global and source parameters (i.e., linked vs. independent, fault lengths, sense of slip, recurrence used, dip angles, b-values, and M_{max}).

7.4.2.2 ASM Team

Figures 7-53 and 7-54 show the contributions of the various source types to the mean hazard. For 10 Hz, both the areal source zones and the single-rupture local faults are the major contributors to the hazard. For 1 Hz, the single-rupture local faults, the areal zones, and the regional faults contribute significantly to the hazard.

Figures 7-55 and 7-56 show the contributions of the most important individual seismic sources from all types of sources. The Walker Lane areal source is dominant, both at 10 Hz and 1 Hz, and its contribution is a factor of two or three larger than that of the next source. Important local faults include Stagecoach Road-Paintbrush Canyon and Solitario Canyon faults. Important regional faults include the Furnace Creek and Death Valley faults.

The 10-Hz deaggregation results (Figure 7-57) show that most of the hazard comes from short distances (<15 km), either M_w 5 to 6.5 events from the areal zones or M_w 5 to 7 events on the local faults. The 1-Hz results (Figure 7-58) show a shift to higher magnitudes for the local faults and areal zones, and a large contribution from regional faults in the 45 to 60 km distance range and magnitudes greater than M_w 7 to 7.5 associated with the Furnace Creek and Death Valley faults.

Figures 7-59 through 7-71 show sensitivity results of the ASM local faults for 10-Hz horizontal spectral acceleration. The major nodes in the ASM global logic tree for local faults consider the existence of a detachment and whether the detachment is seismogenic, the existence of a buried strike-slip fault and whether it is seismogenic, whether the faults merge at depth, the occurrence of simultaneous ruptures, the recurrence approach used, and dip angles. The type of recurrence approach (slip rates versus recurrence intervals) and the occurrence of simultaneous ruptures are the only nodes that show significant sensitivity. Of the source parameters of the Stagecoach Road-Paintbrush Canyon fault system, the recurrence model and recurrence (given the recurrence model and recurrence approach) show significant sensitivity.

Figures 7-72 through 7-75 show sensitivity results of the ASM areal zones for 10-Hz horizontal spectral acceleration. The only node in the ASM global logic tree for areal zones corresponds to the choice of alternative seismicity catalogs. The two areal zones (Walker Lane and Basin and Range) use uniform seismicity. Sensitivity to the catalog used is very low. Sensitivity to source parameters of the Walker Lane source (i.e., recurrence and M_{max}) is low. Figure 7-75 shows the sensitivity to the M_{max} of the Walker Lane source for 1-Hz horizontal spectral acceleration. This sensitivity is also low, although somewhat higher than the one for 10 Hz shown on Figure 7-73.

Figures 7-76 through 7-80 show sensitivity results for the ASM regional faults and 1-Hz horizontal spectral acceleration. The only regional faults that make any significant contribution to the hazard are the Furnace Creek and middle Death Valley faults. The global logic tree for regional faults has nodes to represent recurrence model, recurrence approach, b-value, and maximum depth. Sensitivity to all these nodes is low. Sensitivity to recurrence and M_{max} is also low.

7.4.2.3 DFS Team

Figures 7-81 and 7-82 show the contributions of the various source types to the mean hazard. For 10 Hz, both the individual local faults and the areal zones are the major contributors to the hazard. For 1 Hz, the individual local faults and areal zones contribute equally to the hazard; the regional faults contribute slightly less.

Figures 7-83 and 7-84 show the contributions of the most important individual seismic sources from all source types. The most important local faults are the Stagecoach Road-Paintbrush Canyon fault system and the Solitario Canyon fault. The most important areal zone for both 10-Hz and 1-Hz motions is the East Walker Lane for their Model B, which includes a local host areal zone. The most important regional fault is the Death Valley-Furnace Creek fault system, which is a moderate contributor to hazard at 1 Hz.

The 10-Hz deaggregation results (Figure 7-85) show that most of the hazard comes from short distances (<15 km), and M_w 5 to 6.5 events for local faults or M_w 5 to 7 events for areal sources. The 1-Hz results (Figure 7-86) show a shift to higher magnitudes for the local faults and areal zones (with a shift to longer distances in the latter), and a moderate contribution from regional faults in the 45 to 60 km range and M_w 6.5 to 7.5 associated with the Death Valley, Furnace Creek, and Fish Lake Valley faults.

Figures 7-87 through 7-94 show sensitivity results of the DFS local faults for 10-Hz horizontal spectral acceleration. The major nodes in the DFS global logic tree for local faults consider the presence of independent versus multiple-fault ruptures, the subsurface geometry (planar versus detached, with two planar-fault scenarios) and multiple-fault rupture scenarios, the recurrence model, and the b-value. Sensitivity to the presence of multiple-fault ruptures versus independent faulting is important although the multiple branch has low weight, so that the resulting uncertainty is low. Sensitivity to other nodes in the global logic tree is low. Sensitivity to M_{max} and the recurrence of the Stagecoach Road-Paintbrush Canyon fault system is also low.

Figures 7-95 through 7-99 show sensitivity results of the DFS areal zones for 10-Hz horizontal spectral acceleration. The major nodes in the DFS global logic tree for areal zones represent the catalog used, zonation (one model with three source zones, the other with a single zone), and spatial variability and smoothing of seismicity within a source. The host zones included in both models contain a small local portion with a lower M_{max}. The sensitivity to spatial smoothing is low to moderate; all other sensitivities to global parameters are low. Sensitivities to M_{max} and the recurrence are also low.

Figures 7-100 through 7-104 show sensitivity results for the DFS regional faults and 1-Hz horizontal spectral acceleration. The major nodes in the DFS global logic tree for regional faults represent recurrence model, maximum depth, and b-value. Sensitivity to these three quantities is low. Sensitivity to the slip rate of the Death Valley fault is moderate, but the sensitivity to the corresponding M_{max} is low.

7.4.2.4 RYA Team

Figures 7-105 and 7-106 show the contributions of the various source types to the mean hazard. For 10 Hz, the single- and multiple-rupture local faults, together with the areal zones, are the major contributors to the hazard. For 1 Hz, the regional faults contribute the most, but the other source types also have important contributions to seismic hazard.

Figures 7-107 and 7-108 show the contributions of the most important individual seismic sources from all source types. The most important local faults are the Paintbrush Canyon-Stagecoach Road-Bow Ridge and the West-side coalesced fault systems. The latter involves the Solitario Canyon, Iron Ridge, Windy Wash, and Fatigue Wash faults, and is associated with the multiple-rupture attenuation equations. The most important areal source zones are A2 and A1: two alternative geometries for a small host source. The most important regional faults are the Furnace Creek and Death Valley, which are also the two most important contributors to hazard at 1 Hz.

The 10-Hz deaggregation results (Figures 7-109) show that most of the hazard comes from short distances (<15 km) and M_w 5 to 6.5 events for areal sources and M_w 5 to 7.0 events for local faults. The 1-Hz results (Figure 7-110) show a large contribution from regional faults in the 45 to 75 km range and M_w 6.5 to 7.5 associated with the Death Valley and Furnace Creek faults.

Figures 7-111 through 7-121 show sensitivity results of the RYA local faults for 10-Hz horizontal spectral acceleration. The major nodes in the RYA global logic tree for local faults represent maximum fault depth, coalescence model, b-values, fault lengths, and recurrence approach. Sensitivity is significant only for recurrence approach, and moderate for fault lengths. Other sensitivity branches are low. Sensitivity to the source parameters (recurrence model, M_{max}, and recurrence) of the East-side faults, the Paintbrush Canyon-Stagecoach Road-

Bow Ridge fault system is low to moderate. Sensitivity to the M_{max} and recurrence of the West-side fault system is moderate.

Figures 7-122 through 7-126 show sensitivity results of the RYA areal zones for 10-Hz horizontal spectral acceleration. The major nodes in the RYA global logic tree for areal zones represent choice of catalog used, zonation, and spatial smoothing of seismicity (in all but the host source). Sensitivity to all these branches is low. Sensitivity to the M_{max} and the recurrence of A2 zone is also low.

Figures 7-127 through 7-132 show sensitivity results of the RYA regional faults for 1-Hz horizontal spectral acceleration. The major nodes in the RYA global logic tree for regional faults are the configuration of the Death Valley-Furnace Creek fault system (linked or separate), the recurrence model, the maximum fault depth, and the b-value. Sensitivity to all of these branches is low. Sensitivity to the M_{max} and recurrence of the Furnace Creek fault is also low.

7.4.2.5 SBK Team

Figures 7-133 and 7-134 show the contributions of the various source types to the mean hazard. For 10 Hz, the single-rupture local faults are the major contributors to the hazard. For 1 Hz, the regional faults and the single-rupture local faults are the major contributors.

Figures 7-135 and 7-136 show the contributions of the most important individual seismic sources from all source types. The most important local faults are the Paintbrush Canyon-Stagecoach Road and Solitario Canyon faults. The most important areal zone is the Basin and Range zone, which is the host source zone. The most important regional fault is the Furnace Creek fault, which is also the most important contributor to hazard at 1 Hz.

The 10-Hz deaggregation results (Figure 7-137) show that most of the hazard comes from individual local faults; events at short distances (<15 km) and M_w 5 to 7. The 1-Hz results (Figure 7-138) show a large contribution from regional faults in the 45 to 60 km range and M_w 7 to 7.5 (associated with the Death Valley-Furnace Creek-Fish Lake Valley fault system).

Figures 7-139 through 7-146 show sensitivity results of the SBK local faults for 10-Hz horizontal spectral acceleration. The major nodes in the SBK global logic tree for local faults

represent fault behavior (independent, linked, coalesced, or detachment), fault dip, maximum depth, and b-value. Sensitivity to all of these nodes is low. Sensitivity to recurrence approach and recurrence model of the Paintbrush Canyon-Stagecoach Road fault system is moderate to low; sensitivity to other source parameters (M_{max} and recurrence) is low.

Figures 7-147 through 7-151 show sensitivity results of the SBK areal sources for 10-Hz spectral acceleration. The major nodes in the SBK global logic tree for areal zones represent zonation, choice of catalog (treated as independent across source zones), and adjustment for NTS events. Sensitivity to these nodes is low. Sensitivity to source parameters of the Basin and Range zone is moderate for recurrence and low for M_{max}.

Figures 7-152 through 7-158 show sensitivity results for the SBK regional faults and 1-Hz horizontal spectral acceleration. The major nodes in the SBK global logic tree for regional faults represent the rupture behavior of the Death Valley-Furnace Creek-Fish Lake Valley fault system, sense of slip of the Death Valley fault, maximum depth, dip angles, and b-values. Sensitivity is high for the scenario in which all faults in the Death Valley-Furnace Creek-Fish Lake Valley fault system are linked. The resulting contribution to uncertainty is low, however, because the branch associated with this scenario has a very low probability. Sensitivity to other global branches is low. Sensitivity is low for source characteristics of the Furnace Creek fault (i.e., recurrence approach, recurrence model, M_{max}, and recurrence).

7.4.2.6 SDO Team

Figures 7-159 and 7-160 show the contributions of the various source types to the mean hazard. For 10 Hz, both the single-rupture local faults and the areal source zones are the major contributors to the hazard. For 1 Hz, the single-rupture local faults, the areal zones, and the regional faults contribute equally to the hazard.

Figures 7-161 and 7-162 show the contributions of the most important individual seismic sources from all source types. The most important local fault is Solitario Canyon fault. The most important areal zone is Zone 1, the host zone, which represents the Walker Lane. Zone 1 is also the largest contributor to hazard at both 10 Hz and 1 Hz. The most important regional fault is the Furnace Creek fault.

The 10-Hz deaggregation results (Figure 7-163) show that most of the hazard comes from short distances (<15 km) and M_w 5 to 6.5 events for areal zones or M_w 5 to 7 events for local faults. The 1-Hz results (Figure 7-164) show a large contribution from regional faults, with a peak in the 45 to 60 km distance range and M_w 7 to 7.5 associated with the Death Valley and Furnace Creek faults. In addition, regional faults at other distances significantly contribute.

Figures 7-165 through 7-169 show sensitivity results of the SDO local faults for 10-Hz horizontal spectral acceleration. The SDO global logic tree for local faults considers only the b-value. Multiple-rupture scenarios are treated as part of the aleatory model (e.g., over time, some events involve multiple simultaneous ruptures, others involve single ruptures). Sensitivity to b-values is very low. Source parameters for the local faults include maximum depth, recurrence model, M_{max}, and recurrence. Sensitivity to these parameters is shown for the Solitario Canyon fault, and found to be low.

Figures 7-170 through 7-173 show sensitivity results of the SDO areal zones for 10-Hz spectral acceleration. The major nodes in the SDO global logic tree for areal zones represent choice of catalog and spatial variability and smoothing of seismicity within an areal zone. Sensitivity to choice of catalogs is moderate, with Version 8 giving a hazard that is roughly half the hazard from either of the other two catalogs. Sensitivity to spatial variability is low. Sensitivity to the parameters of Zone 1 (i.e., M_{max} and recurrence) is also low.

Figures 7-174 through 7-177 show sensitivity results for the SDO regional faults and 1-Hz horizontal spectral acceleration. The major nodes in the SDO global logic tree for regional faults represent maximum depth, recurrence model, and b-value. Sensitivity to these nodes is low. Source parameters include fault length, M_{max}, and activity rates. Sensitivity to these parameters for the Furnace Creek fault is low.

7.4.2.7 Overall Trends

The sensitivity results for all SSFD expert teams indicate the following general trends:

- Seismic source parameters with a direct effect on activity rates (e.g., recurrence approach [either slip rates or recurrence intervals], and recurrence model [characteristic,

exponential, or maximum moment] are the parameters that contribute the most to uncertainty in seismic hazard, for the exceedance probabilities of interest in this study.

- M_{max} has a small effect on uncertainty for the exceedance probabilities of interest in this study, especially for 10 Hz, because a large fraction of the hazard comes from more frequent moderate-magnitude events.

- Geometric fault parameters (e.g., rupture lengths, dips, maximum depths) are minor contributions to uncertainty. These parameters have a moderate effect on the locations of earthquakes and an effect on M_{max}, but do not affect earthquake frequency. (Fault geometry affects occurrence rates when activity is specified by slip rates. However, the increased activity that results from increased length of a fault that comes near the site [and whose closest approach to the site is the perpendicular distance] will occur away from the site and will have little effect on the hazard)

- Although expert teams vary somewhat, the dominant sources for seismic hazard at 10 Hz are the Paintbrush Canyon-Stagecoach Road and Solitario Canyon faults (or coalesced fault systems including these two faults), and the host areal zone (not necessarily in that order). At 1 Hz, the dominant sources are the Death Valley and Furnace Creek faults and the same three sources mentioned above.

- Multiple-rupture scenarios of the type with comparable seismic moment release on more than one fault (i.e., those requiring modification of the attenuation equations) make a small contribution to the total hazard for five of the six expert teams.

- All expert teams considered the existence of buried strike-slip faults and seismogenic detachments. Several of them explicitly included these sources in their models. The contribution of these sources to the total seismic hazard is negligible primarily because the corresponding branches in the logic tree have low probabilities. This is also true for volcanic sources of seismicity, which were explicitly considered by only two expert teams.

7.4.3 Sensitivity to Ground Motion Experts and Parameters

Figures 7-178 through 7-187 show the sensitivity of the total hazard to the GM experts and their interpretations. These comparisons all use the seismic source interpretations by the ASM team as an example. Results are shown for 10 Hz, 1 Hz, and 0.3 Hz. Three types of figures are shown, as follows:

1. Mean hazard calculated using the interpretations by each GM expert.

2. Mean hazard curves for all values of $\varepsilon_{\mu,}$, the parameter that scales each expert's median prediction to represent the expert's assessment of epistemic uncertainty in the median ground motion. These figures show the contribution of σ_μ to uncertainty in the hazard. σ_μ also has an effect on the mean hazard, because of the skewness of the lognormal distribution of ε_μ.

3. Mean $\pm$ σ curves showing the effect of σ_σ (each expert's assessment of epistemic uncertainty in σ) on the uncertainty in the calculated hazard (see the discussion of this type of sensitivity results in Section 3.3.2). σ_σ also affects the mean hazard, because the calculated seismic hazard is a nonlinear function of σ (with a positive second derivative).

In general, the most important ground motion contributors to uncertainty in the hazard are σ_μ and σ_σ (i.e., within-expert uncertainties), rather than expert-to-expert uncertainties. The moderate expert-to-expert variation is likely the result of using a common information base and of having an elicitation and feedback format that minimizes differences in knowledge and understanding among experts.

Other sensitivity results (not included in this report) indicate that the effect of σ_μ is higher for Anderson, and to a lesser extent for Boore, than for the other GM experts. This is one of the factors that make Anderson's results higher. The effect of σ_σ is more uniform across GM experts.

The importance of σ_σ increases as frequency decreases. This is consistent with the magnitude-distance-ε distributions on Figures 7-15 and 7-16, which show that the contribution from events with $\varepsilon > 2$ is more important for 1 Hz than for 10 Hz.

The total uncertainty due to ground motion issues (i.e., the combined expert-to-expert and within-expert uncertainties) is larger than the uncertainty due to seismic source-characterization issues. This conclusion may be qualitatively confirmed by comparing Figures 7-5 and 7-179. This is a common situation in multiple-expert PSHA studies.

In summary, the major contributor to epistemic uncertainty in seismic hazard is the uncertainty in ground motion amplitude that was expressed by each individual GM expert (within-expert epistemic uncertainty). Additional contributions to epistemic uncertainty arise from moderate differences among the SSFD expert teams and among the GM experts, as well as from the uncertainties expressed by the seismic source logic trees.

TABLE 7-1
MEAN UNIFORM HAZARD SPECTRAL VALUES (g) AND PGV VALUES (cm/sec) FOR REFERENCE ROCK OUTCROP

Freq. (Hz)	Horizontal		Vertical	
	10^{-3}	10^{-4}	10^{-3}	10^{-4}
0.3	0.051	0.168	0.029	0.105
0.5	0.091	0.278	0.046	0.159
1	0.162	0.471	0.073	0.222
2	0.263	0.782	0.130	0.406
5	0.346	1.083	0.200	0.660
10	0.355	1.160	0.250	0.906
20	0.284	0.951	0.225	0.853
PGA	0.169	0.534	0.112	0.391
PGV	15.3	47.6	7.4	23.4

TABLE 7-2
GUIDE TO WITHIN-TEAM SENSITIVITY RESULTS

Figure Numbers	Team	Description
7-21 through 7-22	AAR	Mean hazard by source group
7-23 through 7-24	AAR	Dominant seismic sources
7-25 through 7-26	AAR	M-R- deaggregation by source group
7-27 through 7-34	AAR	Local faults, sens. to global parameters
7-35 through 7-41	AAR	Local faults, sens. to source parameters
7-42 through 7-43	AAR	Area sources, sens. to global parameters
7-44 through 7-46	AAR	Area sources, sens. to source parameters
7-47 through 7-48	AAR	Regional faults, sens. to global parameters
7-49 through 7-52	AAR	Regional faults, sens. to source parameters
7-53 through 7-54	ASM	Mean hazard by source group
7-55 through 7-56	ASM	Dominant seismic sources
7-57 through 7-58	ASM	M-R- deaggregation by source group
7-59 through 7-67	ASM	Local faults, sens. to global parameters
7-68 through 7-71	ASM	Local faults, sens. to source parameters
7-72	ASM	Area sources, sens. to global parameters
7-73 through 7-75	ASM	Area sources, sens. to source parameters
7-76 through 7-78	ASM	Regional faults, sens. to global parameters
7-79 through 7-80	ASM	Regional faults, sens. to source parameters
7-81 through 7-82	DFS	Mean hazard by source group
7-83 through 7-84	DFS	Dominant seismic sources
7-85 through 7-86	DFS	M-R- deaggregation by source group
7-87 through 7-92	DFS	Local faults, sens. to global parameters
7-93 through 7-94	DFS	Local faults, sens. to source parameters
7-95 through 7-97	DFS	Area sources, sens. to global parameters
7-98 through 7-99	DFS	Area sources, sens. to source parameters
7-100 through 7-102	DFS	Regional faults, sens. to global parameters
7-103 through 7-104	DFS	Regional faults, sens. to source parameters

TABLE 7-2 (continued)

Figure Numbers	Team	Description
7-105 through 7-106	RYA	Mean hazard by source group
7-107 through 7-108	RYA	Dominant seismic sources
7-109 through 7-110	RYA	M-R- deaggregation by source group
7-111 through 7-115	RYA	Local faults, sens. to global parameters
7-116 through 7-121	RYA	Local faults, sens. to source parameters
7-122 through 7-124	RYA	Area sources, sens. to global parameters
7-125 through 7-126	RYA	Area sources, sens. to source parameters
7-127 through 7-130	RYA	Regional faults, sens. to global parameters
7-131 through 7-132	RYA	Regional faults, sens. to source parameters
7-133 through 7-134	SBK	Mean hazard by source group
7-135 through 7-136	SBK	Dominant seismic sources
7-137 through 7-138	SBK	M-R- deaggregation by source group
7-139 through 7-142	SBK	Local faults, sens. to global parameters
7-143 through 7-146	SBK	Local faults, sens. to source parameters
7-147 through 7-149	SBK	Area sources, sens. to global parameters
7-150 through 7-151	SBK	Area sources, sens. to source parameters
7-152 through 7-154	SBK	Regional faults, sens. to global parameters
7-155 through 7-158	SBK	Regional faults, sens. to source parameters
7-159 through 7-160	SDO	Mean hazard by source group
7-161 through 7-162	SDO	Dominant seismic sources
7-163 through 7-164	SDO	M-R- deaggregation by source group
7-165	SDO	Local faults, sens. to global parameters
7-166 through 7-169	SDO	Local faults, sens. to source parameters
7-170 through 7-171	SDO	Area sources, sens. to global parameters
7-172 through 7-173	SDO	Area sources, sens. to source parameters
7-174	SDO	Regional faults, sens. to global parameters
7-175 through 7-177	SDO	Regional faults, sens. to source parameters

a) Seismic source i

Earthquake locations in space (and magnitude-dependent rupture dimensions) lead to a distribution of distance $f_{R(i)|M(i)}(r;m)$

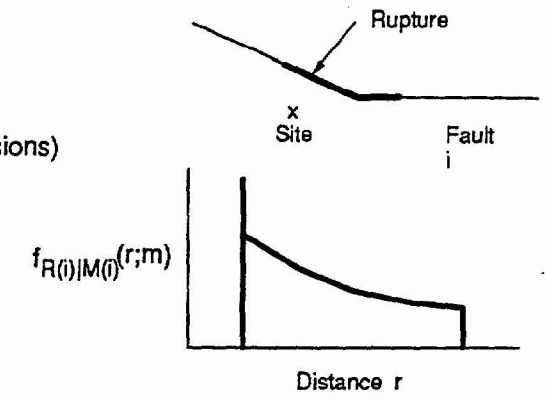

b) Magnitude distribution and rate of occurrence for source i

$f_{M(i)}(m)$, ν_i

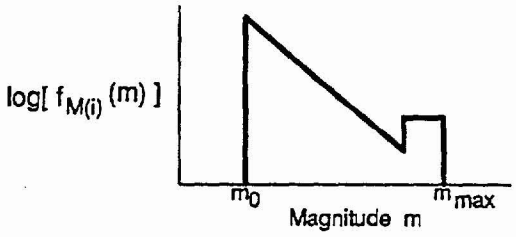

c) Ground-motion attenuation equation

$G_{A|m,r}(a)$

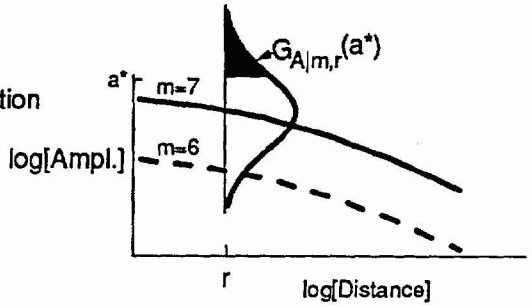

d) Probability analysis: annual exceedence probability

$$\approx \sum_i \nu_i \int_r \int_m G_{A|m,r}(a^*)\, f_{M(i)}(m)\, f_{R(i)|M(i)}(r;m)\, dm\, dr$$

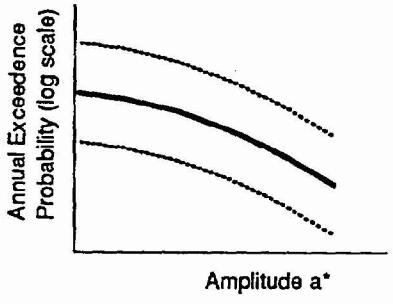

Figure 7-1 Seismic hazard computational model (modified from McGuire and Arabasz, 1990)

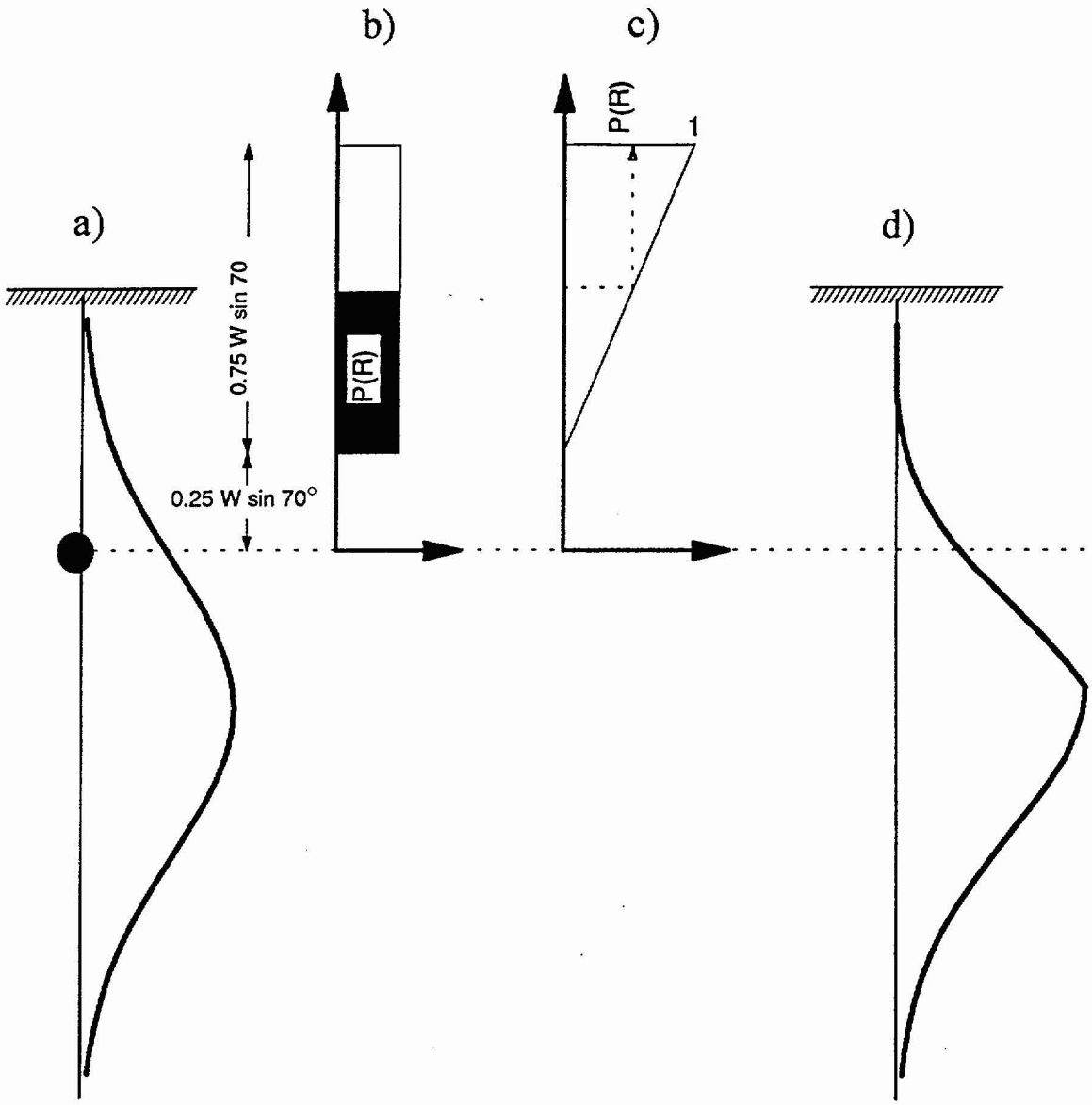

Figure 7-2 Calculation of hypocentral depth distribution for area sources considering the dimensions of the rupture. a) Normal distribution of depth for small events; the solid ellipse indicates a hypothetical hypocentral location. b) probability density function for the location of the top of the rupture. W is the magnitude-dependent rupture width. The probability P(R) that the event is realizable is the probability that the top of the rupture is below the ground surface (the shaded area). c) cumulative distribution function for the location of the top of the rupture, showing P(R). d) Distribution of depth for event with finite width W. This distribution is obtained by multiplying the distribution in (a) by P(R) and normalizing to an area of 1.

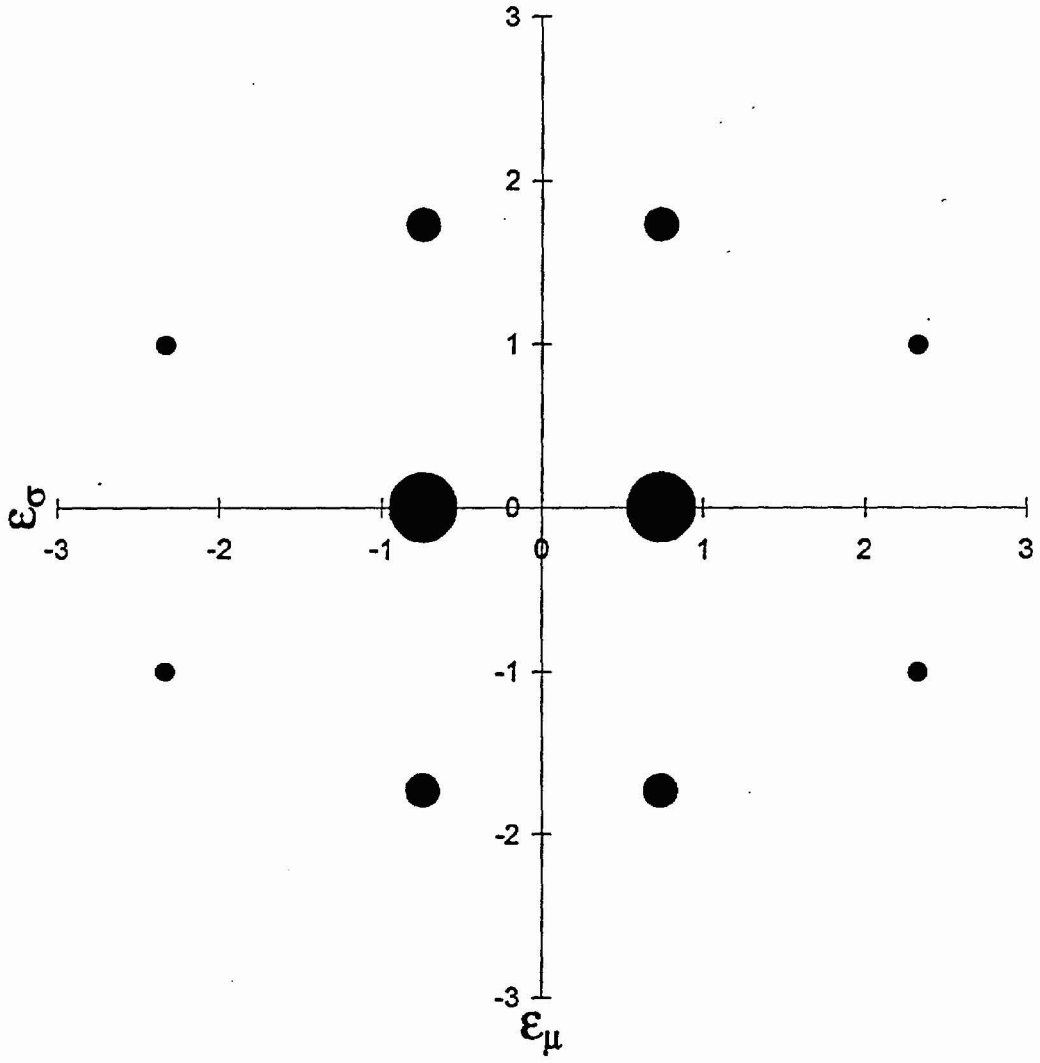

Figure 7-3 Discretization of the joint distribution of ε_μ (horizontal axis) and ε_σ (vertical axis) used to represent within-expert epistemic uncertainty in ground motions. The areas of the circles are proportional to the weights for the corresponding points.

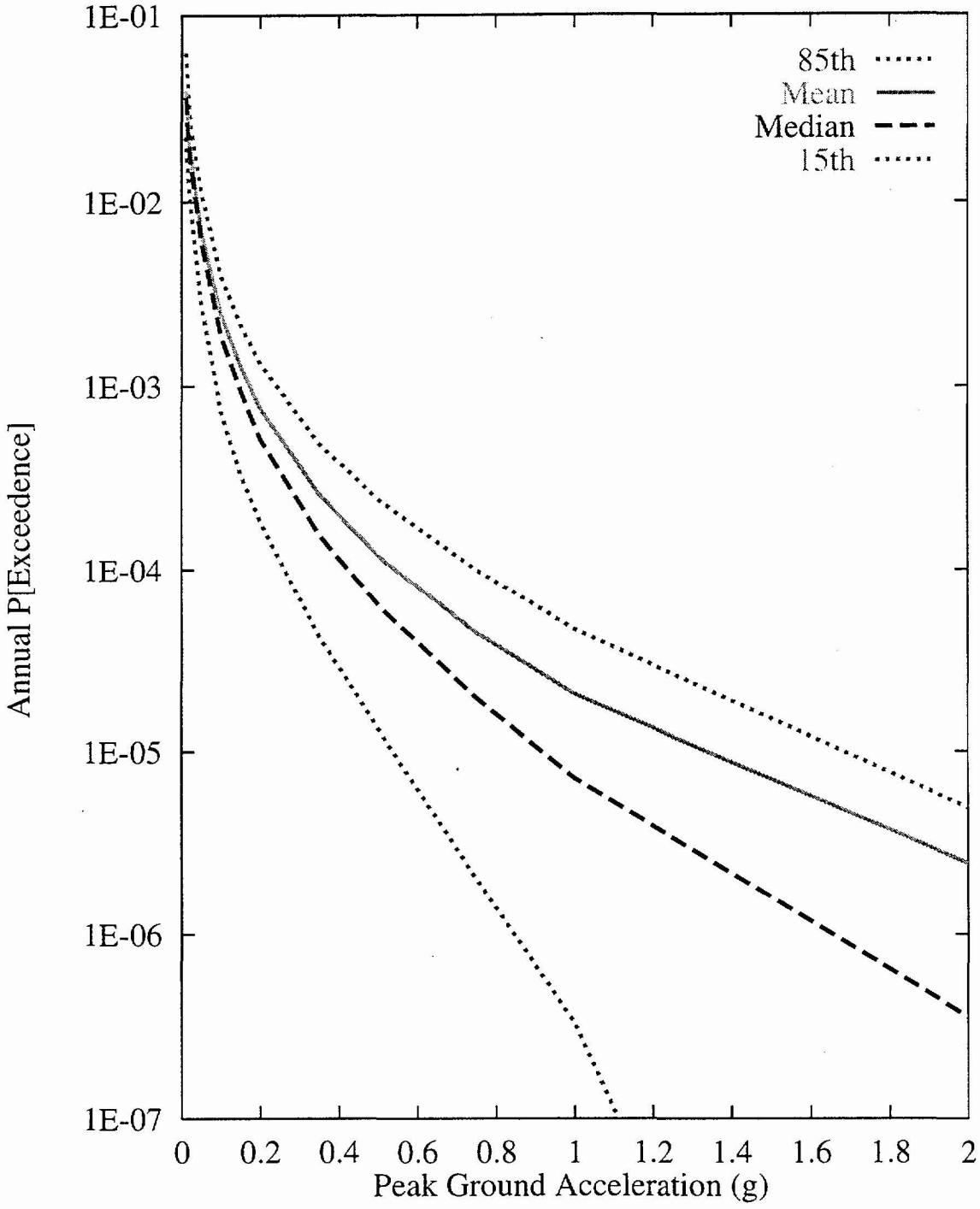

Figure 7-4 Integrated seismic hazard results: summary hazard curves for horizontal PGA

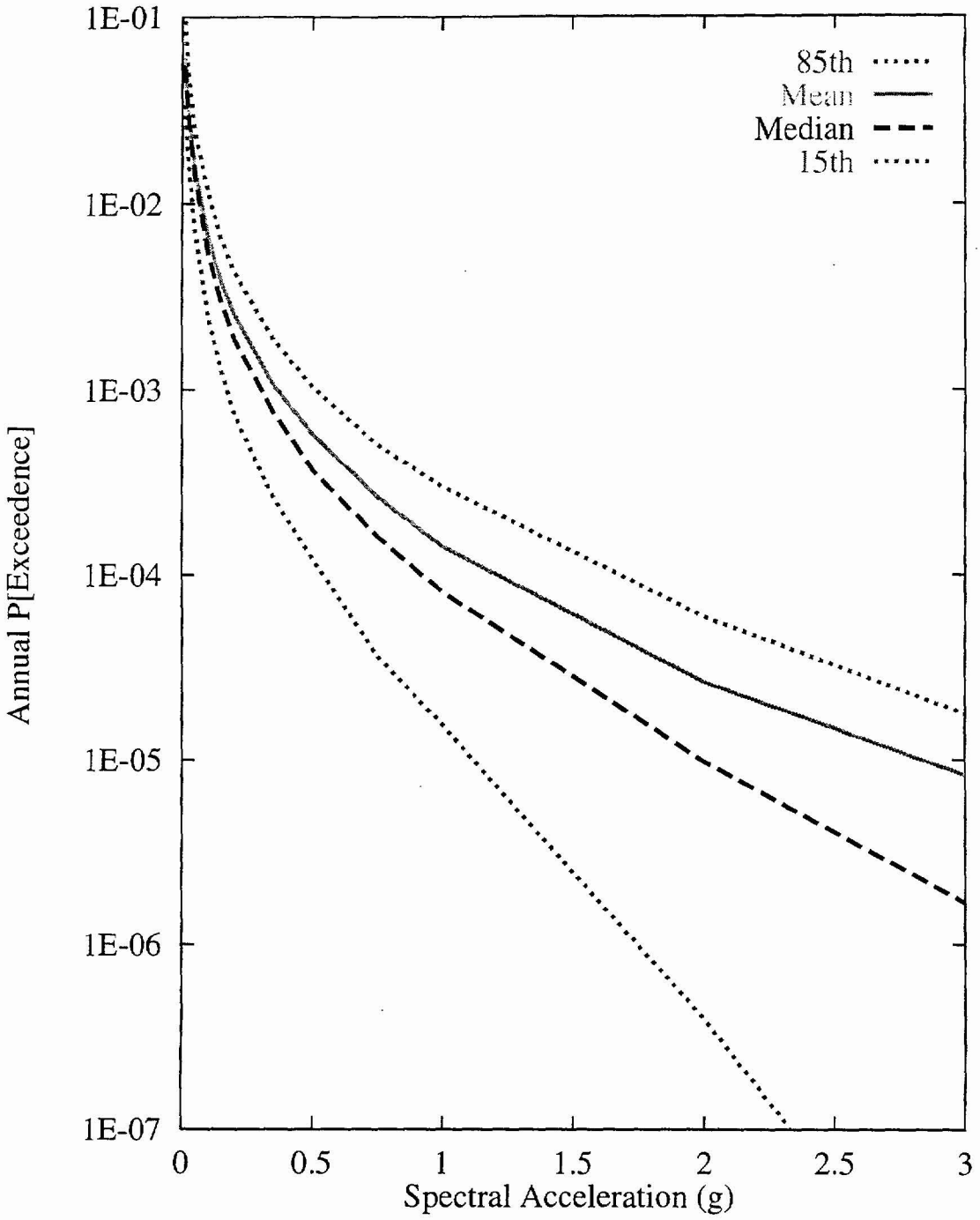

Figure 7-5 Integrated seismic hazard results: summary hazard curves for 10-Hz horizontal spectral acceleration

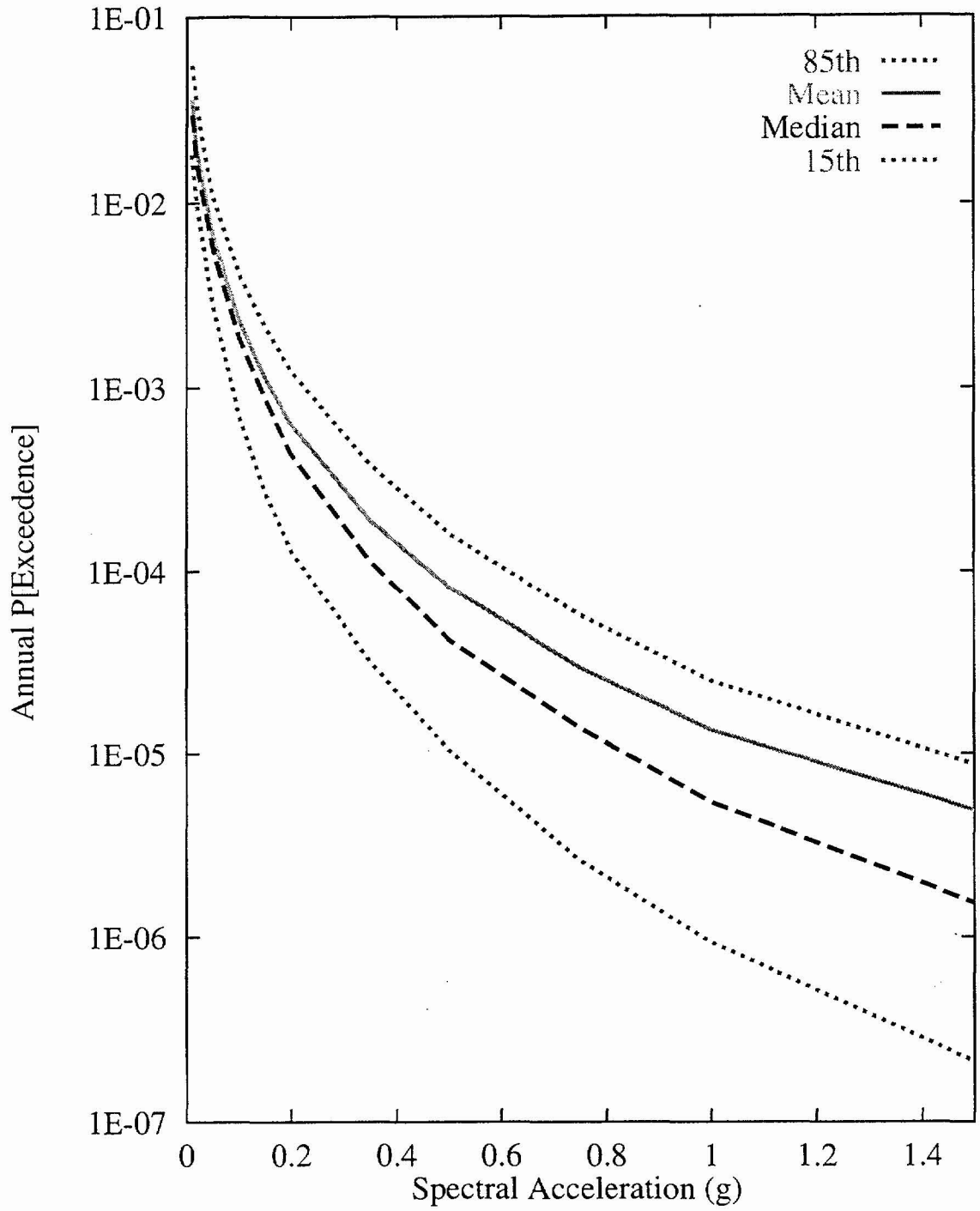

Figure 7-6 Integrated seismic hazard results: summary hazard curves for 1-Hz horizontal spectral acceleration